INFORMATION TO USERS

This manuscript has been reproduced from the microfilm master. UMI films the text directly from the original or copy submitted. Thus, some thesis and dissertation copies are in typewriter face, while others may be from any type of computer printer.

The quality of this reproduction is dependent upon the quality of the copy submitted. Broken or indistinct print, colored or poor quality illustrations and photographs, print bleedthrough, substandard margins, and improper alignment can adversely affect reproduction.

In the unlikely event that the author did not send UMI a complete manuscript and there are missing pages, these will be noted. Also, if unauthorized copyright material had to be removed, a note will indicate the deletion.

Oversize materials (e.g., maps, drawings, charts) are reproduced by sectioning the original, beginning at the upper left-hand corner and continuing from left to right in equal sections with small overlaps.

ProQuest Information and Learning
300 North Zeeb Road, Ann Arbor, MI 48106-1346 USA
800-521-0600

Modeling of a Hybrid-Ventilated Building "Grong School"

Young-Chae Jeong

A Thesis

in

The Department of

Building, Civil and Environmental Engineering

Presented in Partial Fulfillment of the Requirements

for the Degree of Master of Applied Science at

Concordia University

Montreal, Quebec, Canada

June 2002

ABSTRACT

Modeling of a Hybrid-Ventilated Building "Grong School"

Young-Chae Jeong

This thesis reports the results of computer simulation of a hybrid-ventilated building using ESP-r (Environmental Systems Performance for research). A newly constructed school building in Norway was used for this simulation study. The research attempted to verify the use of ESP-r for the simulation of a real building that utilizes hybrid ventilation technologies. The simulations and their analysis focus on the building's thermal interactions and ventilation performance.

The model building has been simulated in three different categories of ESP-r: "building thermal simulation", "airflow simulation", and "building + airflow integrated simulation". Measured weather data were used to define the outdoor conditions of the building. It covers a representative heating period and constitutes of time-series of minutely measured values of air temperature, solar radiations, wind speed, and wind direction. In addition, for validation purpose some measured parameters of indoor environment, such as room temperature, were compared to predicted values by ESP-r.

This thesis concludes that modeling of hybrid ventilation systems is now possible by ESP-r's integral approach and the resultant outputs are feasible and practical in terms of

both thermal and ventilation point of view, but at the same time limitations do exist when it attempts to model really complicated building systems or to model CO_2 based control systems.

ACKNOWLEDGMENTS

I would like to express my deepest gratitude and warm thanks to my supervisor, Dr. Fariborz Haghighat for his great help to make this work successful.

I also would like to acknowledge helpful advices and data presentation from Mr. Bjorn Jenssen and Dr. Per Olaf Tjelflaat of NTNU (Norweigian University of Science and Technology).

Extended thanks go to Dr. Ian Beausoleil-Morrison of Buildings Group of NRCan (Natural Resources Canada) for his offering ESP-r training courses and kind advices by e-mail.

This research is part of the Canadian contributions to the work of Annex 35 of IEA (International Energy Agency).

Finally, I do wish to thank my wife, Insoon Ha, and my parents for their continuous encouragement and support during my studies.

TABLE OF CONTENTS

LIST OF FIGURES

CHAPTER 1

INTRODUCTION

1.1 Hybrid ventilation

Recently the use of mechanical ventilation has been called into question mainly due to high energy consumption. Energy use by ventilation losses and fans accounts for almost 10 % of total energy use in buildings. But this energy use does not result in satisfactory conditions in terms of indoor air quality and thermal comfort in many buildings. Several ventilation techniques are being introduced to improve this situation. One of the most innovative and potentially energy-efficient approaches to building ventilation and cooling is hybrid ventilation system.

According to the Annex text of IEA Annex 35 "Hybrid Ventilation" the definition of hybrid ventilation is: "*Hybrid ventilation is a two-mode system which is controlled to minimize the energy consumption while maintaining acceptable indoor air quality and thermal comfort.*" [IEA annex 35 2000] Also, elsewhere this system was described as one of the following: (1) alternate use of natural and mechanical ventilation, (2) fan assisted natural ventilation, or (3) stack and wind supported mechanical system [W. D. Gids 2000].

Obviously, buildings with hybrid ventilation systems use both mechanical ventilation and natural ventilation strategies. The difference between conventional ventilation system and hybrid ventilation system is that hybrid ventilation can be controlled automatically

between natural and mechanical mode in order to minimize the energy consumption and to maintain satisfactory indoor environment. To say, hybrid ventilation systems have built-in strategies to have the mechanical and natural systems work in conjunction with each other. The main reason of using a hybrid system lies in the fact that it reduces the energy usage of a building considerably. Also, the use of these systems may result in higher occupant satisfaction. This system will lead to controls, which try to maintain the exact required ventilation rates. The driving forces should be minimized so that the system uses the minimum of electrical or mechanical energy.

The hybrid ventilation forms highly integrated and dynamic factors, such as transient thermal storage in building materials, solar gains, ventilation and infiltration due to wind, stack, and mechanical forces, and the non-steady operation of heating equipment. Therefore, like many other design problems, hybrid ventilation systems can only be assessed when treated as a sub-set of some complex set of interactions. In other words, a piecemeal approach, in which a particular region is considered in isolation, will be inappropriate and potentially misleading. One of the most powerful techniques currently available for an integrated approach is modeling and simulation by computers. They have become indispensable engineering techniques in the field of design and operation.

1.2 Building modeling and simulation

With the advent of powerful and inexpensive digital computers, tools which can provide a thorough understanding of the complex energy and mass flows that occur in buildings are simulation and modeling. Modeling is the art of developing a model which faithfully

represents a complex system, and simulation is the process of using the model to analyze and predict the behavior of the real system [Jan L. M. Hensen and J. W. Hand 1993].

Simulation and modeling tools are used to predict the thermal response of buildings when subjected to different energy conservation strategies. In the approach, the building is represented by digital information which can be processed for different energy utilization scenarios in order to optimize performance at acceptable cost. An ASHRAE Task Group [ASHRAE 1975] formulated a definition of system simulation applicable to "Energy Requirements for Heating and Cooling of Buildings" as: *"Predicting the operating quantities within a system (pressures, temperatures, energy and fluid flow rates) at the condition where all energy and material balances, all equations of state of working substances, and all performance characteristics of individual components are satisfied."*

Energy simulation in the building context has until recently been focused primarily on the building side of the overall problem domain. However, buildings are really an integration of energy systems comprising not only the whole of building form and fabric, but also plant and various other environmental control systems. In other words, it is important that when system simulation is used for building performance evaluation the building should not be represented as just another plant components imposing a load on the system, but should be presented taking into account all energy and mass flow paths by modeling the overall system in an integrated fashion. It must be clear that those approaches have much more potential for solving real world problems related to building and plant interactions.

Aforementioned hybrid ventilation systems are usually highly integrated with the building and its mechanical components. The systems form a highly integrated and dynamic system with combination of building, HVAC plants, solar energy features, and dynamic outdoor conditions. To predict the performance of such a configuration, a proper tool must be chosen. For this research, the dynamic thermal simulation tool, ESP-r, developed by the Energy Systems Research Unit (ESRU) – University of Strathclyde, UK, had been used for the extensive parametric simulations. ESP-r is a transient energy simulation system which is capable of modeling the energy and fluid flows within combined building and plant systems when constrained to conform to control actions [ESRU 1997]. The following gives some reasons why it was chosen as the simulation program on which the present study is based:

(1) It is a research-oriented program, with the objective to simulate real buildings as rigorously as possible.

(2) It provides finite volume and conservation based modeling approach for building and plant.

(3) It sets out to take into account all building / plant energy and mass flows and their inter-connections. (Network airflow modeling integrated with building thermal and plant model)

(4) The system is well documented. (It is heavily commented with the code itself: it comes with training and built-in tutorial material: also there is an extensive manual which is updated on a regular basis.)

(5) The system has been (and still is) the subject of various international validation.

1.3 Objectives

This thesis reports a computer simulation of a hybrid-ventilated building using ESP-r. A newly constructed school building in Norway was used for this simulation study. This research attempts to verify the use of ESP-r for the simulation of a real building that utilizes hybrid ventilation technologies. The simulations and their analysis focus on the building's thermal interactions and airflow movements. The objectives of the research are summarizes as follows:

(1) to apply ESP-r to the modeling of a hybrid-ventilated building.

(2) to evaluate thermal and ventilation performance of the model building from simulated results.

(3) to compare some predicted results by ESP-r with measured data, and

(4) finally to estimate the capability of the ESP-r for the simulation of real buildings utilizing hybrid ventilation concepts.

Chapter 2 describes the model building used for the research. It is a new school building in Norway and has been a good example of a design where the total building design was affected by the hybrid ventilation concept. Chapter 3 describes a general overview and theoretical background of ESP-r, a computing environment for building and plant energy simulation. Chapter 4 gives detailed procedures and techniques of the modeling and simulation. Chapter 5 addresses a discussion of the simulation results and some validation procedures, and finally Chapter 6 describes the conclusion drawn from the previous chapters.

CHAPTER 2

GRONG SHOOL

2.1 Overview of the Grong school

The building used for this study is a new single-story school building of brick veneer and wood frame structure. It is an elementary school building of *1.000* m^2, designed to accommodate *223* occupants. It is located in the center of Grong, a small town slightly north of Trondheim, Norway. Grong school was completed in August 1998.

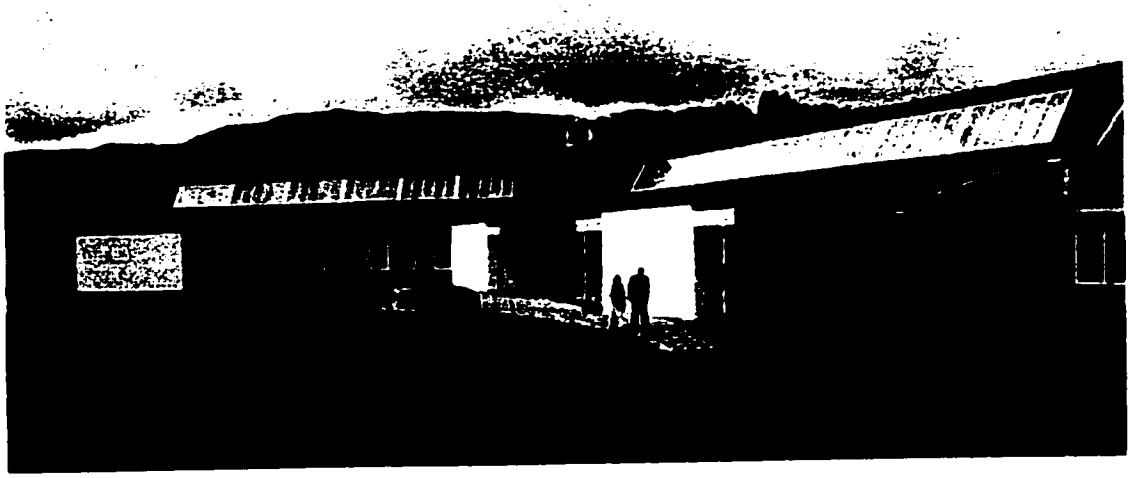

Figure 2.1 Overview of the Grong school (looking towards the north-west)

The classrooms are located on the north side of the building to avoid overheating and thereby reduce cooling demand. Common rooms, rooms for group activities, storage rooms, and locker rooms are located on the south side. North facing classrooms have no need for glare reduction devices or shading systems, but have low heat gains and thus

increased need for heating during winter. To increase solar gains the exhaust air channel (top of the building) is designed as a solar collector, as seen in Figure 1. This gives some heat to the exhaust channel to help buoyancy-driven airflow, and also gives some sunlight into the classrooms. The internal walls of the exhaust channel are glazed in order to allow daylight to reach the back of classrooms.

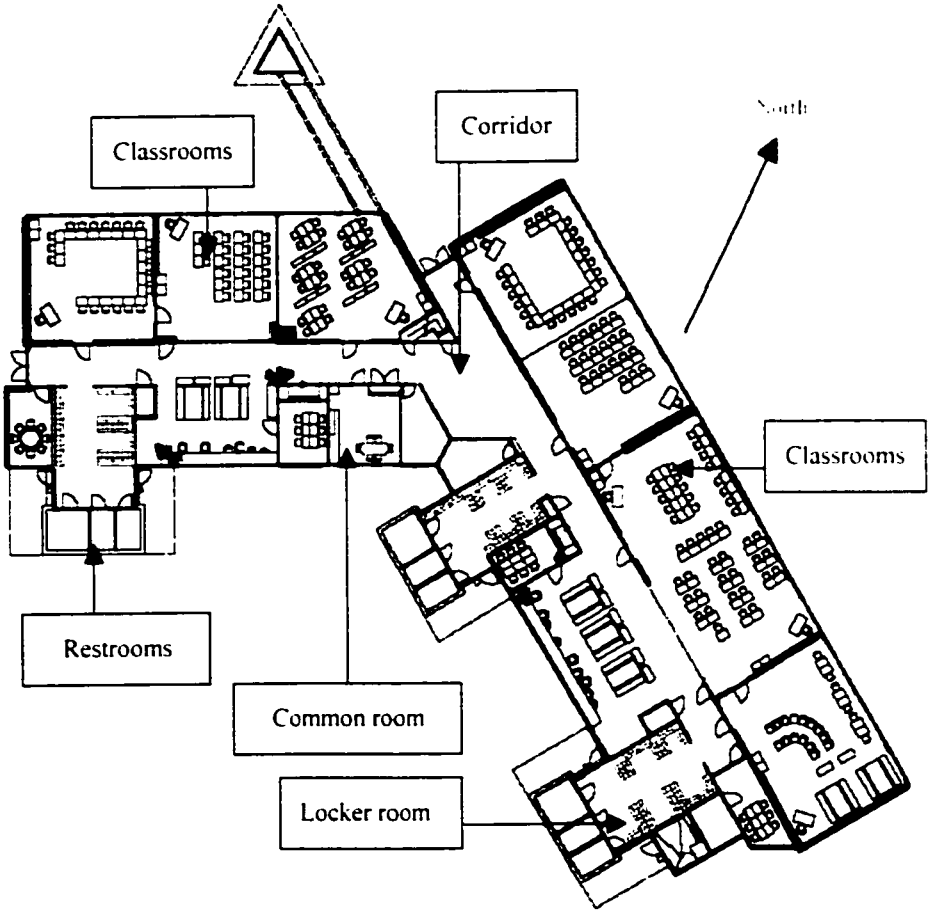

Figure 2.2 Plan of the Grong school

■ **Location and Site situation**

Latitude: 65 N

Longitude: 11 E

Altitude: 50m above sea level

Terrain: Countryside

Air pollutant level: Low

Noise Level: Low

Average wind speed: $0 \sim 5\ m/s$

- **Architect and Consultant**

Architect: Letnes Arkitektkontor AS, Verdal, Norway

HVAC Design: Planconsult VVS, Trondheim, Norway

Research Assistance: SINTEF and NTNU, Trondheim, Norway

Figure 2.3 Interior and exterior views of the Grong school (left: exterior view of exhaust channel and tower on the roof, center: view of classroom towards the corridor, right: view of central corridor)

2.2 Ventilation concepts

The outdoor climate at the site has temperatures below indoors for 95 % of the year. The wind condition is usually gusty on the site. Thus, wind and buoyancy-driven ventilation with fan assistance (hybrid ventilation) has been chosen for this project.

Air enters the building through a separate intake tower, and is fed through an earth channel (underground concrete duct) into a spinal distribution chamber (underground culvert) in the basement. From here, the air is distributed to the classrooms through grilles installed on the floor as required. Exhaust air is entered into the exhaust channel via exhaust dampers (exhaust vents) above the central corridor, and out through the exhaust tower. Figure 4 shows a schematic view of the ventilation concept.

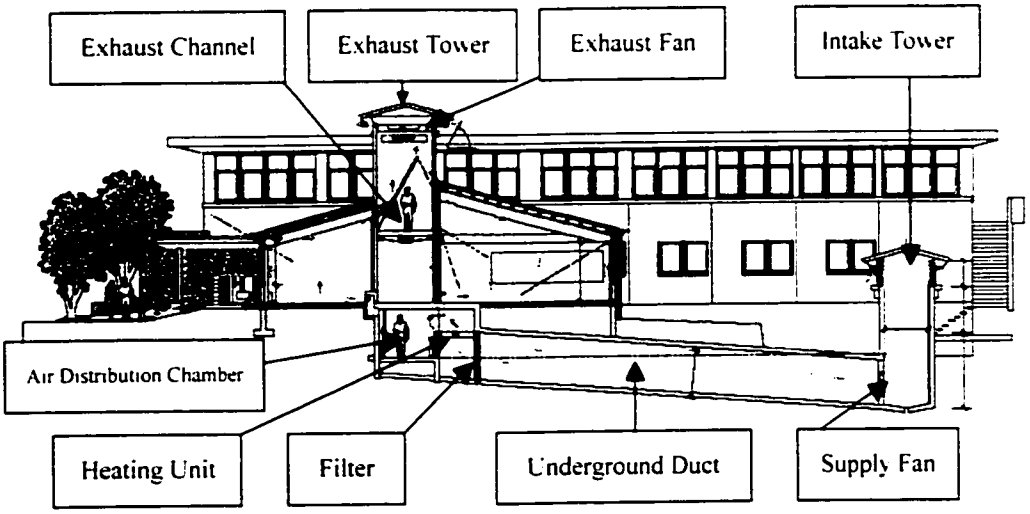

Figure 2.4 Ventilation concept of the Grong school

Before entering the classrooms, the air is filtered and warmed by the heat recovery system and an additional heating element, if required. In wintertime, the underground

duct also serves as a preheating chamber, using heat from the earth to warm cold incoming air. Similarly, it also cools the warm air in the summer.

The ventilation airflow path through the building is sized to allow for velocities up to around *1 m/s*. Therefore, components like filter and heat exchanger unit are much larger than those used for regular mechanical ventilation systems. To overcome the total pressure drop, frequency-controlled fans are installed at the ventilation intake side and at the outlet. Both fans are expected to run when a large airflow rate is needed, for example for free cooling in summer. In a typical winter scenario, only the supply-side fan is expected to run, and at partial speed.

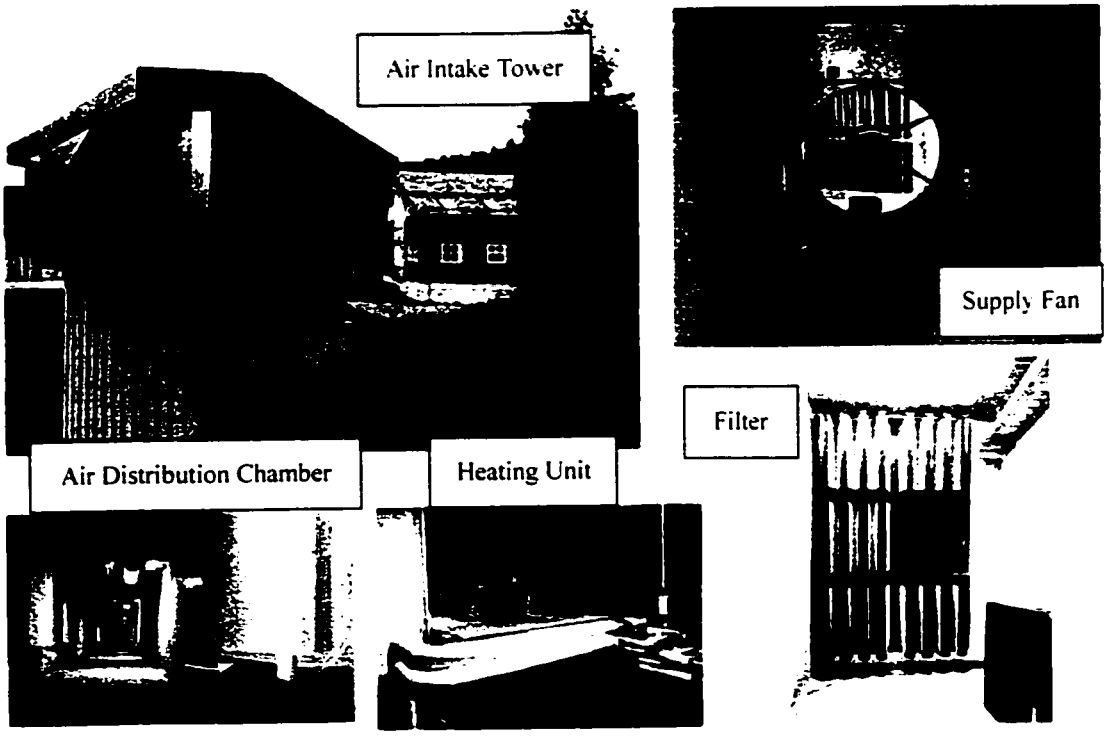

Figure 2.5 Air supply parts of the building

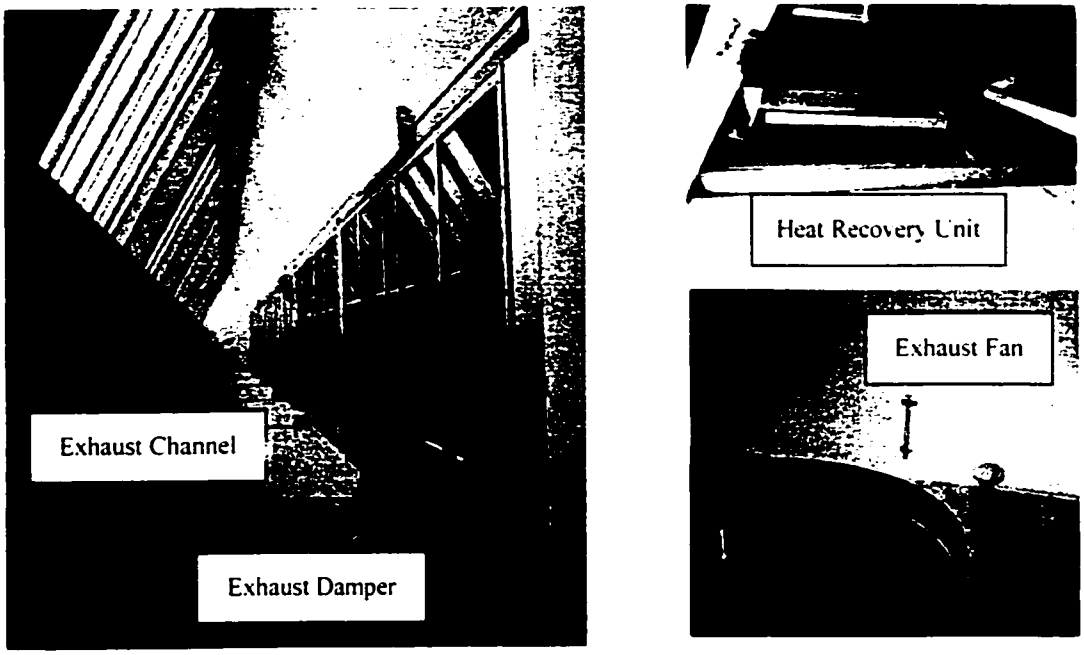

Figure 2.6 Air exhaust parts of the building

The exhaust channel is connected to a centrally located exhaust tower, where the heat recovery system is installed. The heat recovery system exchanges heat from the air leaving the exhaust channel with incoming fresh air, through the water circulation system with an expected efficiency of *55 ~ 60 %*. Solar energy entering the exhaust channel through the glazed roof will add useful heat to the heat recovery system during spring and autumn, and will also increase the buoyancy-driven forces.

2.3 Control strategies

The fresh air supply to the classroom is individually controlled by CO_2 and temperature sensors. The ventilation system is designed to supply an airflow rate which provides just the set air quality or temperature level in the room. When the building is unoccupied the

ventilation airflow rate is low. In this case, the system works only in natural ventilation mode, which gives a continuous and low airflow rate to remove contaminants.

As people enter a room, they generate heat and CO_2. After some time, CO_2 sensor detects high CO_2 level. The CO_2 sensor is connected to BEMS (Building Energy Management System). When the CO_2 concentration reaches a pre-set level, the BEMS signals the exhaust air damper (exhaust vent) of the room to open one step at a time. If the damper is fully opened, and the CO_2 level at the sensor is still too high, the BEMS signals the fans to increase the speed.

The supply and exhaust fans are controlled to each other to ensure that rooms are not pressurized too much. In addition, the supply fan is controlled so that the pressure difference between the underground culvert and exhaust channel is kept to a certain range (e.g. $\Delta P = 20 \sim 25$ Pa). A similar strategy, as used for CO_2 control, is also used for temperature control. The allowed maximum level of CO_2 is set to *660 ppm* above outdoors; i.e. the absolute level of CO_2 should not exceed *1,000 ppm*. The supply air is heated to about *19 °C* by a heating coil unit. The heating power released from the heating unit is controlled based on the air temperature at the outlet of the heating unit.

Radiators are installed below the windows to eliminate heat transmission loss through the building envelope and avoid down draft, releasing sufficient amount of heat. The water temperature to the radiators is set according to the outdoor temperature. The flow through

the radiator is pre-set. Each radiator is equipped with a thermostatic valve and its design set temperature is *22 °C* at *0.8 m* above the floor.

Additional rooms like locker rooms and restrooms have separate exhaust system. Air is allowed to flow through designated openings from occupied areas to those rooms and exhausted by local exhaust fans.

CHAPTER 3

ESP-r

3.1 Overview

ESP-r stands for *Environmental Systems Performance (r for "research")*. This is a transient energy simulation program, which is capable of modeling the energy and fluid flows within combined building and plant systems. This is based on a finite volume and conservation (for energy, mass, momentum, etc.) approach. In this approach, a problem is transformed into a set of conservation equations that are then integrated at successive time-steps in response to climate, occupant and control system.

ESP-r system has been evolved to its present form over more than two decades. From 1974 to 1977 Joe Clarke developed the initial prototype as part of his doctoral research. Then, over the period 1977 to 1988, ESP-r was refined in a number of respects: the system was reorganized and documented; validation trails commenced; multi-zone processing was implemented and a graphics-orientated user interface was established. From 1981 through 1986, ESP-r's capabilities were extended by the addition of dynamic plant simulation, the inclusion of building airflow modeling, a move to low cost Unix workstation technology and the installation of expert system primitives. In 1987, the Energy Simulation Research Unit (ESRU) was formed to address the problems confronting the further evolution of building energy and environmental simulation. After then, more advanced modeling approaches have been incorporated and the scope has been broadened to embrace the simulation of non-energy domains. [ESRU 1997]

3.2 Structure of ESP-r

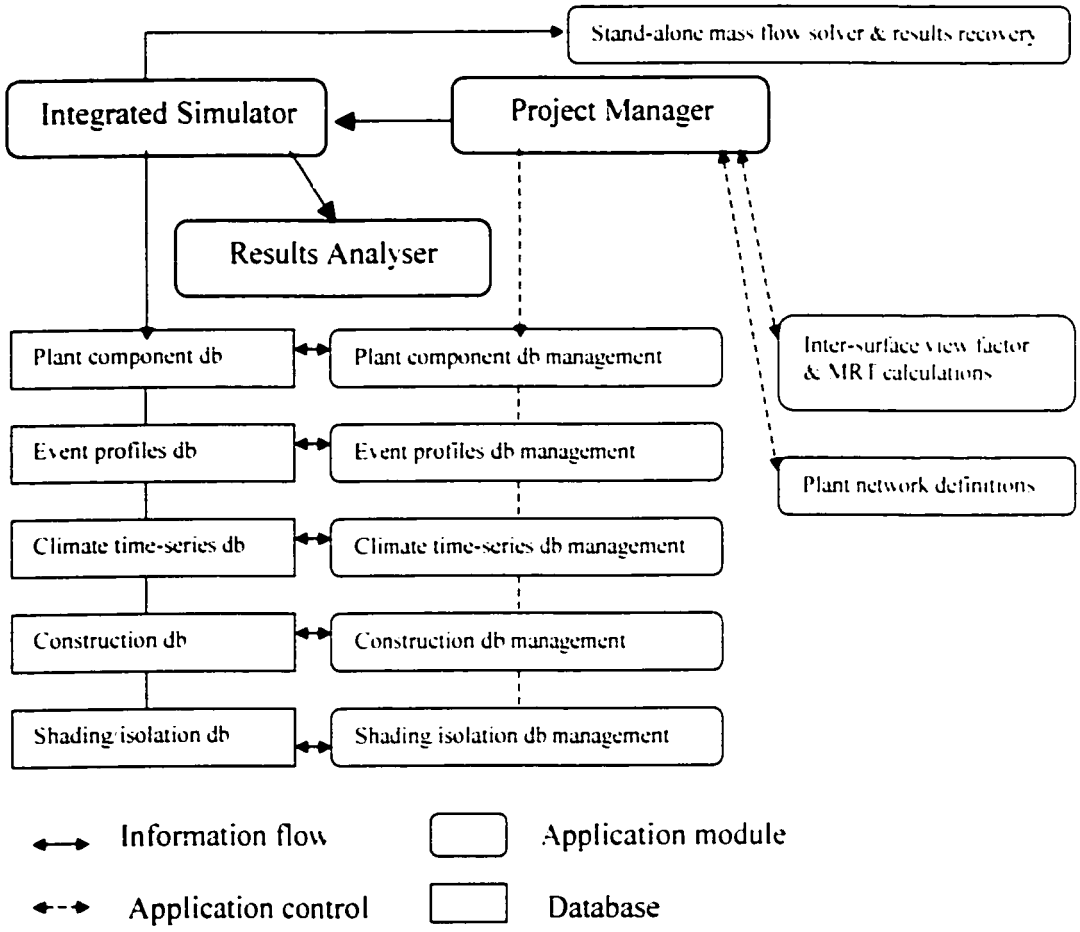

Figure 3.1 Main Structure of ESP-r

The ESP-r package comprises a number of interrelating program modules addressing project management, simulation, results recovery and display, database management and report writing. The simulation module predicts energy and fluid flows of building and plants by a rigorous numerical method. The building or plant network is divided into a large number of finite volumes. Then at each time-step as a simulation proceeds, an energy and mass balance are applied for all volumes, giving rise to a differential matrix

for the entire system. This is then solved by custom matrix processing software in terms of any user-imposed control objectives. Figure 3.1 shows a schematic diagram of ESP-r's main structure.

A number of ESP-r modules create and / or manipulate random access, binary disk files such as the constructions databases, the event profiles databases, and the simulation results database. In normal use, the three main modules, *Project Manager*, *Simulator* and *Results Analyzer*, are used to investigate building and / or plant performance and, by iteration, to assess the sequences of any change to system design or control. Shown in Figure 3.2 are montages of ESP-r's three main modules.

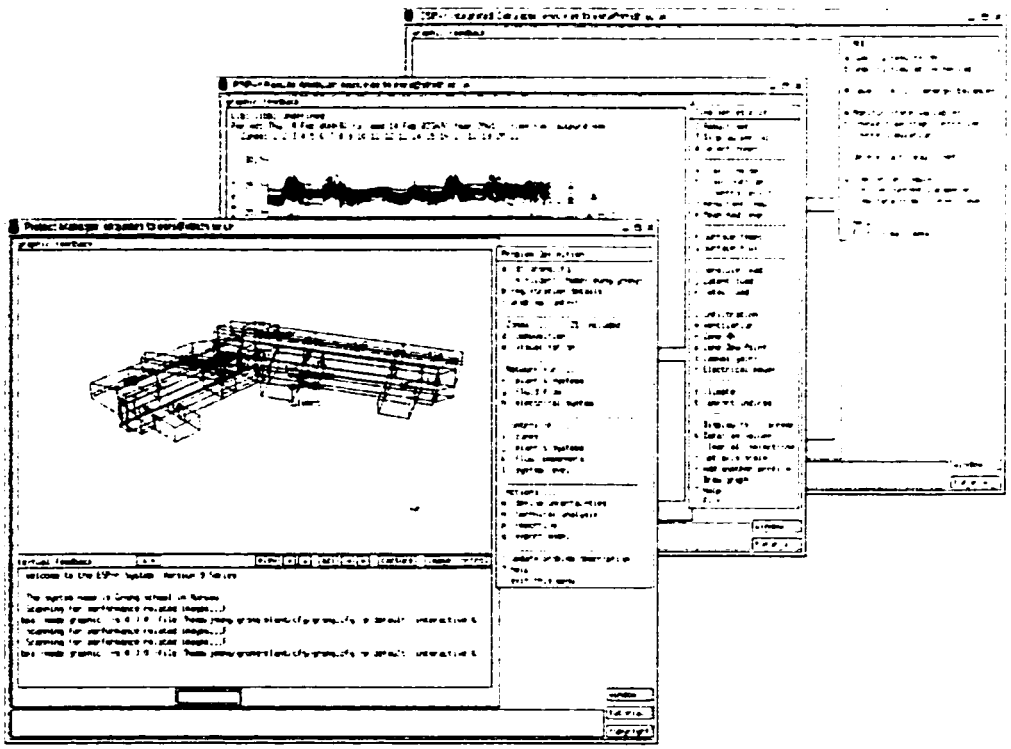

Figure 3.2 Montages of ESP-r's three main modules (Project manager, Result analyzer, and Simulator)

For more detailed information regarding ESP-r's structure, the reader is referred to ESRU (1997). Also, the theories employed by ESP-r to represent heat transfer, fluid flow, plant modeling, and the numerical techniques used to achieve equation integration, are detailed elsewhere (e.g. Clarke 1985, Hensen 1991, Aasem 1993, Beausoleil-Morrison 2000). What follows is some literature review of the basic theories used in ESP-r.

3.3 Thermal model

ESP-r considers a building and its plant as a collection of small finite volumes. These finite volumes represent the various regions of the building and / or plant between which energy and mass can flow. To say, they possess uniform properties that can vary over time, and represent homogeneous and mixed material regions associated with room air, room surface and constructional elements. Then, for each finite volume and at computational time-step, energy and mass conservation equations are generated and passed to a central numerical solver where the equations representing the entire problem are integrated in an essentially simultaneous manner. The coefficients of these equations are developed as a function of the various heat transfers associated with shortwave and longwave radiation, surface convection, casual gains, air leakage behavior and so on.

3.3.1 Heat balance for intra-constructional nodes

As do most simulation programs, ESP-r treats heat transfer through the opaque fabric as a one dimensional conduction only problem with constant thermo-physical properties. By this common approach, each homogenous layer is represented by three nodes (one at each

layer boundary and one within the layer) Figure 3.3 illustrates an intra-constructional node located within a homogeneous material layer.

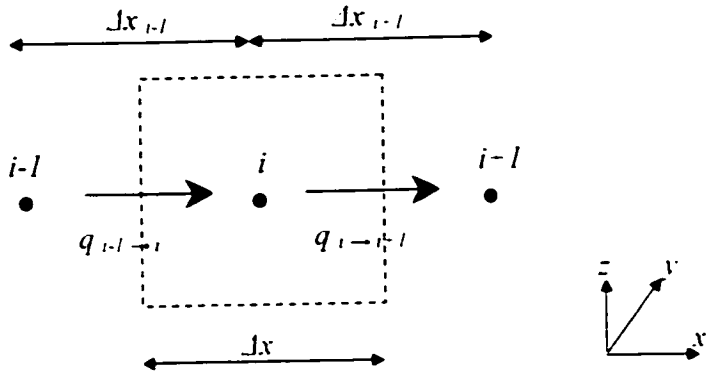

Figure 3.3 Heat balance on a node within homogeneous layer of multi-layer construction

i represents the node under consideration (e.g. insulation part of an exterior wall) while *i-1* and *i-1* represent the immediate neighbors (e.g. *i-1*: gypsum board part, *i-1*: sheathing part of an exterior wall) in *x* direction (the direction of heat flow). The control volume enclosing node *i* is Δx wide and extends Δz in the vertical direction and Δy in the direction perpendicular to the page.

The heat balance for node *i*'s control volume (CV) can be described with three terms:

{storage of heat in CV} = {net conduction into CV} - {source of heat within CV} (3.1)

The storage term represents the rate of change of the control volume's temperature, and the source term represents interaction with a plant component. Given this, the balance of equation 3.1 is expressed in mathematical terms by:

$$\rho c_p \frac{\partial T}{\partial t} = -\frac{\partial q''_x}{\partial x} + q'''_{plant} \qquad (3.2)$$

where c_p is the specific heat $\{J\,kg\,K\}$ and ρ the density $\{kg\,m^3\}$ of the material. T is temperature $\{°C\ or\ K\}$. t is time $\{s\}$. q''_x is the conductive heat flux in the x-direction $\{W\,m^2\}$, and q'''_{plant} is the heat injection from the embedded plant component $\{W\,m^3\}$.

When integrating Equation 3.2 over the control volume ΔV:

$$\int_{\Delta V} \rho c_p \frac{\partial T}{\partial t} dV = -\int_{\Delta V} \frac{\partial q''_x}{\partial x} dV + \int_{\Delta V} q'''_{plant} dV \qquad (3.3)$$

and by representing the first derivative of temperature in time term with a backwards difference scheme over the finite time-step:

$$(\rho c_p \Delta x \Delta y \Delta z)_i \frac{T_i^{t+\Delta t} - T_i^t}{\Delta t} = q_{i-1\to i} - q_{i\to i+1} + q_{plant} \qquad (3.4)$$

T_i^t is the temperature of node i at the beginning of the time-step and $T_i^{t+\Delta t}$ at the end of the time-step. Time t is known as the present time-row and time $t+\Delta t$ as the future time-row.

$q_{i-1\to i}$ and $q_{i\to i-1}$ are the conductive heat flows across the faces of the control volume $\{W\}$. The explicit forms of the $q_{i-1\to i}$ and $q_{i\to i-1}$ when present time-row temperatures are used, are given by:

$$q_{i-1\to i} = \frac{k_{i-1}\Delta y \Delta z}{\Delta x_{i-1}}(T_{i-1}^t - T_i^t) \qquad q_{i\to i+1} = \frac{k_{i+1}\Delta y \Delta z}{\Delta x_{i+1}}(T_i^t - T_{i+1}^t) \qquad (3.5),\ (3.6)$$

where k_{i-1} is the thermal conductivity $\{W/mK\}$ of the material between nodes i and $i-1$, and k_{i+1} is the thermal conductivity $\{W/mK\}$ of the material between nodes i and $i+1$.

Substituting equations 3.5 and 3.6 into equation 3.4 and expressing the plant injection at

the present time-row gives rise to the fully explicit form of the heat balance:

$$\frac{(\rho c_p \Delta x \Delta y \Delta z)_i}{\Delta t}(T_i^{t+\Delta t} - T_i^t) = \frac{k_{i-1}\Delta y \Delta z}{\Delta x_{i-1}}(T_{i-1}^t - T_i^t) - \frac{k_{i-1}\Delta y \Delta z}{\Delta x_{i-1}}(T_i^t - T_{i-1}^t) + q_{plant}^t \qquad (3.7)$$

If the conductive heat flows and the plant terms are approximated using future (rather than present) values. the fully implicit form of the heat balance results:

$$\frac{(\rho c_p \Delta x \Delta y \Delta z)_i}{\Delta t}(T_i^{t+\Delta t} - T_i^t) = \frac{k_{i-1}\Delta y \Delta z}{\Delta x_{i-1}}(T_{i-1}^{t+\Delta t} - T_i^{t+\Delta t}) - \frac{k_{i-1}\Delta y \Delta z}{\Delta x_{i-1}}(T_i^{t+\Delta t} - T_{i-1}^{t+\Delta t}) + q_{plant}^{t+\Delta t} \qquad (3.8)$$

According to Beausoleil-Morrison (2000). ESP-r approximates the heat balance with an equally weighted average of the explicit and implicit relations. (This is known as the Crank-Nicolson difference formulation. and is preferred over the fully explicit and fully implicit schemes for its numerical stability.) Thus. adding equation 3.7 and 3.8. dividing through by volume ($\Delta x \Delta y \Delta z$). and grouping the future time-row terms on the left and the present time-row terms on the right gives:

$$\begin{aligned}
&\left[\frac{2\cdot(\rho c_p)_i}{\Delta t} + \frac{k_{i-1}}{\Delta x \Delta x_{i-1}} + \frac{k_{i+1}}{\Delta x \Delta x_{i-1}}\right]T_i^{t+\Delta t} - \left[\frac{k_{i-1}}{\Delta x \Delta x_{i-1}}\right]T_{i-1}^{t+\Delta t} - \left[\frac{k_{i+1}}{\Delta x \Delta x_{i-1}}\right]T_{i+1}^{t+\Delta t} - \left[\frac{q_{plant}^{t+\Delta t}}{\Delta x \Delta y \Delta z}\right] \\
&= \left[\frac{2\cdot(\rho c_p)_i}{\Delta t} - \frac{k_{i-1}}{\Delta x \Delta x_{i-1}} - \frac{k_{i+1}}{\Delta x \Delta x_{i-1}}\right]T_i^t + \left[\frac{k_{i-1}}{\Delta x \Delta x_{i-1}}\right]T_{i-1}^t + \left[\frac{k_{i+1}}{\Delta x \Delta x_{i-1}}\right]T_{i+1}^t + \left[\frac{q_{plant}^t}{\Delta x \Delta y \Delta z}\right]
\end{aligned} \qquad (3.9)$$

This is the basic equation ESP-r employs to characterize the heat balance for nodes located within homogeneous material layers of opaque multi-layered constructions.

3.3.2 Heat balance for internal surface nodes

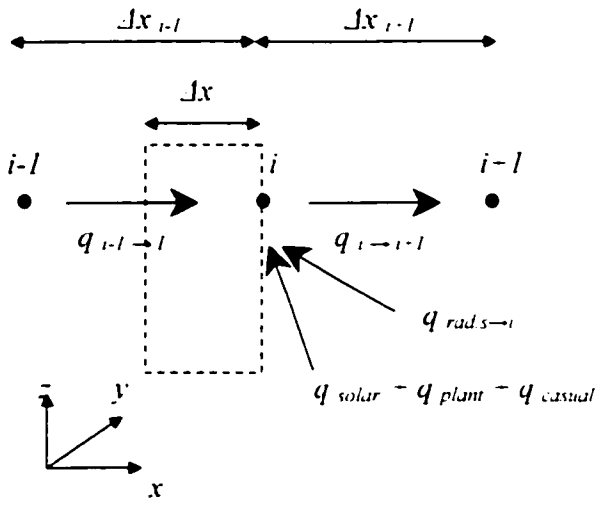

Figure 3.4 Heat balance on a node at internal surface

Here, the control-volume heat-transfer approach focuses on the nodes located at internal surfaces. Figure 3.4 shows a node (i) located on the internal surface of a construction. The left face of the control volume is located between nodes i and i-1. However, the right face is located at the interface of the solid construction and the room air. The neighboring node to the right ($i+1$) represents the room's air point. The heat balance for the control volume of node i is:

{storage of heat in CV} = {net conduction into CV} + {source of heat within CV} + {net longwave radiation into CV} + {net convection into CV} (3.10)

Since conduction into the control volume occurs only at the boundary with the next-to-surface node i-1, the explicit form of the conduction is:

$$\{net\ conduction\ into\ CV\} = q_{i-1\to i} = \frac{k_{i-1}\Delta y\Delta z}{\Delta x_{i-1}}(T^t_{i-1} - T^t_i) \qquad (3.11)$$

and the explicit form of the source term is given by:

$$\{source\ of\ heat\ within\ CV\} = q^{t}_{solar,i} + q^{t}_{cas\text{-}rad,i} + q^{t}_{plant,i} \qquad (3.12)$$

where $q^{t}_{solar,i}$ is the solar radiation absorbed at node i at the present time. $q^{t}_{cas\text{-}rad,i}$ represents the radiant energy absorbed from casual sources such as occupants, lights, office equipment. $q^{t}_{plant,i}$ represents a radiant plant input to node i, perhaps from a radiant heater located within the room.

The longwave radiation term represents the net heat exchange with surrounding surfaces that are in longwave contact (i.e. other internal surfaces of the room) and its explicit form is given by:

$$\{net\ longwave\ radiation\ into\ CV\} = q^{t}_{rad,\rightarrow i} = \sum_{s=1}^{N} h^{t}_{r,s\rightarrow i}\,\Delta y\Delta z(T^{t}_{s} - T^{t}_{i}) \qquad (3.13)$$

where N is the number of surrounding surfaces in longwave contact. $h^{t}_{r,s\rightarrow i}$ is a linearized radiation heat transfer coefficient $\{W/m^2K\}$. These coefficients are recalculated each time-step on a surface-by-surface basis.

The convection term represents heat exchange between the room air and the solid surface, and is modeled using the well-stirred assumption. The explicit form of the convection term is given by:

$$\{net\ convection\ into\ CV\} = q^{t}_{i\rightarrow i+1} = h^{t}_{c,i}\,\Delta y\Delta z(T^{t}_{i+1} - T^{t}_{i}) \qquad (3.14)$$

where $h^{t}_{c,i}$ is the convection heat transfer coefficient $\{W/m^2K\}$ between the surface at

node *i* and the room-air-point, evaluated at the present time low.

Substituting equation 3.11 through 3.14 into 3.10 and representing the storage term with a backward difference scheme, leads to the explicit form of the heat balance. The implicit form of the heat balance results when all terms are evaluated with future values. Concatenating these, dividing through by volume, and rearrangement of the various terms into temperature related coefficients lead to the generalized form of the internal-surface balance. The resultant equation is:

$$\left[\frac{2\cdot(\rho c_p)_i}{\Delta t}+\frac{k_{i-1}}{\Delta x\Delta x_{i-1}}+\frac{h_{c,i}^{t+\Delta t}}{\Delta x}+\frac{\sum_{s=1}^{s} h_{r,s\to i}^{t+\Delta t}}{\Delta x}\right]T_i^{t+\Delta t}-\left[\frac{k_{i-1}}{\Delta x\Delta x_{i-1}}\right]T_{i-1}^{t+\Delta t}-\left[\frac{h_{c,i}^{t+\Delta t}}{\Delta x}\right]T_{i+1}^{t+\Delta t}$$
$$-\frac{\sum_{s=1}^{s} h_{r,s\to i}^{t+\Delta t}}{\Delta x}T_s^{t+\Delta t}-\left[\frac{q_{solar,i}^{t+\Delta t}}{\Delta x\Delta y\Delta z}\right]-\left[\frac{q_{con-rad,i}^{t+\Delta t}}{\Delta x\Delta y\Delta z}\right]-\left[\frac{q_{plant,i}^{t+\Delta t}}{\Delta x\Delta y\Delta z}\right] \qquad (3.15)$$
$$=\left[\frac{2\cdot(\rho c_p)_i}{\Delta t}-\frac{k_{i-1}}{\Delta x\Delta x_{i-1}}-\frac{h_{c,i}^{t}}{\Delta x}-\frac{\sum_{s=1}^{s} h_{r,s\to i}^{t}}{\Delta x}\right]T_i^{t}+\left[\frac{k_{i-1}}{\Delta x\Delta x_{i-1}}\right]T_{i-1}^{t}+\left[\frac{h_{c,i}^{t}}{\Delta x}\right]T_{i+1}^{t}$$
$$+\frac{\sum_{s=1}^{s} h_{r,s\to i}^{t}}{\Delta x}T_s^{t}+\left[\frac{q_{solar,i}^{t}}{\Delta x\Delta y\Delta z}\right]+\left[\frac{q_{con-rad,i}^{t}}{\Delta x\Delta y\Delta z}\right]+\left[\frac{q_{plant,i}^{t}}{\Delta x\Delta y\Delta z}\right]$$

3.3.3 Heat balance for air-point nodes

Figure 3.5 focuses on a node representing the air-point of a zone. In this case, node *i* represents the air-point and the nodes labeled *s* represent the surface nodes of the bounding constructions. Node *j* represents the air-point of another zone while node *o* represents the outdoor air. Consistent with the well-stirred assumption the room air is treated as uniform.

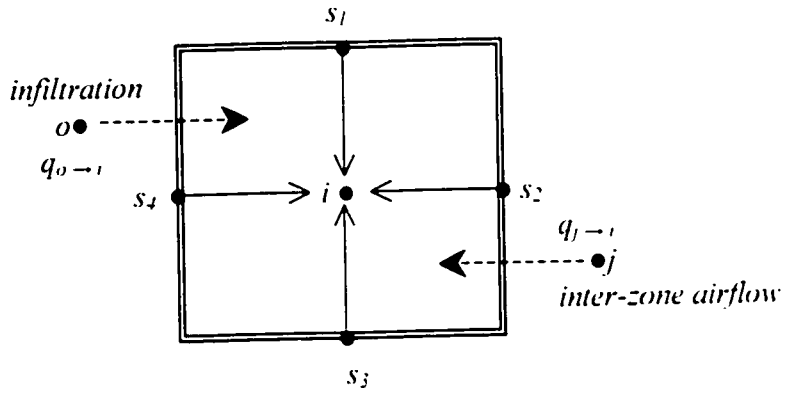

Figure 3.5 Heat balance on an air-point node

The heat balance for the air-point node must consider: bulk air flow from adjacent zones and the outdoors, surface convection at the building fabric components, and convective sources of heat:

{storage of heat in CV} ={net convection into CV} + {advection into CV by inter-zone airflow} + {advection into CV by infiltration} + {source of heat within CV} (3.16)

The convection term represents the total heat transfer from all bounding surfaces (wall,

roof, floor, windows, etc) to the room air, and is given in the explicit form by:

$$\{net\ convection\ into\ CV\} = \sum_{s=1}^{N} h'_{c,s} A_s (T'_s - T'_i) \qquad (3.17)$$

where N is the number of bounding surfaces. A_s is the area $\{m^2\}$, and $h'_{c,s}$ the present time-low convective heat transfer coefficient for surface s.

The advection terms represent the thermal energy carried by air flowing into the control volume from other zones or from the outdoors. The terms are given in the explicit form by:

$$\{advection\ into\ CV\ by\ inter-zone\ airflow\} = \sum_{j=1}^{M} \dot{m}'_{j\to i} C_p (T'_j - T'_i) \qquad (3.18)$$

$$\{advection\ into\ CV\ by\ infiltration\} = \dot{m}'_{o\to i} C_p (T'_o - T'_i) \qquad (3.19)$$

where M is the number of zones supplying air to the control volume. $\dot{m}'_{j\to i}$ is the air flow from zone j to zone i $\{kg/s\}$ at the present time-row and $\dot{m}'_{o\to i}$ is the infiltration rate $\{kg/s\}$ from the outdoors for the present time-low. T'_j and T'_o are the present time-row temperatures of the air-point in zone j and the outdoor air, respectively.

There are various techniques for establishing $\dot{m}'_{j\to i}$ and $\dot{m}'_{o\to i}$. The most general approach is to employ a network airflow model to calculate the infiltration and inter-zone air flows in response to prevailing weather conditions and thermal states within the building. This will be described in Section 3.4.

The source term can be given in discretized explicit form by:

$$\{source\ of\ heat\ within\ CV\} = q^{t}_{cas\text{-}conv,i} + q^{t}_{plant,i} \tag{3.20}$$

where $q^{t}_{cas\text{-}conv,i}$ is the heat transferred convectively from casual sources (such as occupants, lights, office equipment) at the present time. $q^{t}_{plant,i}$ represents a convective plant input to node i at the present time, perhaps from a convective heater located within the room.

When the explicit and implicit forms of the heat balance are added, the equation divided by the volume (VOL_{room}), and the future time-row terms gathered on the left and present time-row terms on the right, the following heat balance for room air-point nodes results:

$$\begin{aligned}
&\left[\frac{2\cdot(\rho c_p)_i}{\Delta t} + \frac{\sum_{s=1}^{N} h^{t+\Delta t}_{c,s} A_s}{VOL_{room}} + \frac{\sum_{j=1}^{M} \dot{m}^{t+\Delta t}_{j\to i} c_p}{VOL_{room}} + \frac{\dot{m}^{t+\Delta t}_{o\to i} c_p}{VOL_{room}}\right] T_i^{t+\Delta t} - \left[\frac{\sum_{s=1}^{N} h^{t+\Delta t}_{c,s} A_s}{VOL_{room}}\right] T_s^{t+\Delta t} \\
&- \left[\frac{\sum_{j=1}^{M} \dot{m}^{t+\Delta t}_{j\to i} c_p}{VOL_{room}}\right] T_j^{t+\Delta t} - \left[\frac{\dot{m}^{t+\Delta t}_{o\to i} c_p}{VOL_{room}}\right] T_o^{t+\Delta t} - \left[\frac{q^{t+\Delta t}_{cas\text{-}conv,i}}{VOL_{room}}\right] - \left[\frac{q^{t+\Delta t}_{plant,i}}{VOL_{room}}\right] \\
&= \left[\frac{2\cdot(\rho c_p)_i}{\Delta t} - \frac{\sum_{s=1}^{N} h^{t}_{c,s} A_s}{VOL_{room}} - \frac{\sum_{j=1}^{M} \dot{m}^{t}_{j\to i} c_p}{VOL_{room}} - \frac{\dot{m}^{t}_{o\to i} c_p}{VOL_{room}}\right] T_i^{t} + \left[\frac{\sum_{s=1}^{N} h^{t}_{c,s} A_s}{VOL_{room}}\right] T_s^{t} \\
&+ \left[\frac{\sum_{j=1}^{M} \dot{m}^{t}_{j\to i} c_p}{VOL_{room}}\right] T_j^{t} + \left[\frac{\dot{m}^{t}_{o\to i} c_p}{VOL_{room}}\right] T_o^{t} + \left[\frac{q^{t}_{cas\text{-}conv,i}}{VOL_{room}}\right] + \left[\frac{q^{t}_{plant,i}}{VOL_{room}}\right]
\end{aligned} \tag{3.21}$$

3.4 Fluid-flow network

This approach is based on the assumption that a building and / or plant can be considered as being composed of a number of zones or nodes. Nodes represent large air volumes with uniform conditions, and predict flow through discrete paths such as doors and cracks. Although the model presumes one-dimensional steady-flow, boundary conditions can vary in time. The basic elements, thermal zones, describe the geometry and fabric of a building. Overlying these basic modeling elements are networks, which are used to describe fluid flow, HVAC, and moisture flow. In ESP-r, fluid flow networks are composed of three basic constituents (i.e. nodes, connecting components, and inter-nodal connections).

3.4.1 Components

Components are defined to represent leakage paths through the fabric, and pressure drops associated with doors, cracks, ducts, pipes, fans, pumps, and so on. The components relate the airflow rate through a connection to the pressure difference across the connection and can be described by the following expression:

$$\dot{m}_{i,j} = f(P_i, P_j) = f(\Delta P_{i,j}) \qquad (3.22)$$

where $\dot{m}_{i,j}$ is the flow rate $\{kg/s\}$ from node i to node j, P_i is the pressure $\{Pa\}$ at node i, P_j is the pressure $\{Pa\}$ at node j, and $\Delta P_{i,j}$ is the pressure difference $\{Pa\}$ between nodes i and j. Currently supported fluid flow component types are summarized as follows.

3.4.1.1 Power law flow component

These types of flow component use one of the following relationships between flow and pressure difference across the component:

$$\dot{m} = \rho\, a\, (\Delta P)^b, \qquad \dot{m} = a\, (\Delta P)^b, \qquad \dot{m} = a \sqrt{\rho}\, (\Delta P)^b \qquad (3.23),\ (3.24),\ (3.25)$$

where $\dot{m}$ is the fluid mass flow rate through the component $\{kg/s\}$, a is a flow coefficient, expressed in $\{m^3/s \cdot Pa^b\}$, $\{kg/s \cdot Pa^b\}$, or $\{(kg \cdot m^3)^{1/2}/(s \cdot Pa^b)\}$, respectively. ΔP is the total pressure loss across the component $\{Pa\}$, and b is the flow exponent $\{-\}$. The value of ρ $\{kg/m^3\}$ depends on the type of fluid and on the direction of flow. (i.e. it is evaluated with the temperature of the sending node.) Theoretically, the value of the flow exponent b should lie between 0.5 (for fully turbulent flow) and 1.0 (for laminar flow).

3.4.1.2 Quadratic law flow component

In this type of component, airflow through a building opening is described by a quadratic relationship between pressure difference across the component and flow rate. The flow equation is divided in a laminar and a turbulent part and expressed in one of the following equations:

$$\Delta P = a \frac{\dot{m}}{\rho} + b \left(\frac{\dot{m}}{\rho} \right)^2, \qquad \Delta P = a\, \dot{m} + b\, \dot{m}^2 \qquad (3.26),\ (3.27)$$

where $\dot{m}$ is the fluid mass flow rate through the component $\{kg/s\}$, a is a flow coefficient, expressed in $\{Pa / (m^3/s)\}$ or $\{Pa / (kg/s)\}$, respectively. ΔP is the total pressure loss across the component $\{Pa\}$, and b is a flow coefficient, expressed in $\{Pa / (m^3/s)^2\}$ or $\{Pa / (kg/s)^2\}$, respectively. ρ is the fluid density $\{kg/m^3\}$ depending on the type of fluid and on the direction of flow.

3.4.1.3 Constant flow rate component

Constant flow rate component uses one of the following relationships:

$$\dot{m} = \rho\, a, \qquad \dot{m} = a \qquad (3.28),\ (3.29)$$

where $\dot{m}$ is the fluid mass flow rate through the component $\{kg/s\}$, a is a constant defining the flow rate in $\{m^3/s\}$ or $\{kg/s\}$, respectively, ρ is the fluid density $\{kg/m^3\}$ depending on the type of fluid and on the direction of flow.

3.4.1.4 Common orifice flow component

Common orifice flow equation is a basic expression for turbulent flow through relatively large openings (e.g. a purposely provided vent). If expressed as mass flow rate, this is given by:

$$\dot{m} = C_d A \sqrt{2\,\rho\,\Delta p} \qquad (3.30)$$

where $\dot{m}$ is the fluid mass flow rate through the component $\{kg/s\}$, C_d is the discharge factor $\{-\}$, and A is opening area $\{m^2\}$, ρ is the fluid density $\{kg/m^3\}$, and ΔP is the total pressure loss across the component $\{Pa\}$.

3.4.1.5 Laminar pipe flow component

This is for laminar flow through openings with relatively long flow paths (e.g. a narrow crack in the building fabric).

$$\dot{m} = \frac{\rho \Delta P \pi r^4}{8 \mu L} \qquad (3.31)$$

where $\dot{m}$ is the fluid mass flow rate through the component $\{kg/s\}$, ρ is the fluid density $\{kg/m^3\}$, ΔP is the total pressure loss across the component $\{Pa\}$, r is the radius of opening $\{m\}$, L is the length of the flow path $\{m\}$, and μ is the fluid dynamic viscosity $\{kg/m \cdot s\}$. Both the fluid density ρ and the dynamic viscosity μ depend on the type of fluid flow and on the temperature of the sending node.

3.4.1.6 Specific airflow components

(1) Specific airflow opening component

This component is actually identical to the orifice flow component with fluid type set to air and with discharge factor C_d equal to 0.65.

(2) Specific airflow crack component

For this component, the relation between mass flow rate and pressure difference is given by:

$$\dot{m} = \rho \, k \, \Delta P^x \qquad (3.32)$$

where $\dot{m}$ is the fluid mass flow rate through the component $\{kg/s\}$, ρ is the fluid density $\{kg/m^3\}$, ΔP is the total pressure loss across the component $\{Pa\}$, and

$x = 0.5 + 0.5 \exp(-500 W)$ $\{-\}$,

$k = L9.7 (0.0092)^x / 1000$ $\{m^3/s. Pa^x\}$

where W is the crack width $\{m\}$, and L is the crack length $\{m\}$.

(3) Specific airflow door component

With large vertical openings such as doorways, it is unlikely that unidirectional flow can be assumed. If a temperature difference exists across such an opening, airflow can occur in both directions due to the action of small density variations over the door height. For this type of connection the following expression is used:

$$\dot{m} = \rho (2/3)[C_d W H (2/\rho)^{1/2} (C_a^{3/2} - C_b^{3/2})/C_t] \qquad (3.33)$$

where

$C_a = (1 - r_p) C_t + (P_n - P_m)$ {Pa}.

$C_b = (P_n - P_m) - r_p C_t$ {Pa}.

$C_t = g P_o H / R (1/\Theta_m - 1/\Theta_n)$ {Pa}.

and C_d is the discharge factor {-}, W is the opening width {m}, H is the opening height {m}, $r_p = H_r/H$ {-}, g is the acceleration due to gravity ($=9.81\ m\ s^{-2}$), P_o is the atmospheric pressure ($=101325\ Pa$), R is the gas constant for dry air ($=287.1\ J/kg{\cdot}K$), Θ_m and Θ_n are temperatures at node m and n {K}, and H_r is the node reference height above base of doorway {m}.

3.4.1.7 General flow conduit component

For fluid flow through a conduit (i.e. a duct or pipe) with uniform cross-sectional area, no pressure gain due to fan or pump, and steady state conditions, the sum of all friction and dynamic losses {Pa} is found from:

$$\Delta P = f L \rho \bar{v}^2 / 2D_h + \sum C_r \rho \bar{v}^2 / 2 \qquad (3.34)$$

where ΔP is the sum of all losses {Pa}, f is the friction factor {-}, L is the conduit length

$\{m\}$, D_h is the hydraulic diameter (=4 * *cross-sectional area / perimeter of the cross-section*) $\{m\}$, $\bar{v}$ is the average velocity $\{m\ s\}$, and C_i is the local loss factor due to fitting i $\{-\}$.

The friction factor in the first term in the equation above depends on the type of flow, which can be characterized by the Reynolds-number. The local loss factor in the second term in the equation above represents dynamic losses resulting from disturbances caused by fittings. The mass flow rate, $\dot{m}$ $\{kg\ s\}$, through a conduit can now be calculated from a known pressure difference by:

$$\dot{m} = A\sqrt{\frac{2\rho\Delta p}{f\,L/D + \Sigma C_i}} \qquad (3.35)$$

3.4.1.8 Conduit and junction with flow ratio dependent dynamic losses

As do all other fittings, flow junctions (tees, wyes, crosses, etc) cause frictional and dynamic losses. Actually, dynamic losses occur along a duct / pipe length and cannot be separated from frictional losses. For ease of calculations however, dynamic losses are assumed to be concentrated at a section (local) and to exclude friction. The most common technique of describing local dynamic losses for junctions is by equations of the form:

$$\Delta P_{t,p} = C_{c,p}\rho\bar{v}_c^2/2 \qquad (3.36)$$

where $\Delta P_{t,p}$ represents the total pressure losses through section p of the junction $\{Pa\}$, and $C_{c,p}$ is the dimensionless local loss factor for part p of the junction referenced to the velocity pressure at section c of the junction (usually this is a function of q_p/q_c (v_p/v_c)).

Subscript c indicates the common flow path, and subscript p indicates either straight or branch flow path. Values for $C_{c,p}$ can be found in several handbooks (e.g. ASHRAE 1997). ESP-r derives each flow path's local loss coefficient by curve fitting on data encountered in literature or found from experiments.

3.4.2 Nodes

Node represents a volume of air or liquid which is internal (with a known pressure or pressure to be solved) or a boundary condition (with a known pressure or wind induced pressure). Nodes are given a specific temperature or can inherit the temperature of a zone as a simulation proceeds. The nodes are connected together by the components to form the flow network.

The mass balances written for each node relate the flow rates through the connections associated with that node. As mass is conserved and a steady-state solution is sought at each time-step, the sum of the mass flows to a node must equal zero:

$$\sum_{j=1}^{n} \dot{m}_{i,j} = 0 \qquad (3.37)$$

where n is the number of nodes connected to node i. Substituting the flow components relations into above equation gives the following form for the nodal mass balance:

$$\sum_{j=1}^{n} f(\Delta P_{i,j}) = 0 \qquad (3.38)$$

Evaluating the above equation for each node gives rise to a set of non-linear equations. ESP-r solves the equations using a trial–and-error iterative procedure. The iterative

approach for correcting the pressure estimates is based on a Newton-Raphson technique.

Wind induced boundary nodes essentially represent wind impinging upon a surface. This pressure is a function of the wind velocity, direction, surrounding terrain, building height and surface orientation:

$$P_i = \frac{1}{2} C_p \rho V^2 \qquad (3.39)$$

The orientation of the surface in relation to wind direction is expressed in terms of a pressure coefficient *Cp*. Determination of *Cp* can be obtained from wind tunnel model tests of the specific site and building. It varies according to wind direction and position of the building surface. For low-rise buildings, up to three stories, pressure coefficients may be expressed as an average value for each face of the building and for each compass direction. ESP-r has a database of *Cp* coefficients for different types and orientations of surfaces, which is based on published measurement results by Liddament (1986).

Also, the wind speed reduction factor, the ratio of the wind speed in the locality of the building to the climate wind speed, is calculated from some assumed wind speed profile. This accounts for any difference between measurement height and building height and for intervening terrain roughness. The wind speed profile depends on upstream terrain roughness and the vertical stability of the boundary layer. However, due to lack of information, in building engineer it is usually assumed that there is no vertical heat flow. Hensen (1991) describes how ESP-r offers several user selectable wind profiles for evaluation of the wind speed reduction factor as follows:

(1) Power low wind profile (Liddament 1986): in this case the casual wind speed profile is approximated by an empirical exponential expression in which the coefficient and exponent account for terrain roughness differences between local site and measurement site:

$$\frac{U_l}{U_{10}} = K z_l^{\alpha} \qquad (3.40)$$

where U_l $\{m/s\}$ is the local wind speed at a height z_l $\{m\}$ above the ground, U_{10} $\{m/s\}$ is the wind speed measured in open countryside at a standard height of 10 m, and K, α are terrain dependant constants.

(2) Logarithmic wind profile (Simiu & Scanlan 1986): it was found – both theoretically and experimentally – that the wind speed is a logarithmic function of height:

$$\frac{U_l}{U_m} = \frac{U_{*,l}}{U_{*,m}}\left[\left(\ln\frac{z_l - d_l}{z_{0,l}}\right)\Big/\left(\ln\frac{z_m - d_m}{z_{0,m}}\right)\right] \quad where \quad \frac{U_{*,l}}{U_{*,m}} \approx \left(\frac{z_{0,l}}{z_{0,m}}\right)^{0.1} \qquad (3.41)$$

U_m $\{m/s\}$ is the wind speed measured at the meteorological site at a height of z_m $\{m\}$ above the ground, U_* $\{m/s\}$ is the atmospheric friction speed, z_0 $\{m\}$ is the terrain dependant roughness length, and d $\{m\}$ is the terrain dependant displacement length.

(3) LBL model wind profile (also reported in Liddament 1986): for reasons of completeness the Lawrence Berkeley Laboratory (LBL) air infiltration model wind profile (basically a power law profile) is also available in ESP-r:

$$\frac{U_l}{U_m} = \frac{\alpha_l (z_l/10)^{\gamma_l}}{\alpha_m (z_m/10)^{\gamma_m}} \qquad (3.42)$$

where α, γ are terrain dependant constants.

3.4.3 Connections

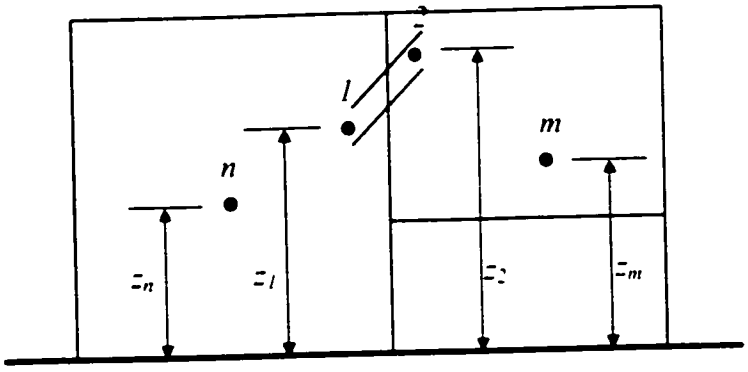

Figure 3.6 Two volume connections

Connections are defined in terms of linking one node to the other node via a component. The height of the connection inlet and outlet relative to the nodes it connects is required for the calculation of stack effect on network flow. This can be well explained with Figure 3.6 which shows two volumes connected by a fluid flow component. It is assumed that each volume can be characterized by a single temperature and a single static pressure at some height relative to a common data plane. Analysis of fluid flow through a component i is based on Bernoulli's equation for one-dimensional steady flow of an incompressible Newtonian fluid including a loss term:

$$\Delta P_i = (p_1 + \frac{1}{2}\rho V_1^2) - (p_2 + \frac{1}{2}\rho V_2^2) + \rho g(z_1 - z_2) \qquad (3.43)$$

where ΔP_i is the sum of all friction and dynamic losses $\{Pa\}$, p_1, p_2 are entry and exit static pressures $\{Pa\}$, V_1, V_2 are entry and exit velocities $\{m/s\}$, ρ is the density of the fluid flowing through the component $\{kg/m^3\}$, g is the acceleration of gravity $\{9.81\ m/s^2\}$, and z_1, z_2 are entry and exit elevations $\{m\}$.

ρ may be either ρ_n or ρ_m depending on the direction of flow. In ESP-r, ρ is based on the most recently computed flow direction. The equation can be simplified for use in the fluid flow algorithm by defining several related terms. Dynamic pressures are the $\frac{1}{2}\rho V^2$ terms, and the total pressure is defined to be the sum of static pressure and dynamic pressure; i.e. $P = p + \frac{1}{2}\rho V^2$. If nodes n and m represent large volumes (e.g. a room), the dynamic pressures are effectively zero. If the nodes represent some point in a duct or pipe network, there will be a positive dynamic pressure. The pressure at the inlet and outlet of the flow component can be related to the node pressures by the hydrostatic law:

$$P_1 = P_n + \rho_n g(z_n - z_1) = P_n - \rho_n g h_1 \qquad where \quad h_1 = z_1 - z_n \quad and$$
$$P_2 = P_m + \rho_m g(z_m - z_2) = P_m - \rho_m g h_2 \qquad where \quad h_2 = z_2 - z_m \qquad (3.44)$$

The relative heights, h_1 and h_2, are a convenient way of expressing the flow component inlet and outlet heights. Using above equations, Bernoulli's equation can be re-written to:

$$\Delta P_i = P_n - P_m + \rho g(z_n + h_1 - z_m - h_2) - \rho_n g h_1 + \rho_m g h_2 \qquad (3.45)$$

The term $[\rho g(z_n+h_1-z_m-h_2)-\rho_n g h_1+\rho_m g h_2]$ is collectively called the stack pressure acting on component i. ρ may be either ρ_n or ρ_m depending on the direction of flow (e.g. for flow in the positive direction $\rho = \rho_n$).

3.5 Plant modeling

In ESP-r, plant system modeling is achieved by a modular, component-wise approach. Each plant component model consists of one or more finite volume, state-space equations, representing the conservation of heat and mass. The plant system is a combination of component models forming a complete set of state-equations for the whole system. [Hensen 1991]

ESP-r's plant network modeling capability allows the calculation of time varying heat and mass transfers associated with HVAC systems. HVAC systems may be modeled in isolation or as part of an integrated building model incorporating other elements such as thermal zones and explicit fluid flow. Plant modeling is used when greater realism in performance is required or where system processes need to be modeled explicitly.

3.5.1 Mass and energy balance in plant modeling

Figure 3.7 shows a part of an imaginary plant consisting of three components / nodes which are linked by plant connections. Component i is linked to one or more other components j, $j+1$, etc from which it receives a mass flow. A mass flow is either a single phase fluid (e.g. water or dry air) or a fluid mixture incorporating two phases simultaneously (e.g. dry air and water vapor mixture). Here, the states represented by the model nodes are: temperature T, first phase mass flow rate $\dot{m}_a$, and second phase mass flow rate $\dot{m}_v$. Component i exchanges heat with the environment e, and there might be generation of heat $\emptyset$. The subscripts refer to: a for air, e for environment, i, j and $j+1$ for the respective components, and v for water vapor.

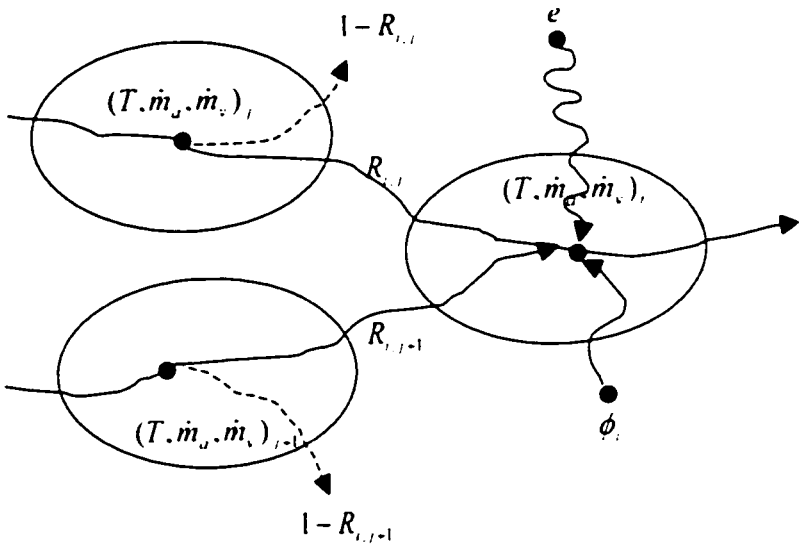

Figure 3.7 Diagrammatic state-space representation of an imaginary plant part

The energy balance $\{W\}$, at any point in time, for node i is:

$$R_{i,j}\dot{m}_{a,j}c_{p,a}(T_j-T_i)+R_{i,j}\dot{m}_{s,j}c_{p,s}(T_j-T_i)+R_{i,j+1}\dot{m}_{a,j+1}c_{p,a}(T_{j+1}-T_i)+R_{i,j+1}\dot{m}_{s,j+1}c_{p,s}(T_{j+1}-T_i)$$
$$+UA(T_e-T_i)+\phi_i=\frac{\bar{c}_i M_i \partial T_i}{\partial t} \qquad (3.46)$$

where $\dot{m}$ is the mass flow rate $\{kg/s\}$, $R_{i,j}$ denotes the ratio between the mass flow rate received by node i and the mass flow rate through node j, c_p is the fluid specific heat $\{J/kg\cdot K\}$, T is the nodal temperature $\{°C\}$, U is the component's total heat loss coefficient $\{W/m^2\cdot K\}$ from node i to the environment and A is corresponding area $\{m^2\}$, Φ_i represents any heat generated and released at node i, c is the component's mass weighted average specific heat $\{J/kg\cdot K\}$, and M is the component's total mass $\{kg\}$. It is assumed that the mass flow diversion ratio R is identical for both mass flow phases.

The mass weighted average of the specific heat of the N component parts is:

$$\bar{c} = \sum_{j=1}^{N} (c_j M_j) / \sum_{j=1}^{N} M_j \qquad (3.47)$$

Equation 3.46 can be solved by numerical approximation, the same method used to solve the building side energy equations. Using the current (known) time step temperature T_i^t, the fully explicit formulation of Equation 3.46 is given by:

$$C_{i,j}^t (T_j^t - T_i^t) + C_{i,j+1}^t (T_{j+1}^t - T_i^t) + UA^t (T_e^t - T_i^t) + \phi_i^t \approx \frac{\bar{c}_i M_i (T_i^{t+\Delta t} - T_i^t)}{\Delta t} \qquad \{W\}$$

$$where \quad C_{i,j}^t = (R_{i,j} \dot{m}_{a,j} c_{p,a} + R_{i,j} \dot{m}_{s,j} c_{p,s}) \ \ at\ current\ time\ step \qquad \{W/K\} \qquad (3.48)$$

If the equation is approximated using future (rather than present) values, the fully implicit form of the heat balance results:

$$C_{i,j}^{t+\Delta t} (T_j^{t+\Delta t} - T_i^{t+\Delta t}) + C_{i,j+1}^{t+\Delta t} (T_{j+1}^{t+\Delta t} - T_i^{t+\Delta t}) + UA^{t+\Delta t} (T_e^{t+\Delta t} - T_i^{t+\Delta t}) + \phi_i^{t+\Delta t} \approx \frac{\bar{c}_i M_i (T_i^{t+\Delta t} - T_i^t)}{\Delta t} \qquad \{W\}$$

$$where C_{i,j}^{t+\Delta t} = R_{i,j} \dot{m}_{a,j} c_{p,a} + R_{i,j} \dot{m}_{s,j} c_{p,s} \ \ at\ future\ time\ step \qquad \{W/K\} \qquad (3.49)$$

Weighted summation (with weight factor $\alpha \leq 1$) of equation 3.48 and 3.49 and rearrangement of the various terms into temperature related coefficients leads to:

$$\begin{aligned} &\left[\alpha(-C_{i,j}^{t+\Delta t} - C_{i,j+1}^{t+\Delta t} - UA^{t+\Delta t}) - \frac{\bar{c}_i M_i}{\Delta t}\right] T_i^{t+\Delta t} + \alpha C_{i,j}^{t+\Delta t} T_j^{t+\Delta t} + \alpha C_{i,j+1}^{t+\Delta t} T_{j+1}^{t+\Delta t} \\ &= \left[(1-\alpha)(C_{i,j}^t + C_{i,j+1}^t + UA^t) - \frac{\bar{c}_i M_i}{\Delta t}\right] T_i^t - (1-\alpha) C_{i,j}^t T_j^t - (1-\alpha) C_{i,j+1}^t T_{j+1}^t \\ &+ \left[-\alpha UA^{t+\Delta t} T_e^{t+\Delta t} - (1-\alpha) UA^t T_e^t - \alpha \phi_i^{t+\Delta t} - (1-\alpha)\phi_i^t\right] \qquad \{W\} \end{aligned} \qquad (3.50)$$

Depending on the value α, the above equation will be identical to the fully implicit

formulation (α =1). the fully explicit formulation (α =0). or for instance the Crank-Nicolson formulation (α =0.5). In the current program. value α is a user definable parameter. However. the default treatment is to switch it dynamically during simulation process.

3.5.2 Plant components

In ESP-r. plant is described using a network consisting of an interconnected group of components. The plant component in ESP-r describes a physical entity (e.g. heat exchanger or cooling coil). As with all other areas of ESP-r. control volumes are used in the modeling of plant components. All component models comprise one or more control volume. Each plant component is made discrete by subdivision into one or more interconnected finite volumes. For each finite volume (or node) up to three conservation equations are developed to represent heat and mass transfer. In case a node represents a solid region there is only one equation (heat). for a node representing water there are two equations (heat + water flow). and for a node representing air there will be three equations (heat + dry air + water vapour).

In ESP-r, many component templates have been developed and these are held in a plant components database which are grouped into four basic types: (1) air conditioning (fans. duct. humidifier. etc). (2) water heating (pumps. pipe. radiators. etc). (3) primitive parts (fundamental elements of components). and (4) miscellaneous (solar collector. etc). Detailed information regarding theoretical background of the plant components can be found elsewhere (e.g. Henssen 1991. Aasem 1993).

3.6 Control

In ESP-r a control can be imposed on several aspects of a model (i.e. zones, flow components, and / or plant components). A control is defined by *sensor location*, *actuator location*, and *control law*. A *sensor* exists to measure some variable for transmission to the control law representing the active controller. The control variable may be any nodal state variable active within a simulation, an outdoor condition, one of the plant component additional variables, or some derived combination of the previous.

Actuators exist to transmit the output of a controller to some building zone or plant component, usually to reduce the deviation of the sensed control variable from some user-specified set point. Actuator locations can be set to any building side node (air, surface, intra-construction, etc), or some plant component participating in a simulation.

A *control law* is an algorithm which represents the logic of some controller. Its purpose is to translate (algorithmically) the sensed condition to the actuated state in terms of the control system characteristics (e.g. building pre-heating, fixed heat injection or extraction, PID control, ideal controller, etc). For each control loop, in addition to specifying sensor, actuator, and control law data, the user has to specify items such as periods of validity and operation, component output capacity, set point, throttling range, and so on.

At each time-step as a simulation proceeds, the nodal property detected by the sensor is fed to the control law algorithm, which then acts to fix or limit some other nodal property.

via the actuator node, prior to matrix reformulation for the current time-step. In this way, simulation control is achieved based on some function of a prevailing control point.

CHAPTER 4

MODELING AND SIMULATION

4.1 Building modeling

To perform building side simulation, it is necessary to define thermal zones that consist of building geometry and opaque or transparent envelope components, and to apply boundary conditions to each of these zones. In addition, it is essential to establish a weather data file for a time period to be considered.

4.1.1 Defining building zones

The first step to model the building side simulation is to define thermal zones, the basic elements of ESP-r, which describe the geometry and fabric of a building. The geometry should be based on the architectural layouts and sections of the building under consideration. Main floor layout and vertical section are shown in Figure 4.1 and 4.2.

There are some limitations when defining geometry in ESP-r. Currently maximum number of zone allowed in ESP-r is *21*, and number of surfaces within a zone should not exceed *24*. To avoid unnecessary complexity, and to conform to the maximum number of zones allowed within a project, it is needed to simplify the building to a certain extent. For example, restrooms in a locker room were assumed to be included in the locker room, but in the airflow network, the effects of local exhaust fans were definitely considered. In addition, small storage rooms near the corridor and group activity rooms (e.g. room 111, 132) were assumed to be a part of those rooms.

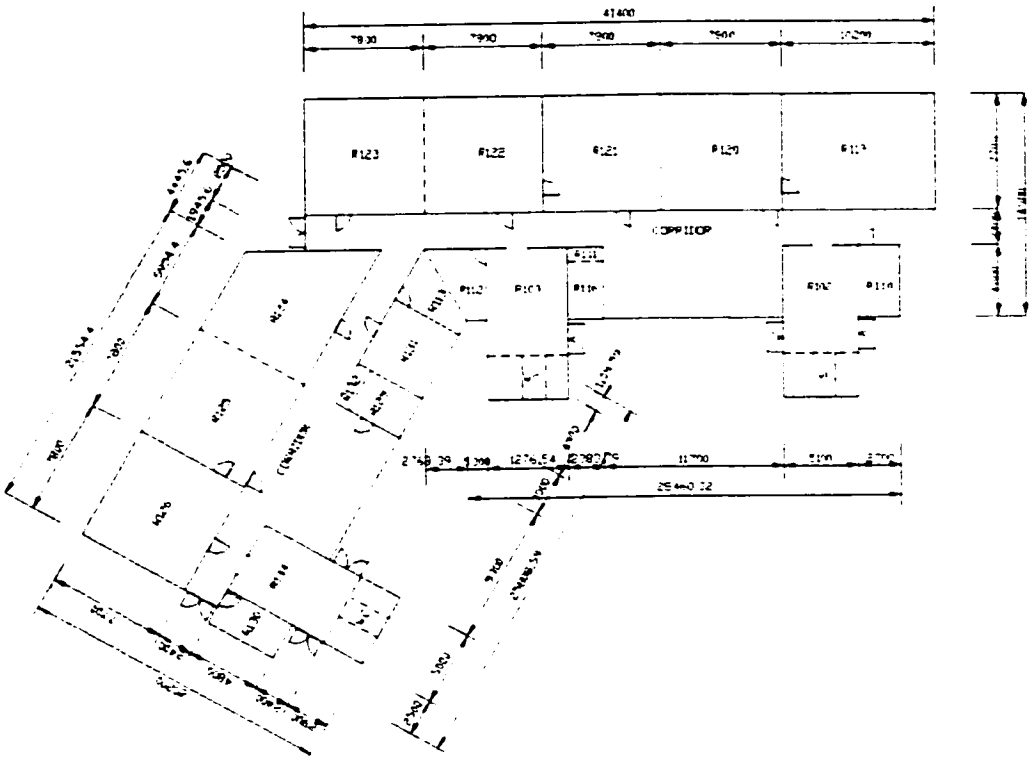

Figure 4.1 Main floor layout of the Grong school (Unit: mm)

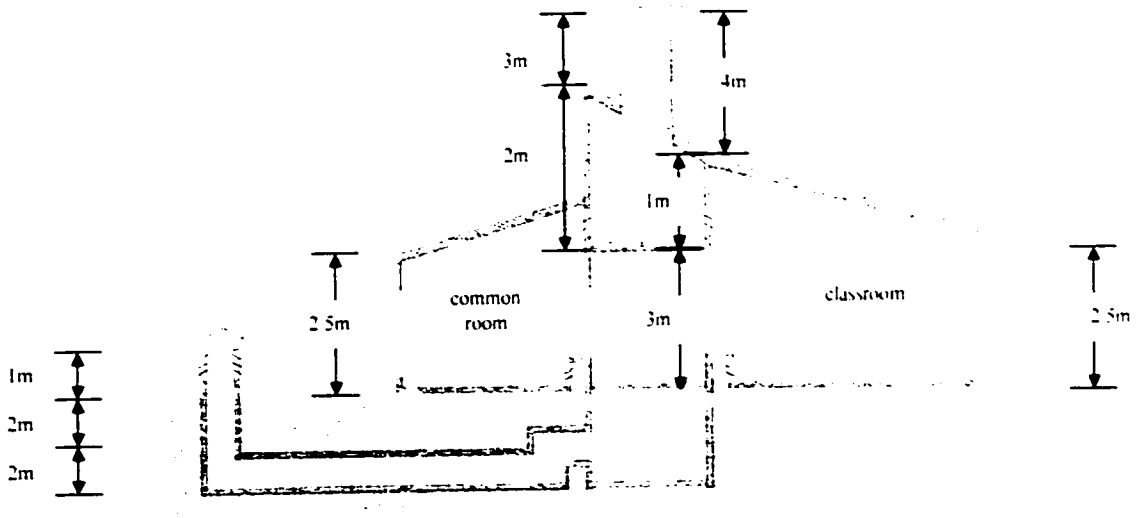

Figure 4.2 Vertical section of the Grong school

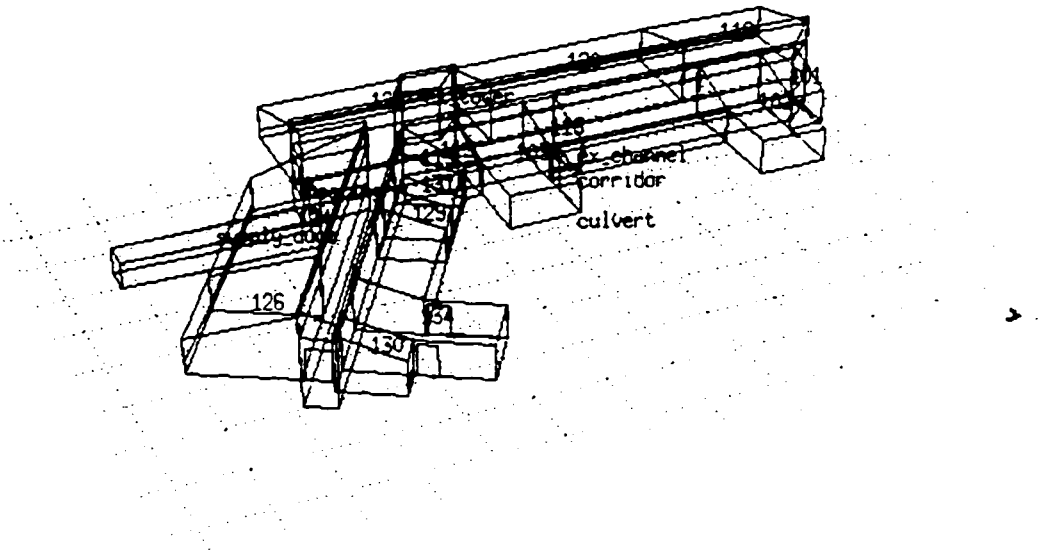

Figure 4.3 Montage of the Grong school implemented in ESP-r

The building comprises *21* zones, each representing a distinct area of the building. A montage of the building implemented in ESP-r is shown in Figure 4.3. Also, detailed information regarding area, volume, and surface area for each zone is summarized in Appendix A. Each zone comprises at least six surfaces that are either opaque or transparent to form an enclosed volume. Each surface is defined by coordinates of vertex points and must be attributed by assigning multi-layer constructions from database. The multi-layer construction is generated by adding materials beginning with the outside face and working into the layer that faces the zone. ESP-r's construction material database contains many standard materials, each of which is characterized by its thickness, conductivity, density, specific heat, surface emittance, and so on. Windows (transparent multi-layer constructions) are created in similar fashion as opaque multi-layer

constructions, but need additional optical properties such as solar reflectance, absorptance, and transmittance. Appendix B shows construction details of the building.

4.1.2 Applying boundary conditions

Multi-layer constructions have inside and outside surfaces. The inside surface faces the zone's air point, and is handled automatically in ESP-r. The boundary condition for outside surface must be defined by one of the following categories: (1) it is exposed to outdoors; (2) it faces another zone; (3) it is exposed to fixed temperature and radiation source; (4) it is connected to ground by user-defined monthly temperature profile; (5) it is exposed to same conditions as inside; or (6) adiabatic.

Exterior wall, window and roof are connected to exterior, the thermal properties of which are characterized by a defined weather file. Floor is connected to the ground that has steady state temperature of *3.6* °C in February by ESP-r's standard monthly ground temperature profile. Underground walls on air distribution culvert are connected to ground having same temperature profile. However, the surfaces of main concrete duct are linked to the different ground temperature profile. Their applied ground temperature in February is *6.1* °C because they are located below the air distribution culvert. These ground temperatures may add some error when predicting room temperatures because of the difficulty of estimating them.

4.1.3 Establishing weather file

The weather data used for this research are based on actual measurements. It covers a

representative heating period and constitutes time-series of minutely measured values of air temperature, solar radiations, wind speed, and wind direction. The measurements were performed by SINTEF (The Foundation for the Scientific and Industrial Research at the Norweigian Institute of Technology) and NTNU (Norweigian University of Science and Technology) during Feb.1st to 28th, 2001 inclusive. Since ESP-r utilizes only hourly written weather data, it needed to modify the measured weather data into an hourly written format. The weather file is attached in Appendix C for reference.

4.2 Airflow modeling

4.2.1 Defining nodes

In ESP-r, fluid flow networks are composed of three basic constituents. These are (1) nodes, (2) connecting components, and (3) inter-nodal connections. As mentioned in the previous chapter, nodes are the points in the network where the pressure is calculated, and connected together by the components to form the flow network. Internal nodes are automatically inferred from the zone information such as volume and reference height. On the other hand, external (boundary) nodes must be defined by the user. All nodes are given a reference temperature in the case where the flow network is integrated with building or building and plant. For example, currently *22 °C* is used for reference temperature of all occupied rooms, but this value has actually no significant meaning because it will be overwritten by the values calculated on the building or plant side simulation. The reference height h_1 and h_2 are required for the calculation of stack effect on the network flow as explained in Chapter 3. The height of the internal node such as a classroom was assumed to be half of the averaged room height.

4.2.2 Defining flow components

Flow components describe the mathematical relationship between the flow through an airflow path and the pressure drop across the path. ESP-r provides the user with many mathematical types to choose. Each of these flow components was described in Chapter 3. Choosing appropriate components is one of the most important parts of airflow network because it directly affects the results of airflow calculations. Appendix D shows a summary of these components used for this research.

For air intake louvers, specific airflow openings were used. Because air intake tower has three separate louvers, it is needed to define three airflow components. Each louver has its net area of $0.62\ m^2$. They were connected to the exterior, imposing wind-induced pressures by logarithmic wind speed profile and wind pressure coefficients for low-rise buildings described in Chapter 3. The same method, as used for the air intake tower, was also used for the exhaust tower.

As illustrated in the Chapter 2, the air is supplied into each room through circular holes on the floor from underground culvert. For instance, room 126 has four circular holes on the floor having the diameter of $250\ mm$ each. In ESP-r, In order to model these holes, the airflow conduit components seem to be the best choice. However, the problem is that this increases the number of flow connections significantly. For example, room 126 needs 4 and corridor needs 14 flow connections to link air flows from culvert to the room. Finally, if it is applied to all room, the total number of the connections will exceed the

maximum number allowed in ESP-r (e.g. 99 connections for current version of ESP-r). Because of this problem, another type of flow component, specific airflow opening, had to be used. The area of *0250* opening is about *0.05* m^2, and this value is multiplied by the actual number of holes in the room under consideration, as can be seen in Appendix D.

Air exhaust vent is a kind of motorized damper between exhaust channel and upper part of a room. A room has one, two or more dampers according to the size of the room in order to have required ventilation. The actual exhaust vent is *0.3 m* long and *0.6 m* high. To avoid unnecessary complexity and to satisfy the connection limitation of ESP-r mentioned above, it was assumed that each room had just one representative opening. For instance, room 119 has actually two vents having each area of *0.18* m^2. Therefore, the room is considered to have a representative vent, the area of which is *0.36* m^2 (*2* · *0.18* m^2). Later, these exhaust vents will be incorporated with a control strategy that opens or closes them or adjusts them incrementally according to set temperatures. For example, a controller can be applied to them in such a way that they are opened when room temperature rises above *22* ℃ or closed when room temperature drops below *20* ℃.

For the exterior and interior doors, specific airflow crack component was selected for the model component. Since the exterior doors are weather-stripped double door, the crack width is considered to be very small (e.g. 0.5 *mm*). The height of all exterior doors is *2.2 m* and the width *1.8 m*. Therefore the evaluated crack length for an entire exterior door is estimated as *10.5 m* (*2.2 m* × *3* + *1.8 m* × *2*). For interior doors, the crack width was considered to be *1 mm* for all. They are single doors, the height of which is *2.1 m* and the

width *0.9 m*. Therefore corresponding crack length is estimated as *6 m* (*2.1 m* × *2* + *0.9 m* × *2*).

There is a vertical opening (doorways) on each of the walls between corridor and locker rooms (room 102, 103 and 134). Because it is reasonable that bi-directional flow is assumed, specific airflow door component is applied to those openings. If temperature difference exists across such an opening, the airflow will occur in both directions due to the action of small density variations over the door height. In case there is no or only a very small temperature difference (e.g. < *0.01 K*), a door component is treated as an ordinary airflow opening because in those cases the buoyancy may be disregarded. In Grong school each doorway has a height of *2.1 m* and width of *1.4 m*.

In the laundry room (room 110), there is a purposely provided opening under door (under-cut). Air is sucked into the room from the corridor through this opening and exhausted by a local exhaust fan to exterior. For this, specific airflow opening component is considered to be most suitable. The length of the opening is *0.9 m* and width *0.02 m*.

In addition, there are a few constant flow components. These are applied to the restroom exhaust fans and laundry room exhaust fan. All locker rooms have three separated restrooms each of which has exhaust fan having *10 l/s* of airflow rate. Also, the capacity of the exhaust fan in the laundry room is *10 l/s*. These fans are assumed to operate continuously, which might be a little different from real operation situation.

Next, it is necessary to model the main supply and exhaust fan. Each of the fans has maximum volumetric airflow rate of *10,000 m^3/hr*. Because the exhaust fan was installed to make a higher airflow rate available for cooling purpose in summer, this study does not consider its operation. The supply fan can be controlled by temperature or pressure sensors in conjunction with the exhaust dampers. A flow network control regime can be imposed on this flow component, allowing it to be switched in on/off mode or proportionally operated. Detailed description regarding controls of both exhaust damper and supply fan is supplied in Section 4.4.

Last, one other important factor to be considered is pressure losses through mechanical parts of the ventilation system such as filter and heat exchanger. Actually, the installation of air filter, heat exchangers and other air handling equipment may cause the biggest pressure losses in the entire ventilation system. According to SINTEF and NTNU (1997), the estimated pressure loss through the fine filters is about *20 Pa*, and also expected pressure loss is *25 Pa* for the inlet heat exchanger and *28 Pa* for the exhaust air heat exchanger under fan operating situation. One of the most effective ways to model this pressure drop is to use power-law relationship, as expressed in Equation 3.24 of Chapter 3. The flow exponent *b* is typically between a *0.6* and *0.7* according to the G. N. Walton et al (2000). The flow coefficient *a* can be estimated from the known pressure difference and maximum flow rate. For example, the pressure loss for the fine filter (*20 Pa*) with the maximum flow rate (*10,000 m^3/h* ≈ *3.333 kg/s*) and the flow exponent (*0.7*) yields approximate flow coefficient of *0.41*. The detailed information on these power-law flow components is also included in Appendix D.

4.2.3 Defining connections

Connections are defined in terms of linking a start-node to an end-node via a component. The height of the connection inlet and outlet relative to the nodes it connects is required for the calculation of stack effect on network flow. Appendix D gives all connection details used for the simulation. There, h_1 is the height difference between flow component and start-node ($h_{component}$ - h_{node1}), and h_2 is the height difference between flow component and end-node ($h_{component}$ - h_{node2}).

4.3 Simulation

4.3.1 Building thermal simulation

The goal of the first simulation is to check that the modeled building is well implemented in ESP-r. Since the building thermal simulation can be a basic model for integrated simulations (e.g. building + airflow network), it is important to look at how the building responds according to the dynamic outdoor conditions and imposed internal heat gains.

The classrooms and common rooms are assumed to be occupied during normal school time (9:00 ~ 18:00), with the resulting sensible energy gains due to occupants, lighting and equipment. The imposed internal loads are basically identical to the design values by SINTEF and NTNU (1997). They are as follows: (1) Lighting load = *13* W/m^2; (2) Occupants load = *22* W/m^2; (3) Equipments load = *2* W/m^2. Loads are assumed to be on 9 hours a day (9:00 ~ 18:00) during weekdays.

A simulation is now performed via the simulator using the defined weather file. The simulation is run over the period of Feb. 8th to Feb. 14th inclusive, with an hour time step. This time period includes a Saturday (10th) and Sunday (11th). There is no control imposed on this stage of simulation, which means the building will be free-floating according to variable outdoor condition.

Graphical outputs of the simulation are presented in Figure 4.4. The results show temperature variations of several representative zones according to dynamic outdoor condition and imposed internal heat gains throughout simulation time period. The variation of supply duct temperature from the first output of Figure 4.4 indicates that the long underground concrete duct could dampen swings in supply air temperature compared to outdoor temperature.

From the results, room 119, 126, 102 and 134 show similar temperature pattern throughout the entire time period, even though room 119 and 126 are a little more sensitive to the change of outdoor condition compared to room 102 and 134. Probably this can be attributed to the existence of window in room 119 and 126. Also, the effect of the imposed internal heat gains can be observed from temperature patterns of those occupied rooms. Note that there is no internal heat load during weekday unoccupied time period and weekend.

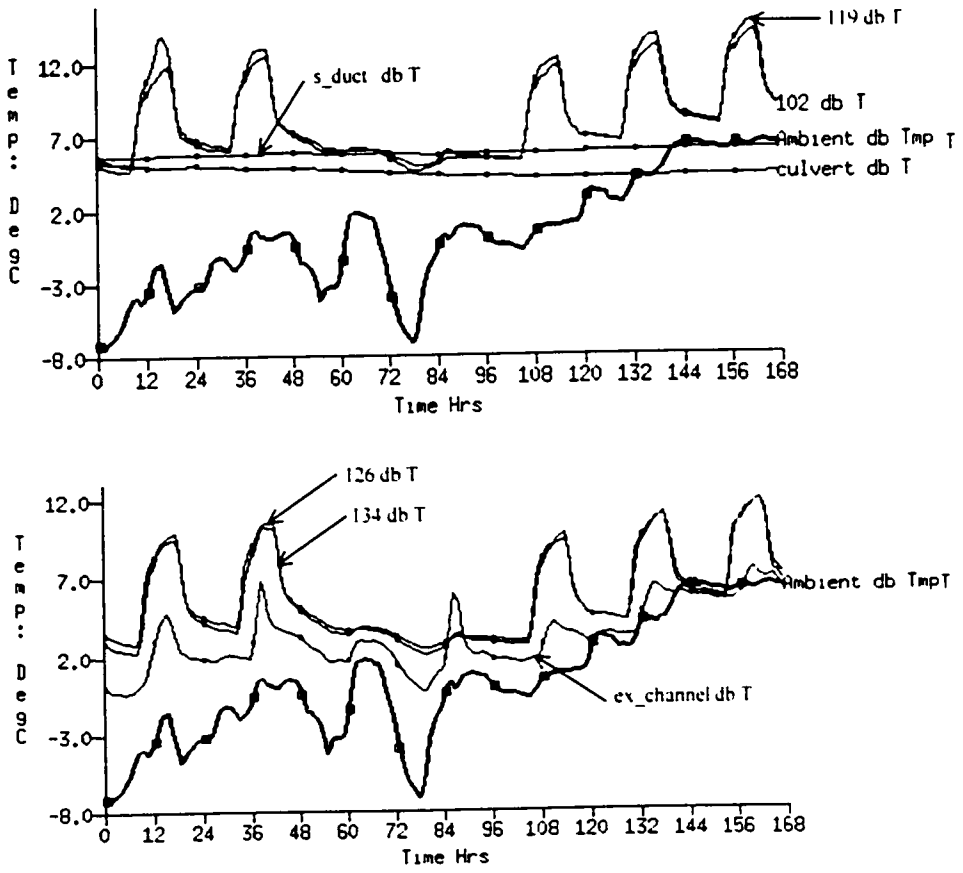

Figure 4.4 Outputs of the building thermal simulation (Unit: *℃*, *119* and *126*: classrooms, *102* and *134*: locker rooms, *s_duct*: main supply duct, *culvert*: underground air distribution culvert, *ex_channel*: exhaust channel, *Ambient*: outdoor air temperature)

Zone heating load can be obtained conducting one more simulation using an ideal thermal controller. For instance, imposing an ideal control with heating set point *22 ℃* to room 122&123 gives sensible heating load to keep the set temperature of the room as shown in Figure 4.5. Later this predicted heating load will be used for estimating capacity of radiator. All outputs of the estimated heating load were gathered in Appendix E.

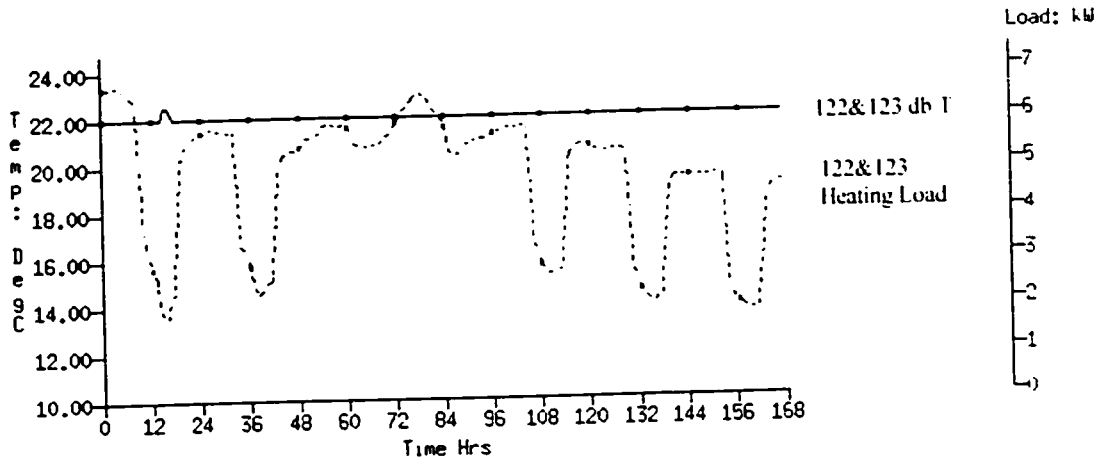

Figure 4.5 Output of zone heating load for room 122&123 (Unit: *℃* for room temperature and *kW* for heating load)

4.3.2 Airflow simulation

The goal of this simulation is to check how the modeled airflow network makes sense from ventilation point of view. This flow network simulation will also be a foundation for the integrated simulations that will be performed next. *22* ℃ was used for reference temperatures of all rooms, *-15* ℃ for supply duct, *19* ℃ for underground culvert and heating coil section, and *15* ℃ for exhaust channel and tower, to give some stack pressures throughout the entire building. Again, when performing an integrated simulation, these reference values will be overwritten by the values calculated on the building side simulation. The exhaust dampers were set to being fully opened in order to allow maximum airflow through them, and the supply fan operation was not considered at this time. The simulation was carried out using the same time period and interval as before.

Some simulation results are gathered in Figure 4.6. presenting entering or leaving airflow rate variations of several zones throughout the simulation time period. The gathered results show that incoming air through the underground duct fluctuates near the flow rate of about $2.600\ m^3/h$ and leaving air through the exhaust tower fluctuates near $2.000\ m^3/h$. The discrepancy can be attributed to the fact that some air is exhausted through restrooms and laundry room by local exhaust fans and the effect of pressure drops through the entire flow components. It should be also noted that the volumetric flow rate difference between entering and leaving air in a zone is because the flows originate from nodes with different temperatures.

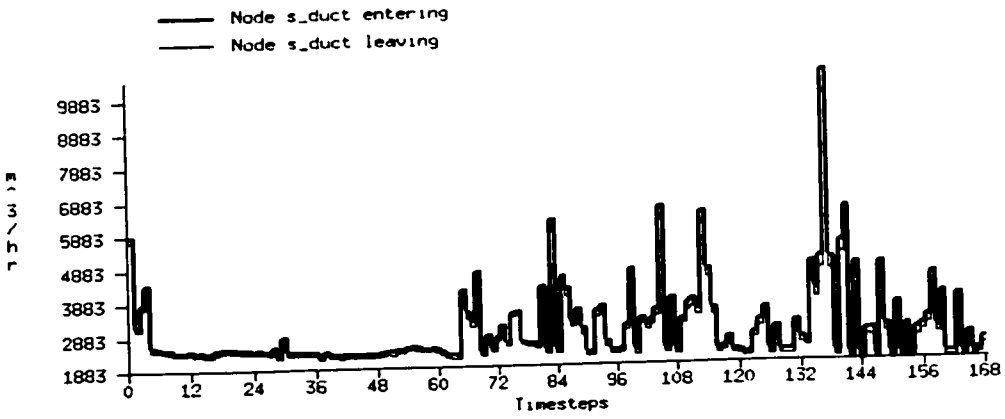

< main supply duct >

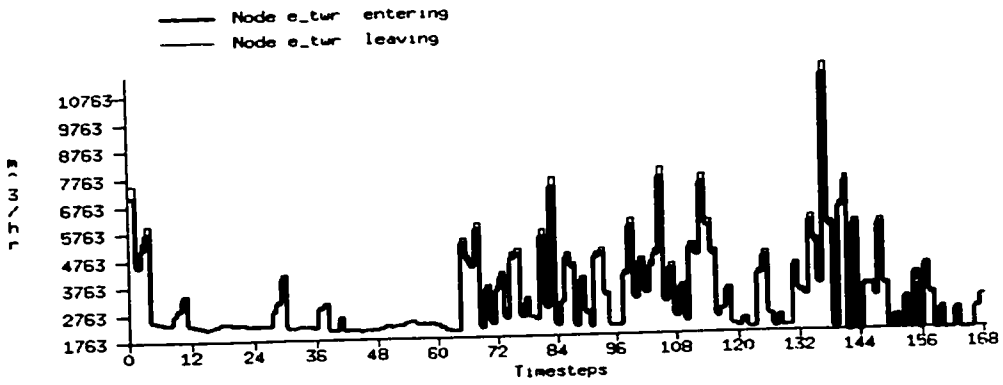

< exhaust tower >

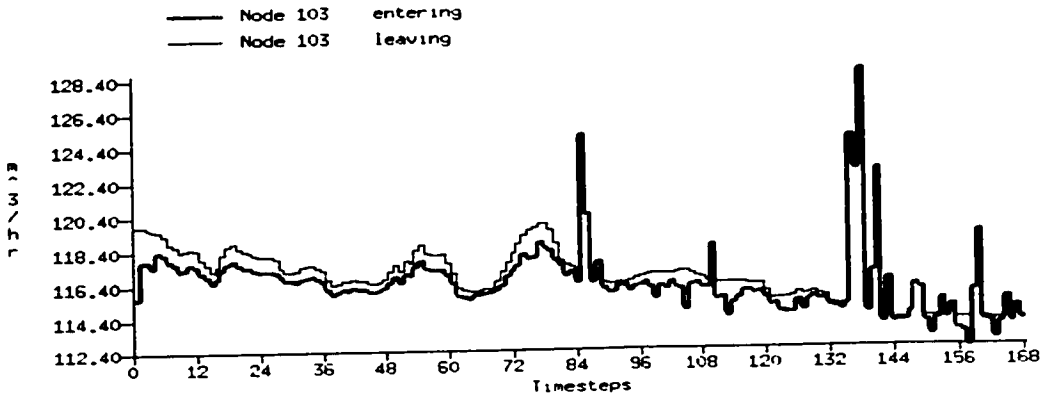

< room 103: locker room >

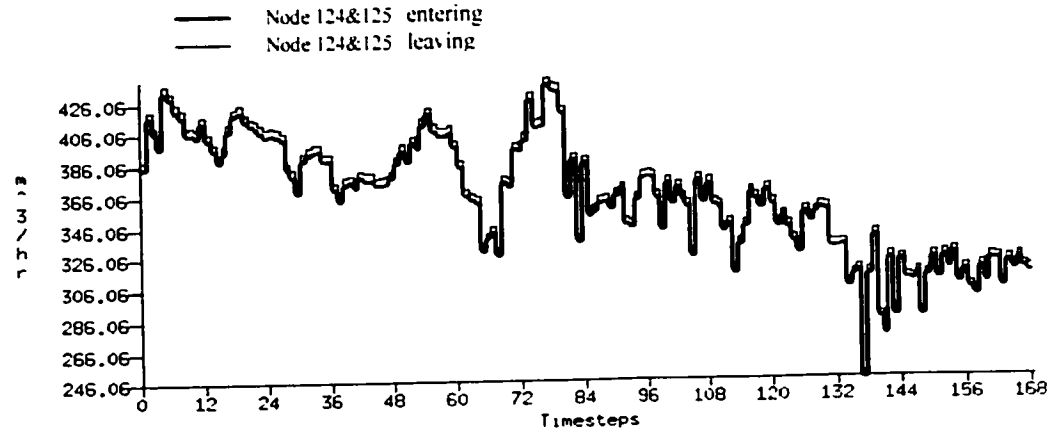

< room 124&125: classroom >

Figure 4.6 Outputs of the airflow simulation (Unit: m^3/hr; in ESP-r *kg/s* or *ACH (Air-Change per Hr)* unit is also available; in the case of m^3/hr or *ACH* unit, the density of the fluid flow is taken into account)

4.3.3 Building + airflow integrated simulation

It is worthy mentioning that actually many errors (e.g. input error, geometry inconsistency, airflow-connection error, etc) have been corrected going through the previous two simulations. An integrated simulation is now carried out, which puts the building and airflow-network together on same simulation time period. In this stage of

simulation, the hybrid ventilation concept of the modeled building can be applied through pre-defined building and airflow network together with some control strategies. The goal of this simulation is to apply the hybrid ventilation concept of the Grong school to ESP-r.

A control strategy has been suggested to keep the air temperature of heat exchanger section and underground culvert constant to *19 °C* with their ideal heat flux controller. Set-point temperature of *19 °C* is identical to the supply set temperature of the actual system. Also, the main supply fan was set to operate continuously to provide ventilation but to stop if a room temperature reaches a certain set-point (e.g. *18 °C* of corridor temperature for this simulation). Simulation is employed to access this proposed control strategy.

A simulation is now performed via the simulator using the defined climate file and control file. The simulation is run over the period of 8^{th} to 14^{th} of February. The time-step used on the simulation is 60 minutes. Simulation results are gathered in Figure 4.7 for temperature outputs of the entire zones and in Figure 4.8 for airflow outputs of several representative zones.

The temperature outputs represent the heating set point temperature never occurs for this system (even though the result shows temperature reaches the set-point for a short time period, i.e. around 14 simulation processing hour; probably this is due to the unusually intensive solar radiation at that time period). In other word, supply air temperature has to

be set more highly or additional heating devices should be installed in order to come up with the proposed control room temperature.

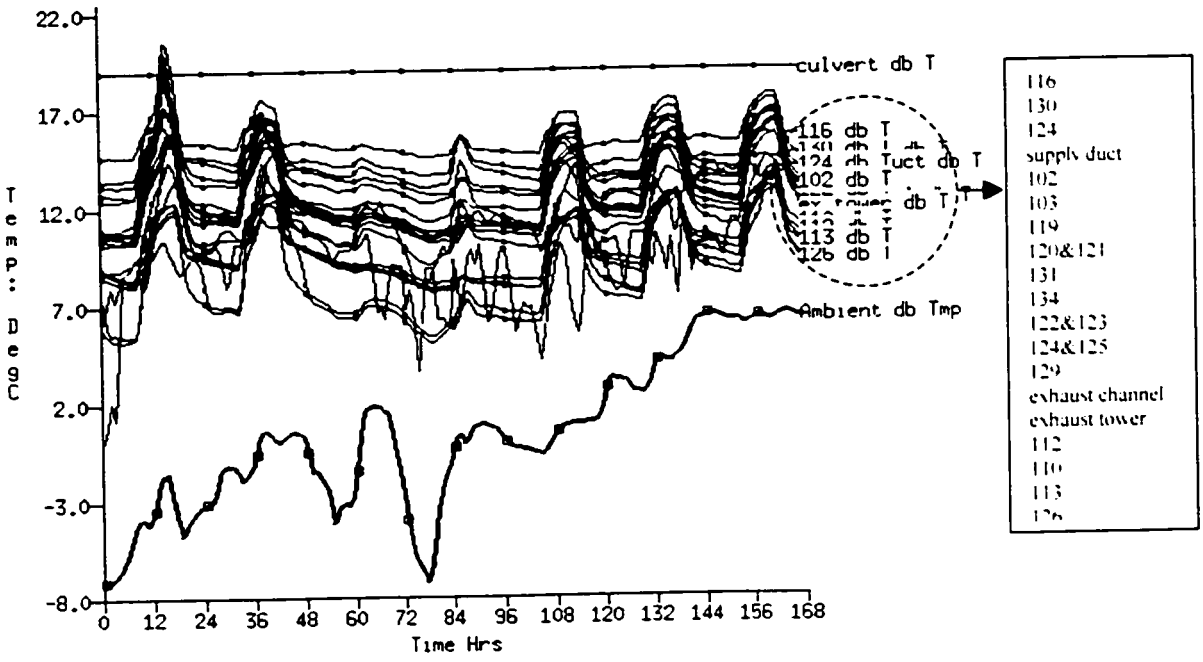

Figure 4.7 Temperature outputs of the building + airflow integrated simulation without zone temperature control (Unit: °C, *culvert*: underground air distribution culvert, *Ambient*: outdoor air temperature)

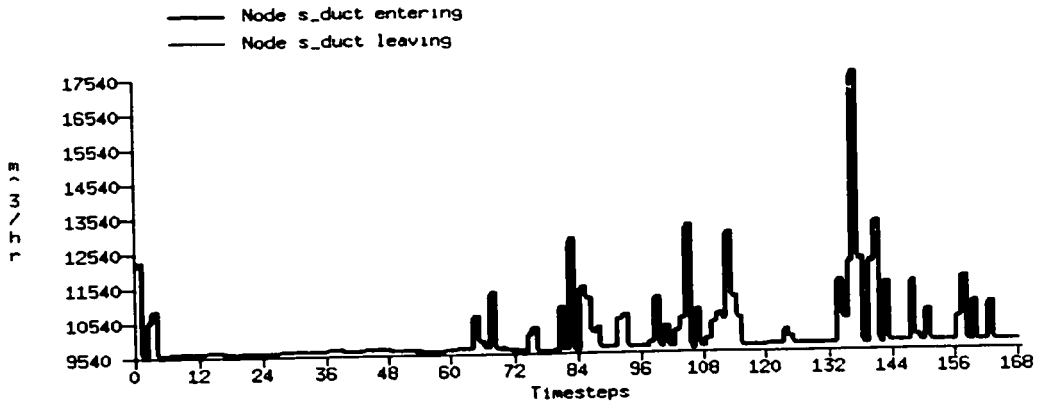

< main supply duct >

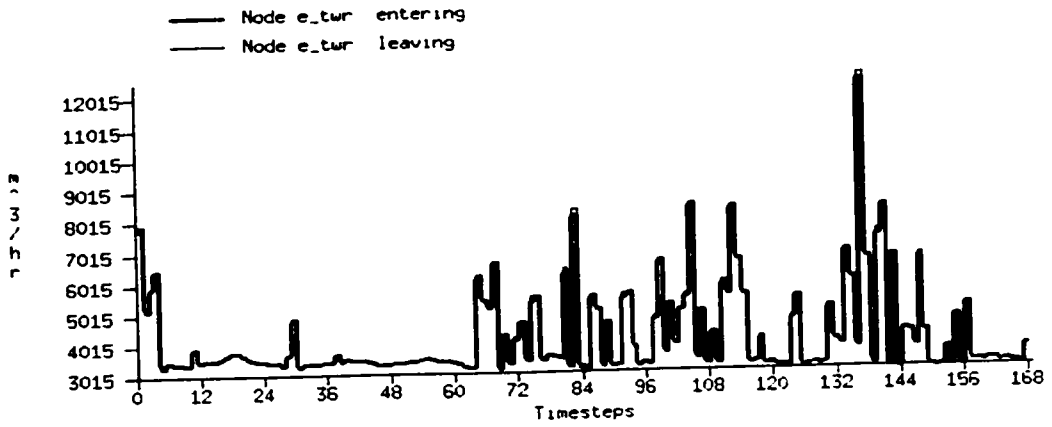

< exhaust tower >

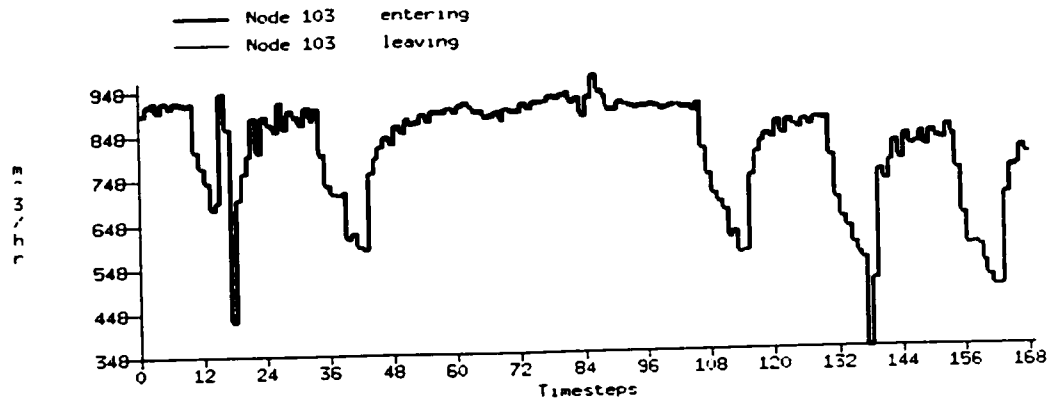

< room 103: locker room >

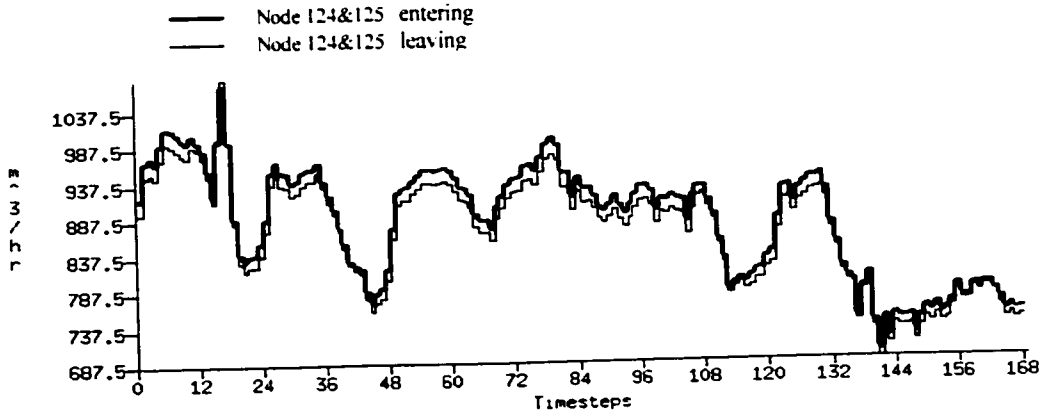

< room 124&125: classroom >

Figure 4.8 Airflow outputs of the building + airflow integrated simulation without zone temperature control (Unit: m^3/hr)

Airflow output of the supply duct in Figure 4.8 shows that the supply fan is continuously operating because room temperature never reaches the control set point. Several unusually highest airflow rates of the supply duct and exhaust tower (e.g. near the simulation processing time of 136 hr) can be attributed to the strong wind velocity at that time. When comparing these results with those of the previous section (Section 4.4.2), it is apparent that flow rate difference between natural ventilation and mechanical ventilation is considerable for this building.

Actually, the real building has additional heating system; i.e. hydraulic radiators are installed under the windows in order to compensate the heat loss from the building envelope and thus give rise to the room temperature. In this stage of simulation, plant components such as radiators can be modeled using a related control strategy.

To model the radiators, a control was defined in proportional control mode to actuate the radiator's heat flux based on a zone air temperature within which it is located. This controls heat injection into each zone in order to keep room air temperature within certain range. The heating set point for this controller was set to *22* ℃ with a throttling range of *2* ℃. The maximum heat flux of the radiator in a zone was estimated by performing building only simulation with ideal zone control as described in Section 4.4.1.

One other control method was added for more realistic simulation. This is used to actuate the exhaust damper that is opened or closed according to room temperature variation.

This control is carried out within airflow-network control domain. Exhaust dampers were set to operate proportionally according to room temperature variation (e.g. *20 ~ 24 °C*) within pre-defined maximum airflows. Maximum airflow rate of each zone can be estimated by previous simulation. Notice that the previous simulation was done with full damper opening and fan operation. For example, in Figure 4.8 the maximum airflow rate of room 124&125 is estimated as *1.000 m^3/h*. Therefore, the exhaust damper of room 124&125 will operate within a range of *0 ~ 1.000 m^3/h* by the control.

Last, the main supply fan was modified to operate in on/off mode to satisfy the set-pressure difference between underground culvert and exhaust channel. It was set to operate to maintain the pressure difference between *20 Pa* and *25 Pa* by on/off controller. This control could keep pressures in the system above a certain limit and also prevent the excessive pressure rise between underground culvert and exhaust damper, particularly when most of exhaust dampers are closed. It should be noted that the actual ventilation system is controlled by the temperature sensor, pressure sensor, CO_2 sensor or a combination of them. The control by the temperature sensor is expected for the night time temperature set-back mode, preheating mode, or cooling mode. For typical winter operations, the fan is expected to be controlled by either CO_2 sensor or pressure sensor, or controlled by a combination of them. The problem is that controls by CO_2 sensors are not available in ESP-r at this time. This might act as the weakest part in modeling hybrid ventilation systems using ESP-r, adding some prediction errors to the resultant outputs.

Now Simulation is employed to access these proposed control strategies. The simulation was conducted using the same time step and period as before. Some simulation results are presented in Figure 4.9 for temperature outputs and in Figure 4.10 for airflow outputs of several representative zones. Also, temperature and airflow results for the entire zones are gathered in Appendix F. Figure 4.9 shows that the room temperatures experience continuous fluctuations because of the controller action to maintain them within the throttling range specified. It can also be seen the airflow variation tend to fluctuate rapidly; this is due to the fact that supply fan and exhaust dampers are continuously adjusted by imposed on/off or proportional control mode.

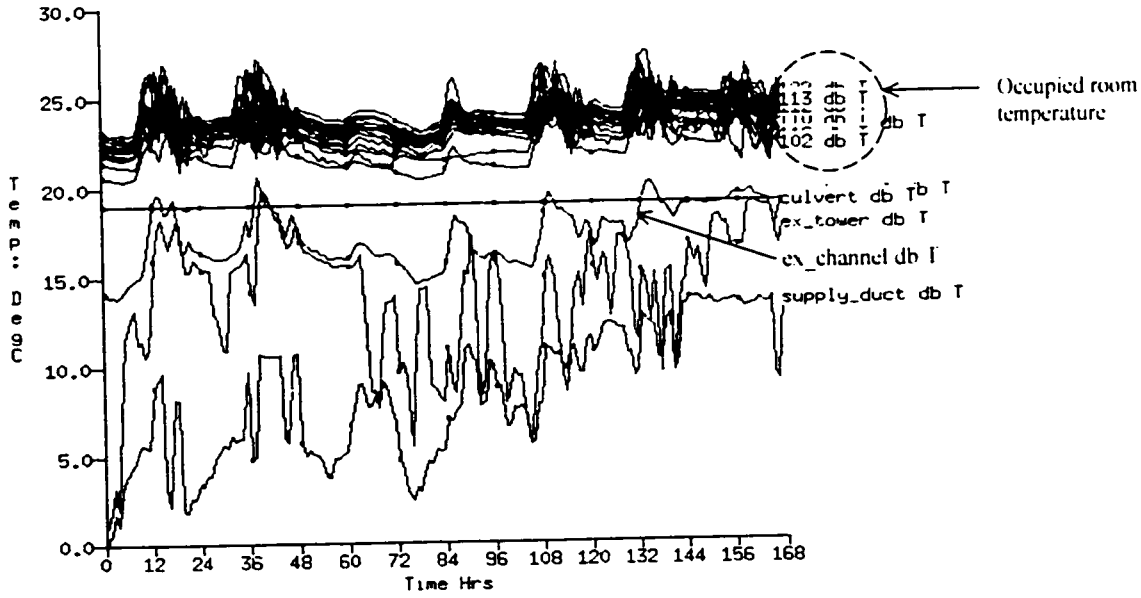

Figure 4.9 Temperature outputs of the building + airflow integrated simulation with zone temperature control by radiator (Unit: *°C*, *122...102*: occupied room temperature, *supply_duct*: main supply duct, *culvert*: underground air distribution culvert, *ex_channel*: exhaust channel, *ex_duct*, exhaust duct)

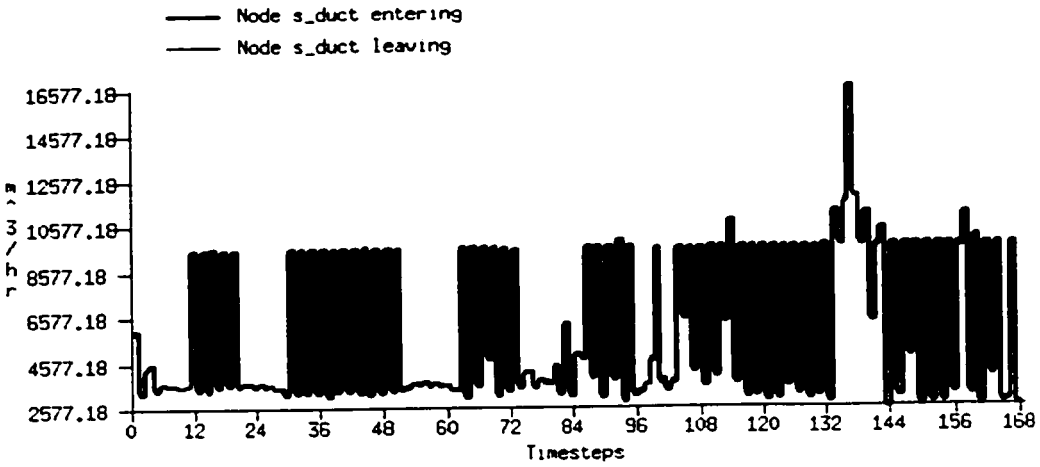

< main supply duct >

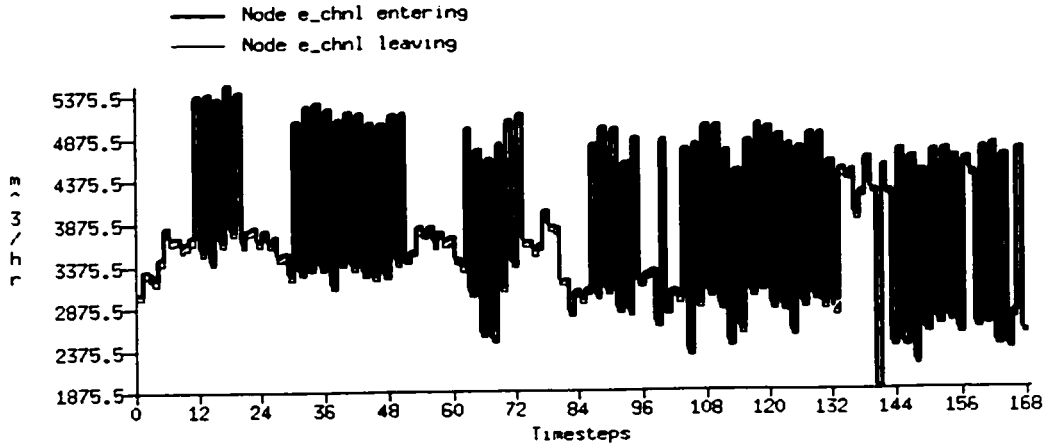

< exhaust channel >

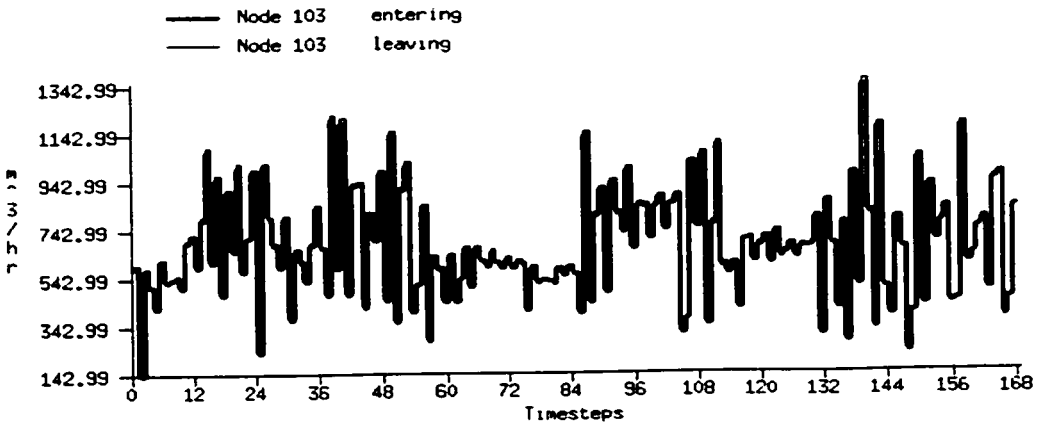

< room 103: locker room >

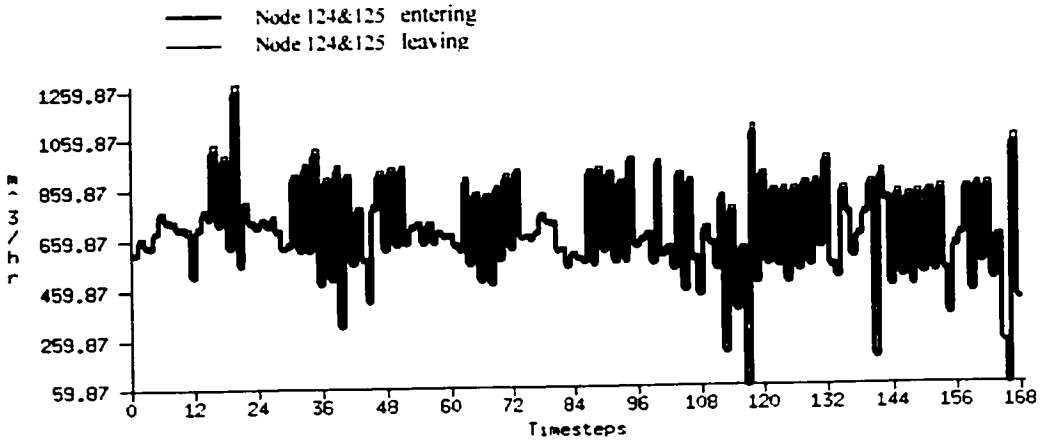

< room 124&125: classroom >

Figure 4.10 Airflow outputs of the building + airflow integrated simulation with zone temperature control by radiator (Unit: m^3/hr)

CHAPTER 5

DISCUSSION

This chapter is made to address discussions on the simulation results and some validation procedure. Obviously the simulation results from the previous chapter provide much information regarding the building's thermal and ventilation performance. Hybrid ventilation performance of the building will be evaluated in this chapter.

5.1 Evaluation of the building

5.1.1 infiltration and ventilation

The infiltration through exterior doors seems to be negligible compared to the airflow rates through other components. Shown in Figure 5.1 is infiltration through room 102's exterior door and through room 134's exterior door, respectively. The results are based on building + airflow integrated simulation with zone temperature control by radiator, discussed in Section 4.4.3. From the outputs, the average infiltration through an exterior door is estimated as *10 ~ 15* m^3/h.

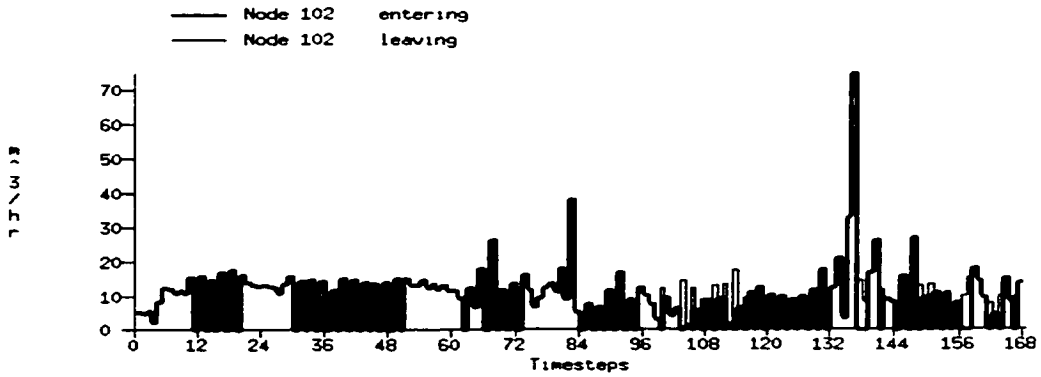

< airflow through an exterior door of room 102 >

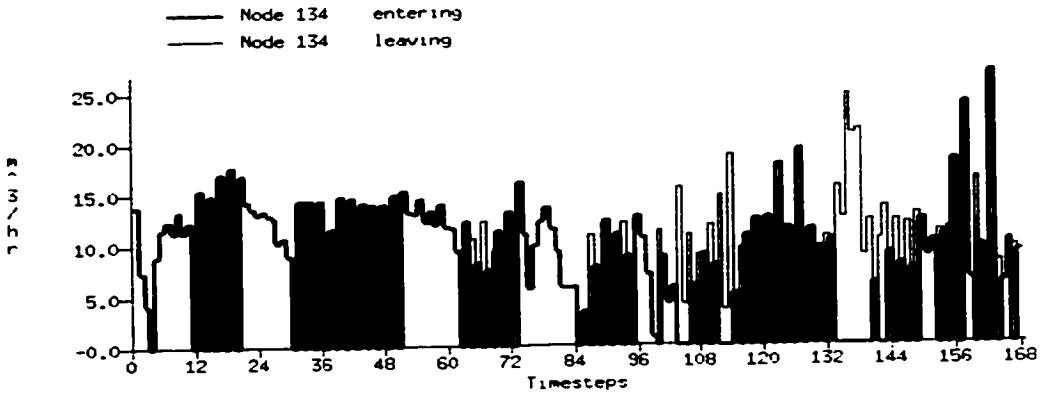

< airflow through an exterior door of room 134 >

Figure 5.1 Infiltration through exterior doors (Unit: $m^3 h$)

Also, Figure 5.2 shows airflow between room 119 and corridor through an interior door and airflow between room 126 and room 124&125 through an interior door, respectively. Results represent airflow rate fluctuates within $2\ m^3 h$ for both cases, which leads to the conclusion that airflow between interior doors is also negligible.

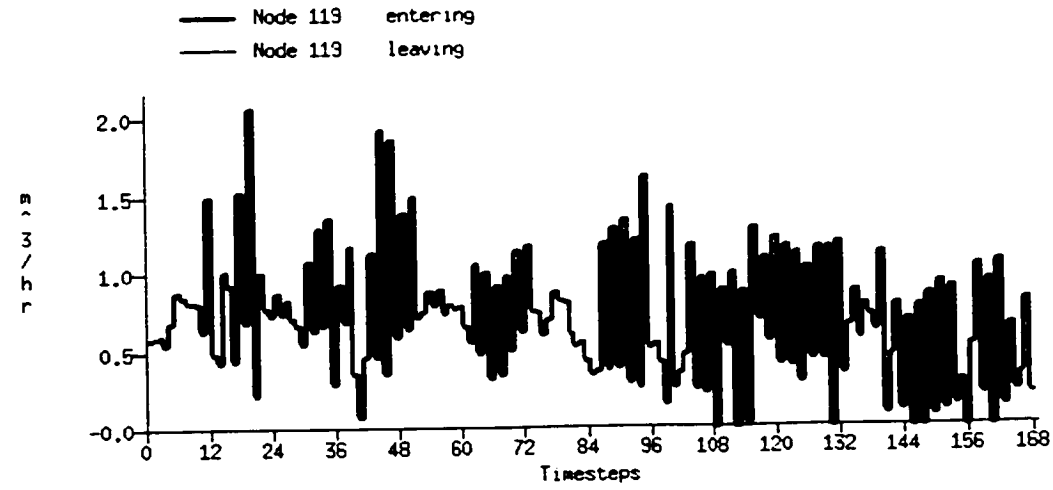

< airflow through an interior door between room 119 and corridor >

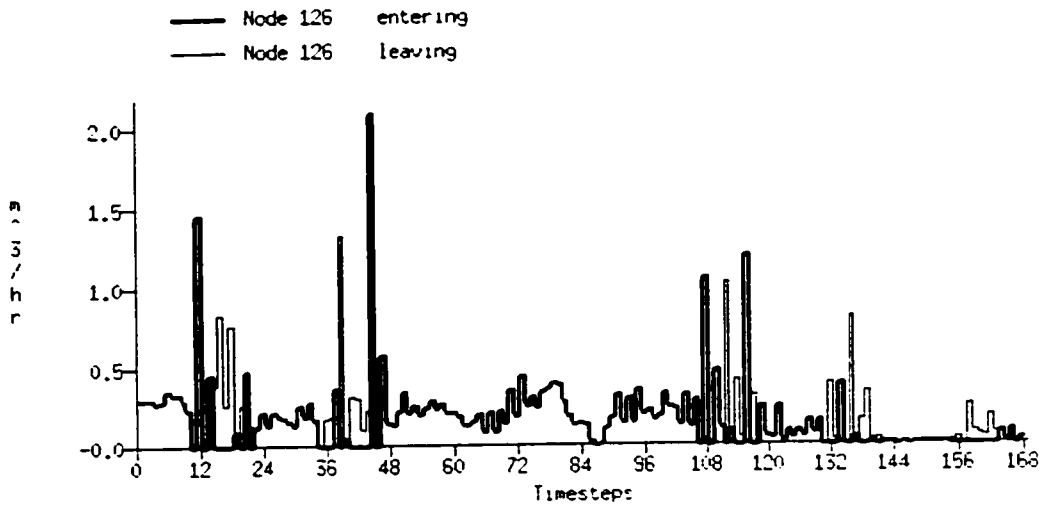

< airflow through an interior door between room 126 and room 124&125 >

Figure 5.2 Airflow through interior doors (Unit: m^3 h)

Simulation results carried out in Section 4.4.2 (airflow simulation) represent a typical natural ventilation characteristic of the building in winter season. From the results, natural ventilation performance of the classroom was roughly estimated to be between *0.7* and *1.1 Air-Change per Hour* (*ACH*), locker room was between *0.7* and *0.8*, and corridor was between *0.6* and *0.9 ACH* for a typical winter time period.

The building's hybrid ventilation performance can be estimated by the integrated simulation (Section 4.4.3). From the integrated simulation (with zone temperature control by radiator), ventilation rates were estimated to be between *1.0 ~ 2.5 ACH* for classrooms, *1.0 ~ 6.0 ACH* for locker rooms, and *2.0 ~ 4.0 ACH* for corridor. It is interesting that locker rooms and corridor have higher *ACH* than classrooms. Essentially this is because the corridor and southern side of the building have lower floor height than classrooms. Also, it can be attributed to the fact that the local exhaust fans allow more air to flow

from corridor to designated common areas. Some of the airflow results from the integrated simulation are presented in Figure 5.3 with the unit of *ACH* for reference.

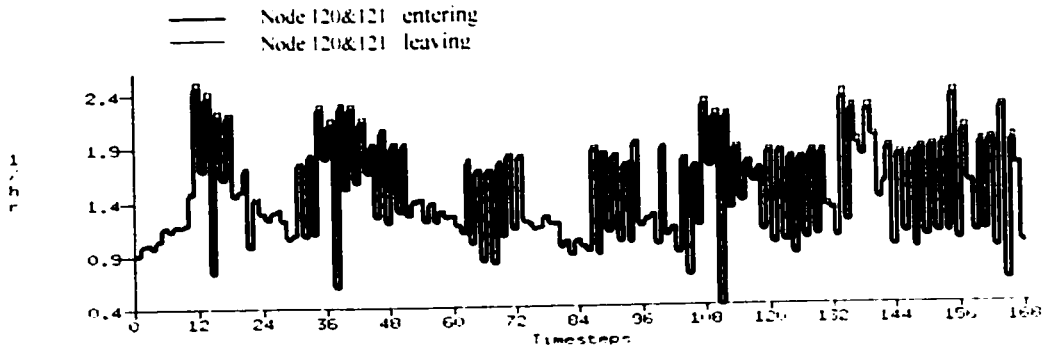

< room 120&121: classroom >

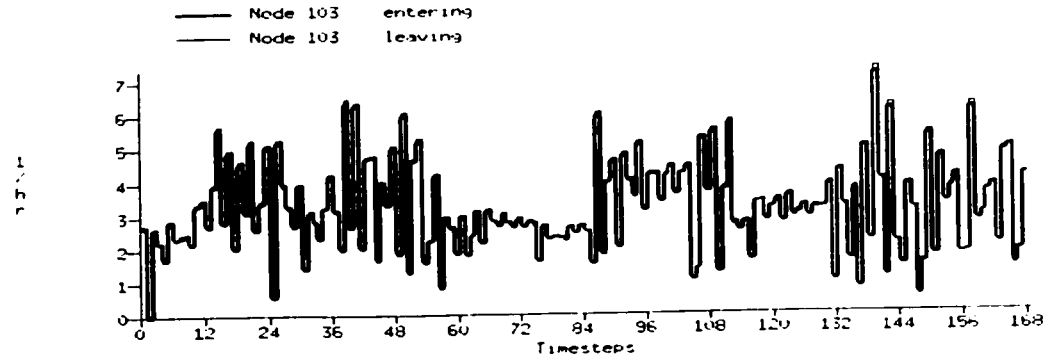

< room 103: locker room >

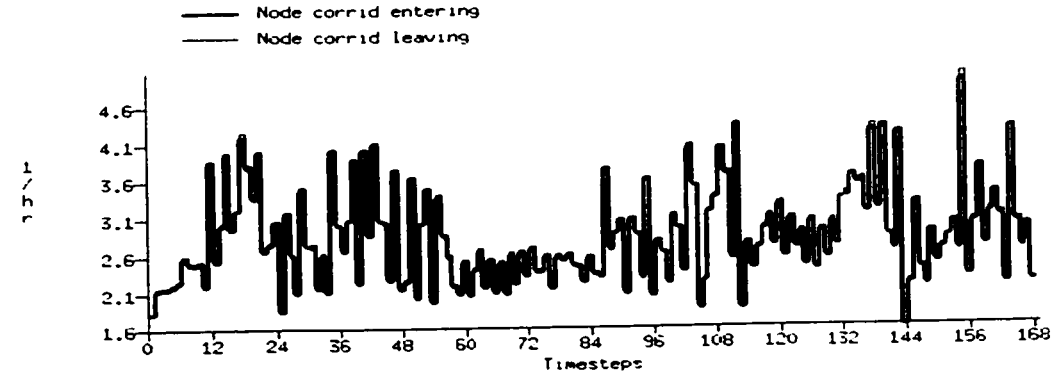

< corridor >

Figure 5.3 Ventilation results with *ACH* unit

When comparing airflow results from airflow simulation (Section 4.4.2) with integrated simulation (Section 4.4.3), it can be concluded that operations of the supply fan can increase ventilation performance significantly (e.g. up to 400% when just comparing airflows fed through main supply duct). When assuming operations of both supply and exhaust fan in summer season, more increased ventilation rates would be expected. Unfortunately, because measurements for the summer period have not been performed so far, this task will require future work.

Wind speed and direction seem to influence the building's ventilation performance significantly. This can be better verified by Figure 5.4, which shows different airflow characteristics of the air intake tower for different directions. It can also be observed from the outputs that the airflow variation is more pronounced between 4th and 7th day of the simulation because of the gusty wind condition during that time period.

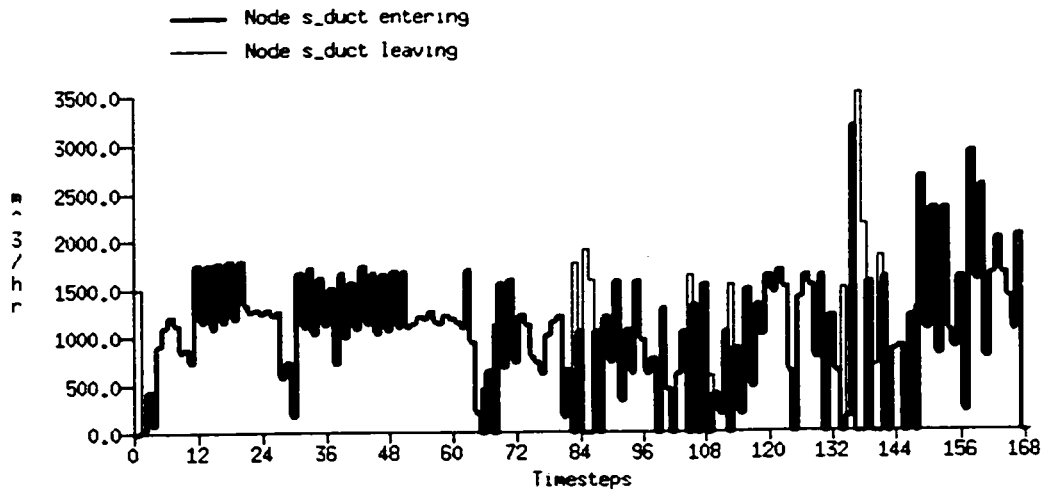

< supplied airflow rate via North-facing louver >

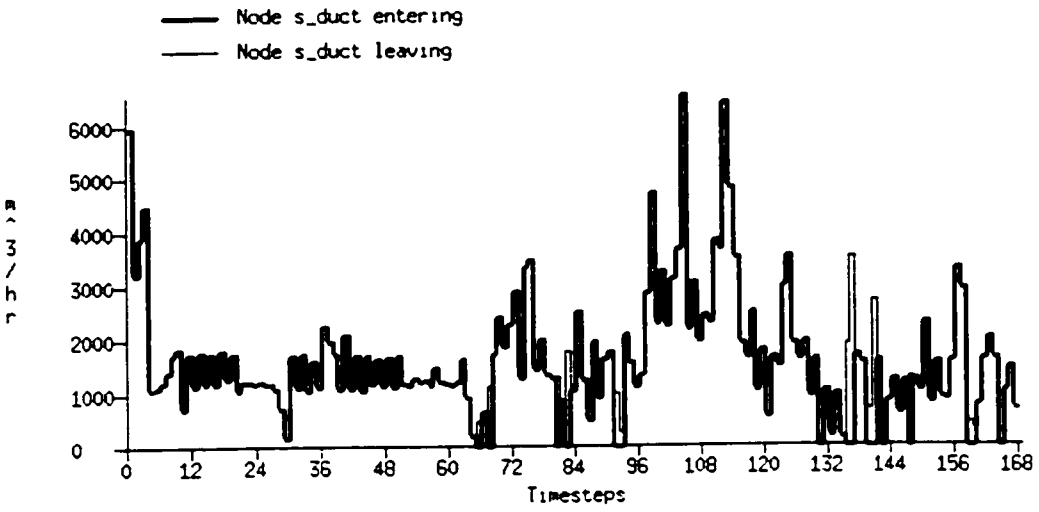

< supplied airflow rate via SE-facing louver >

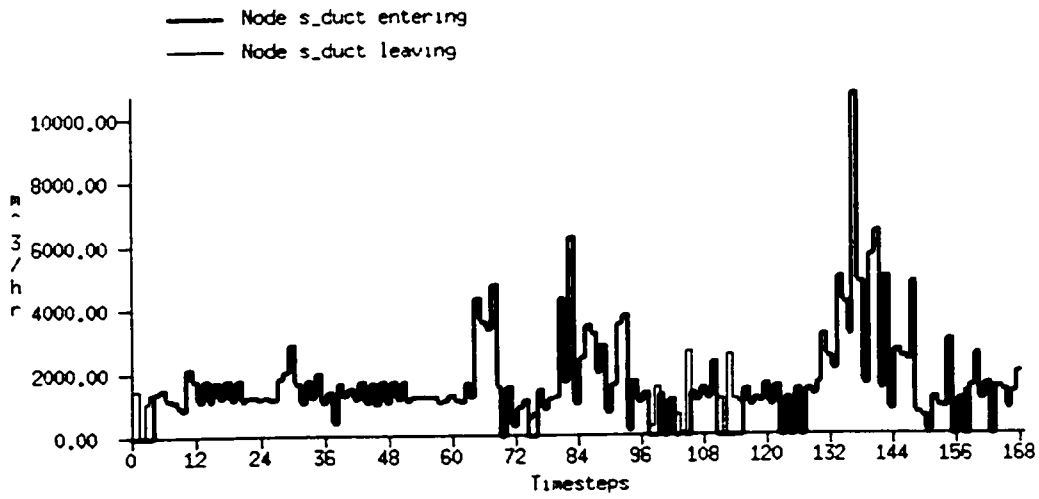

< supplied airflow rate via SW-facing louver >

Figure 5.4 Airflows from three separate air-intake louvers (Unit: m^3/h, outputs from the integrated simulation with zone temperature control by radiator)

The pressure losses through mechanical components such as heat exchanger turned out to be substantial. This effect can be observed by performing one more simulation. This was carried out on the basis of the integrated simulation without zone temperature control

discussed in Section 4.4.3. but at this time three main mechanical components (e.g. filter. heating coil and heat exchanger) were deleted from the airflow-network. The airflow results were compared to the earlier simulation results that appeared in Section 4.3.3. and for the purpose of simple comparison airflows of exhaust tower part for these two simulations were presented in Figure 5.5. The results indicated that airflows could increase significantly without these mechanical components.

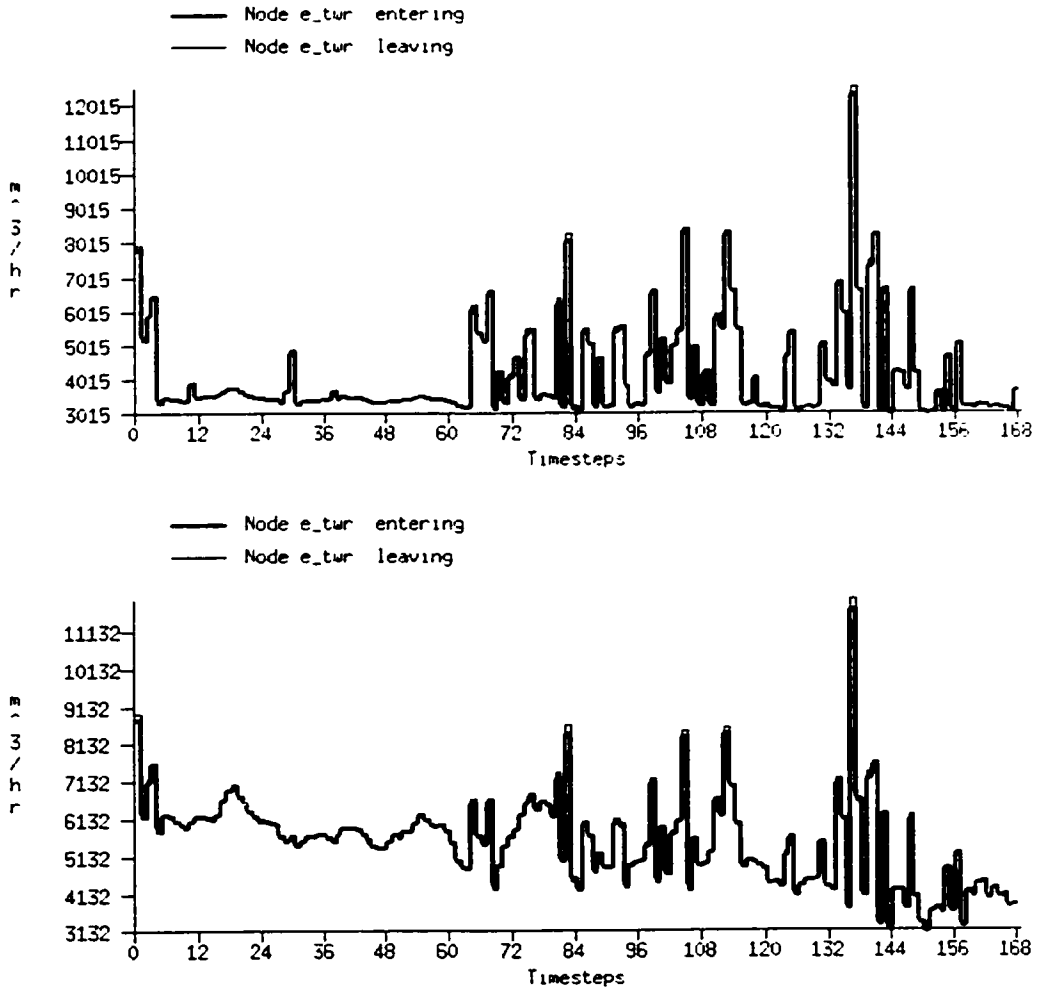

Figure 5.5 Comparison of airflows through exhaust tower between two simulations (Here. the first one is considering mechanical components. but the second is not.)

5.1.2 Thermal performance

Simulation results from section 4.4.1 represent the building's thermal characteristic assuming no ventilation and infiltration throughout the time period. In general, the room temperatures tend to be higher during the day, and become less during the night due to the ambient temperature difference between day and night and the existence of internal load and solar radiation for daytime. From Figure 4.4 of Chapter 4, it can be observed that this effect is less pronounced during weekend that has no internal gains. The temperature of the exhaust channel is free-floating between 0 °C and 7 °C, which is much higher than ambient air. It is apparent that the transparent roof of the exhaust channel is increasing the air temperature to a certain extent.

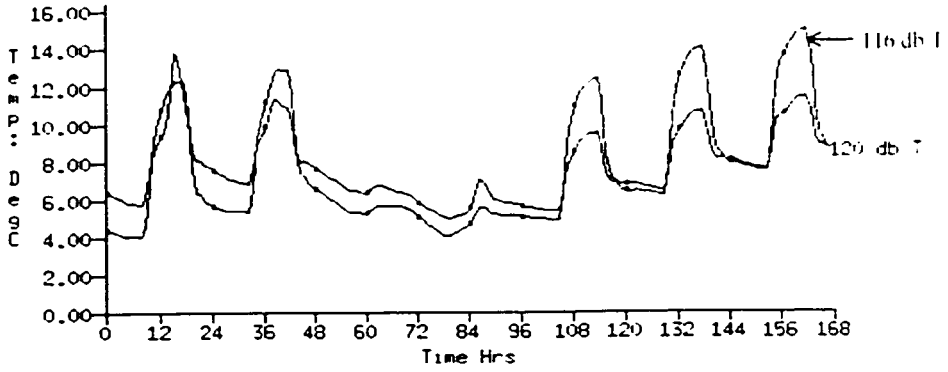

Figure 5.6 Output from the building thermal simulation (Unit: °C, *120*: classroom, *116*: group activity room)

Also from the building thermal simulation, it can be seen that the common rooms located in the southern side of the building (e.g. room 116, 129, or 130) show a little higher room temperature pattern compared to the classrooms located in the northern side of the

building because of the solar radiations. This can be well observed by Figure 5.6. which shows another output from the building thermal simulation. According to SINTEF and NTNU (1997), the initial intention of the design was to make the classrooms have no need for cooling or shading system for daytime by locating them on the northern side of the building even though this might increase heating load during winter time.

The ventilation load can be estimated from the integrated simulation. The following (Figure 5.7) shows sensible heating load of the "heating coil unit section" from the integrated simulation with zone temperature control by radiator (Section 4.3.3). The maximum ventilation heating load is estimated as about *55 kW*.

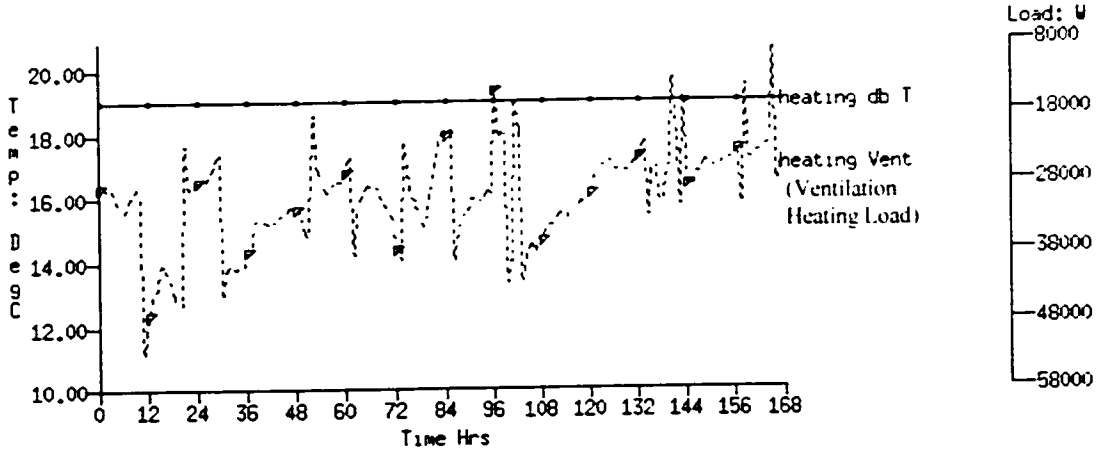

Figure 5.7 Ventilation heating load (Unit: *W*)

5.2 Validation

The validation process is based on the comparison of the simulated results with some measured data. Some building performance parameters were measured by SINTEF and NTNU as a part of project for evaluating the building's indoor condition. This covers

minutely measured values of temperature at underground culvert, room 129, 130 and 131, and exhaust channel, as well as pressure difference in several flow points. The time series of the measurements is exactly same as that of the weather data (from Feb. 1st to 28th, 2001 with one minute interval). During the measurements the building was set to keep the temperature level all day (no night time temperature reduction). The measured data showed that room temperatures were being kept at set-point temperature (e.g. 22 °C) with deviation of *-3 °C* and *-1 °C*, representing tendency of a little overheating during daytime. However, it is difficult to compare these room temperatures with predicted values by ESP-r because both of them are intentionally controlled values and their variation ranges are too small to be compared.

One possible parameter available for the comparison is exhaust channel temperature. Since exhaust channel is free-floating according to the outdoor conditions as well as incoming ventilated air, it would be interesting to perform a comparison between its measured and predicted temperatures for a given time period. The first comparison was performed based on a weekend time period (e.g. Sunday, Feb. 11th, 2001) during which the school was unoccupied. The second comparison was on a weekday time period (e.g. Tuesday, Feb. 13th, 2001). Shown in the Figure 5.8 are comparisons of the predicted exhaust channel temperature (based on the integrated simulation with zone temperature control by radiator) with the measured value for 24-hour time period.

The first comparison shows that the prediction by ESP-r approaches to the measured data within *2.2 °C*. The discrepancy is much smaller during daytime. However, in the second

comparison the predicted values give less convergence to measured data. One possible reason for this discrepancy is the action of CO_2 controller during weekday, making different performance of exhaust dampers in actual operation compared to prediction. On the other hand, during weekend the CO_2 level in the building is relatively low because of no occupancy, which means CO_2 sensors have no influence on the building controllers in real operation.

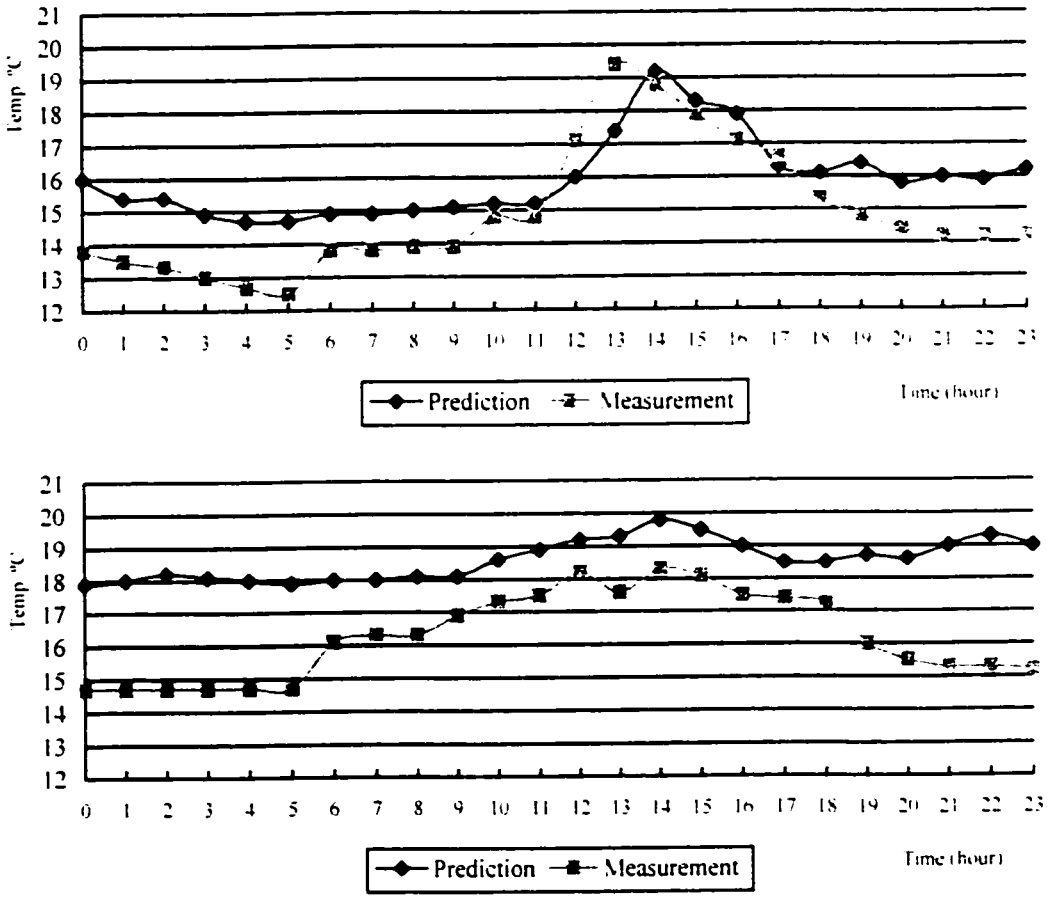

Figure 5.8 Comparison of the simulated temperatures of the exhaust channel with measured data (The first one is based on a weekend, and the second one is on a weekday time period.)

The measured indoor and ambient data could be suspected. However, the measurement itself is considered reliable because when looking at them, minutely variation of the measured temperature is within ± 0.1 °C, which represents good accuracy of the measurement. The wind speed and direction were measured *10 m* above ground level at western end of the building to make similar condition as meteorological station.

5.3 Accuracy of the simulation

This section deals with discussions about accuracy of the simulation that could happen throughout this research. Computer simulation of a building and its plant may be considered as a two-step process: modeling of the real physical processes at play that allows the problem to be solved more easily within practical limitations, and numerical solution of the model. Both steps involve many simplifications and assumptions, and are likely to introduce errors in the resultant solution. The remaining of this chapter focuses on finding possible sources of those errors.

First of all, the heat and mass transfer mechanisms employed in ESP-r could be different from actual situations. As mentioned in Chapter 3, ESP-r's basic heat transfer mechanism is to treat heat transfer through the opaque fabric as one dimensional conduction only problem with constant thermophysical properties. However, in actual situation two and three dimensional conduction effects are assumed and also the thermophysical properties could vary dynamically with temperature. When it comes to the airflow mechanism, the basic assumption of the airflow modeling in ESP-r is well-mixed condition that assumes

uniform temperature in a zone. However, it is hard to consider the model building has uniform room temperature because it is using displacement ventilation concept. It should be noted however that inaccurate prediction results are not always due to the theory or coding of the program itself.

One possible factor to cause prediction error is the difference between the actual thermal and physical properties of the building and input values. For example the properties of the window such as conductivity and solar transmittance are difficult to predict accurately because they are different for different manufactures. However, when performing some parametric sensitivity analysis, the effects of changing U-values of a building envelope within *10 %* are not significant both in airflow and thermal results. The imposed internal heat gains (occupant, light, and equipment loads) might be a little different from actual situation. Particularly, occupant's behaviors and those effects in a building seem to be more difficult to predict.

Aside from the error sources mentioned above, it is also worthy mentioning that essentially predicted results are affected by the modeling process itself. This means that the simulated results are definitely dependant on the skills of the user's abstracting the essence of the problem into a model, choosing appropriate flow or plant components, setting up suitable controls. The effects of choosing different flow components and controls on resultant outputs may be observed by performing more parametric sensitivity analysis. However, due to the time limitation for the current research, this task will also require future work.

CHAPTER 6

CONCLUSION

6.1 Conclusion

This thesis has dealt with computer simulation of a hybrid-ventilated building. A building having hybrid ventilation technologies is considered as a very complicated dynamic energy system, consisting of building, HVAC plant, solar energy features, and dynamic outdoor conditions. To predict the performance of such a configuration, a dynamic thermal simulation tool, ESP-r has been used for the extensive parametric simulations. A newly constructed school building in Norway was used for the simulation study. The simulations and their analysis focused on the building's thermal interactions and airflow movements.

From this perspective, the main objective of this thesis is to investigate the capability of the ESP-r for the simulation of a real building utilizing hybrid ventilation concept. In this thesis, the school building has been simulated in three different categories: building thermal simulation, airflow simulation, and building + airflow integrated simulation.

From the building thermal simulation, it could be observed that the building responded properly to the dynamic outdoor conditions and some imposed internal heat loads. The airflow simulation provided natural ventilation characteristics of the building for a typical winter time period. The predicted airflow rate through the main supply duct fluctuated

near *2,600 m^3/h*, and ventilation performance of the classrooms was between *0.7* and *1.1 ACH* for a typical winter season. The building's hybrid ventilation performance could be predicted by building + airflow integrated simulation with proper control strategies. The resultant airflow rate through a zone experienced rapid fluctuation due to the actions of both supply fan and exhaust damper that were continuously adjusted by imposed on/off or proportional control mode. The air change per hour was roughly estimated to be between *1.0 ~ 2.5* for classrooms, *1.0 ~ 6.0* for locker rooms, and *2.0 ~ 4.0* for corridor. The heating load of both heating coil and radiators could be estimated from simulations with ideal controllers. The air temperature of exhaust channel was compared to the measured data. The first comparison, based on a weekend time period, showed that the prediction by ESP-r approached to the measured data within *2.2* °C. However, the discrepancy was a little higher from the second comparison based on a weekday time period. From the discussion, the action of CO_2 sensors in actual operation was suspected to be a main factor for causing different results between two comparisons. The maximum heating load for the ventilation was estimated as *55 kW* from the integrated simulation.

The discussions from Chapter 5 indicate that it is now feasible and practical to solve a complex building / plant / flow-network for the hybrid ventilation system. This is due to the capabilities of ESP-r that enables an integrated approach for modeling a building, flow-network, environmental control system, and plant. On the other hand, this research also points out that in order to allow for the implementation of much more realistic modeling to ESP-r, more control regimes, for example CO_2 controller should be developed. In addition, the maximum number of zones and flow-connections allowed in

ESP-r should be expanded for modeling of more complicated building and its flow components.

This thesis concludes that modeling of hybrid ventilation systems is now possible by ESP-r's integral approach and the resultant outputs are feasible and practical in terms of both thermal and ventilation point of view, but at the same time limitations do exist when it attempts to model really complex buildings and to model CO_2 based control systems.

6.2 Future work

It might be considered that the present work is merely a step toward complete simulation of the hybrid-ventilated building. A lot of work remains to be done. Most of all, it is necessary to simulate the model building for a summer time period, focusing the study on cooling by hybrid ventilation. In addition, some efforts should be directed towards performing intensive parametric sensitivity analysis for the better understanding of ESP-r.

Last, the present work did not cover modeling of the heat recovery system (air-to-water heat exchanger). This kind of simulation requires detailed information on water circulation system (e.g. pipe, pump, fittings, etc.) as well as information on the heat exchanger itself (e.g. overall heat transfer coefficient, heat exchange area, etc). If these kinds of information are provided, more specific approach to estimating energy consumption of the building could be attempted.

REFERENCES

1. ASHRAE (1975) "Procedures for simulating the performance of components and system for energy calculations", ASHRAE (American Society of Heating. Refrigerating and Air-conditioning Engineers)

2. ASHRAE (1997) "1997 ASHRAE Handbook - Fundamentals", ASHRAE (American Society of Heating. Refrigerating and Air-conditioning Engineers)

3. D. Etheridge (1996) "Building Ventilation – Theory and Measurement", John Wiley & Sons (U.K.)

4. E. Simiu and R. H. Scanlan (1986). "Wind effects on structures: an introduction to wind engineering", Wiley - Interscience. Chichester (UK)

5. E. O. Aasem et al. (1994). "Current systems modeling potential of ESP-r", ESRU (Energy Simulation Reseach Unit), University of Strathclyde (UK)

6. E. O. Aasem (1993), "Practical simulation of buildings and air-conditioning systems in the transient domain", Ph.D. Thesis, University of Strathclyde (UK)

7. ESRU (1997), "The ESP-r system for building energy simulation user guide version 9 series", Energy System Research Unit, University of Strathclyde (UK)

8. F. Haghighat (1989), "Air infiltration and indoor air quality models – a review", International Journal of Ambient Energy Vol.10, pp. 115-122

9. F. Haghighat and A. C. Megri (1996), "A comprehensive validation of two airflow models – COMIS and CONTAM", Indoor Air 1996; 6, pp.278-288

10. G. N. Walton et al. (2000), "CONTAMW 1.0 User Manual", NIST (National Institute of Standards and Technology), U.S.A.

11. H. B. Awbi (1991) "Ventilation of Buildings", E & FN SPON (U.K.)

12. H. Lee (2002), "Validation of three multi-zone airflow models", M.A.Sc. Thesis, Concordia University (Canada)

13. Ian Beausoleil-Morrison (2000), "The adaptive coupling of heat and air flow modeling within dynamic whole–building simulation", Ph.D. Thesis, University of Strathclyde (UK)

14. IEA Annex 35 (2000), "Annex 35 HybVent - Hybrid Ventilation", IEA (International Energy Agency) - ECBCS (Energy Conservation in Buildings and Community Systems), Aalborg Technical University (Denmark)

15. J. A. Clark (1985), "Energy simulation in building design", Adam Hilger Ltd., Bristol (UK)

16. Jan L.M. Hensen (1991). "On the thermal interaction of building structure and heating and ventilation system", Ph.D. thesis, Technische Universiteit Eindhoven (OO)

17. Jan L. M. Hensen and J. W. Hand (1993). "Use of sophisticated building energy simulation tools", Proceeding of 3rd European Conference on Architecture "Solar energy in architecture and urban planning", pp. 354-357

18. Jan L.M. Hensen (1994). "Modelling coupled heat and air flow: ping-pong vs onion", ESRU (Energy Simulation Reseach Unit), University of Strathclyde (UK)

19. Jan L.M. Hensen (1995). "On system simulation for building performance evaluation", Proceeding of 4th IBPSA World Congress on Building Simulation, pp. 259-267

20. J. A. Fox (1977) "An Introduction to Engineering Fluid Mechanics", The Macmillan Press Ltd. (U.K.)

21. J. P. Chastain et al. (1987) "Computation of discharge coefficients for Laminar flow in rectangular and circular openings", ASHRAE Transaction 1987 Part 2 (U.S.A.)

22. M. W. Liddament (1986), "Air infiltration calculation techniques – an application guide", IEA (International Energy Agency) - AIVC (Air Infiltration And Ventilation Centre), Bracknell (UK)

23. R. M. Olson (1980) "Essential of Engineering Fluid Mechanics", Harper & Row Publishers (U.S.A.)

24. R. L. Mott (1979) "Applied Fluid Mechanics", Charles E. Merrill Publishing Company (U.S.A.)

25. SINTEF and NTNU (1997). "The Grong school in Norway", Project report. SINTEF (The Foundation for the Scientific and Industrial Research at the Norweigian Institute of Technology) and NTNU (Norweigian University of Science and Technology)

26. Willem de Gids (2001), "Hybrid ventilation concepts classification and challenges", Proceedings of the 4th International Conference on Indoor Air Quality, Ventilation & Energy Conservation in Buildings Vol. 1, pp.133-139

27. William J. Kosik (2001), "ASHRAE (American Society of Heating, Refrigerating and Air-conditioning Engineers) Journal", October 2001, pp.18-24

APPENDICES

Appendix A

Summary of Zones

Zones		Floor Area (m^2)	Volume (m^3)	Opaque surface area (m^2)	Transparent surface area (m^2)
Name	Details				
Supply duct	Underground supply air duct from air intake tower to heating coil unit section	36.00	72.00	141.60	0.00
Heating coil unit	Heating coil unit section	3.00	6.00	20.60	0.00
Culvert	Underground culvert for fresh air distribution into the rooms	157.54	315.08	588.49	0.00
Room #102	Locker room	51.51	160.65	189.33	5.10
Room #103	Locker room	53.53	166.95	194.50	5.30
Room #110	Laundry room	12.96	42.12	75.29	0.00
Room #112	Storage	12.75	41.70	74.04	4.05
Room #113	Storage	12.02	40.72	72.68	3.89
Room #116	Group activity room	11.44	37.19	67.74	2.38
Room #119	Classroom	78.54	274.90	250.31	34.68
Room #120,121	Classroom	120.12	420.43	354.29	53.04
Room #122,123	Classroom	120.12	420.43	354.29	53.04
Room #124,125	Classroom	123.02	436.29	371.05	53.43
Room #126	Classroom	60.06	210.20	204.09	26.52
Room #129	Group activity room	14.40	46.80	69.69	10.50
Room #130	Group activity room	12.00	39.12	64.61	7.50
Room #131	Group activity room	23.52	76.45	97.01	14.21
Room #134	Locker room	50.50	157.50	186.75	5.00
Corridor	Corridor	261.34	847.83	997.01	21.00
Exhaust channel	Exhaust channel above the corridor	160.54	333.14	386.80	159.72
Exhaust tower	Air exhaust tower	10.57	42.28	77.10	0.00

Appendix B

Construction Details of the Building

Exterior wall				
Material	Thickness (mm)	Conductivity (W/mK)	Density (kg/m^3)	Specific heat (J kgK)
Brick	100	0.96	2000	650
Air layer	48	-	-	-
Plywood board	12	0.15	700	1420
Glass wool	150	0.04	250	840
Vapor barrier	0.2	-	-	-
Gypsum board	12	0.19	950	840
Roof				
Material	Thickness (mm)	Conductivity (W/mK)	Density (kg/m^3)	Specific heat (J kgK)
Aluminum plate	2	210	2700	880
Air layer	12	-	-	-
Plywood board	12	0.15	700	1420
Glass wool	350	0.04	250	840
Vapor barrier	0.2	-	-	-
Gypsum board	12	0.19	950	840
Floor				
Material	Thickness (mm)	Conductivity (W/mK)	Density (kg/m^3)	Specific heat (J kgK)
Concrete	100	1.4	2100	653
Sand	50	1.83	2200	712
Ceiling				
Material	Thickness (mm)	Conductivity (W/mK)	Density (kg/m^3)	Specific heat (J kgK)
Wood board	12	0.18	700	2390
Air layer	240	-	-	-
Gypsum board	12	0.19	950	840
Underground wall				
Material	Thickness (mm)	Conductivity (W/mK)	Density (kg/m^3)	Specific heat (J/kgK)
Concrete	180	1.4	2100	653
Interior wall				
Material	Thickness (mm)	Conductivity (W/mK)	Density (kg/m^3)	Specific heat (J/kgK)
Gypsum board	12	0.19	950	840
Glass wool	150	0.04	250	840
Gypsum board	12	0.19	950	840
Door				
Material	Thickness (mm)	Conductivity (W/mK)	Density (kg/m^3)	Specific heat (J/kgK)
Wood	35	0.18	700	2390
Window				
Material	Thickness (mm)	U-value (W/m^2K)	Others	
Double glazing window	4-12-4	1.14	Clear glass, Argon-gas filled	

Appendix C

Weather Data

Date	Time	outdoor temp. [°C]	diffuse radiation [W/m^2]	direct radiation [W/m^2]	wind speed [m/s]	wind direction [clockwise from N]
2/8/2001	00:00:00	-7.2000	11.7812	0.0000	4.2021	116.4375
2/8/2001	01:00:00	-7.1500	11.7812	0.0000	2.2219	118.1250
2/8/2001	02:00:00	-6.9000	11.7812	0.0000	2.4517	134.8875
2/8/2001	03:00:00	-6.7000	11.7812	0.0000	2.9440	134.8875
2/8/2001	04:00:00	-6.4500	11.7812	0.0000	0.7560	202.0500
2/8/2001	05:00:00	-6.0000	11.7812	0.0000	0.7122	247.0500
2/8/2001	06:00:00	-4.9500	11.7812	0.0000	0.3293	69.6375
2/8/2001	07:00:00	-4.5500	11.7812	0.0000	0.6356	112.3875
2/8/2001	08:00:00	-3.7500	11.7812	0.0000	1.1279	89.6625
2/8/2001	09:00:00	-3.9500	12.1875	18.3618	1.0842	113.7375
2/8/2001	10:00:00	-4.2000	118.2188	114.4568	1.4233	247.0500
2/8/2001	11:00:00	-4.1000	121.8750	97.6597	0.3293	292.1625
2/8/2001	12:00:00	-2.8000	71.9063	57.0342	0.3293	292.0500
2/8/2001	13:00:00	-2.1000	89.7813	69.5344	0.3293	269.5500
2/8/2001	14:00:00	-1.1500	361.5625	232.4271	0.3293	157.2750
2/8/2001	15:00:00	-1.8500	41.8437	29.2995	0.3293	314.6625
2/8/2001	16:00:00	-3.4500	11.7812	5.8617	0.3403	202.1625
2/8/2001	17:00:00	-4.5500	11.7812	0.0000	0.3184	67.3875
2/8/2001	18:00:00	-4.9000	11.7812	0.0000	0.3184	134.8875
2/8/2001	19:00:00	-4.1500	11.7812	0.0000	0.3184	45.0000
2/8/2001	20:00:00	-3.8500	11.7812	0.0000	0.5591	45.0000
2/8/2001	21:00:00	-3.7000	11.7812	0.0000	0.3184	45.0000
2/8/2001	22:00:00	-3.4000	11.7812	0.0000	0.3293	45.0000
2/8/2001	23:00:00	-3.0500	11.7812	0.0000	0.3293	45.0000
2/9/2001	00:00:00	-3.4000	11.7812	0.0000	0.3293	45.0000
2/9/2001	01:00:00	-3.2500	11.7812	0.0000	0.3293	45.0000
2/9/2001	02:00:00	-2.9500	11.7812	0.0000	0.3293	45.0000
2/9/2001	03:00:00	-1.7000	11.7812	0.0000	1.3249	202.1625
2/9/2001	04:00:00	-1.3000	11.7812	0.0000	1.3249	247.1625
2/9/2001	05:00:00	-1.2500	11.7812	0.0000	2.0469	246.9375
2/9/2001	06:00:00	-1.4500	11.7812	0.0000	0.3293	148.8375
2/9/2001	07:00:00	-1.9000	11.7812	0.0000	0.3293	67.9500
2/9/2001	08:00:00	-2.0500	11.7812	0.0000	0.3293	269.5500
2/9/2001	09:00:00	-2.1500	11.7812	3.9085	0.4715	247.0500

2/9/2001	10:00:00	-1.6500	11.7812	18.7525	0.7779	247.0500
2/9/2001	11:00:00	-1.3500	24.3750	46.4872	0.3293	67.5000
2/9/2001	12:00:00	-0.2000	181.5938	269.9276	1.1061	135.0000
2/9/2001	13:00:00	0.7000	65.0000	117.1912	1.1936	140.1750
2/9/2001	14:00:00	0.5000	11.7812	26.9557	0.3621	113.7375
2/9/2001	15:00:00	0.3000	11.7812	18.7525	0.6247	202.2750
2/9/2001	16:00:00	0.2000	11.7812	3.1273	0.9310	135.1125
2/9/2001	17:00:00	-0.0500	11.7812	0.0000	0.3293	224.6625
2/9/2001	18:00:00	0.1500	11.7812	0.0000	0.3293	45.0000
2/9/2001	19:00:00	0.1500	11.7812	0.0000	0.3293	45.2250
2/9/2001	20:00:00	0.5500	11.7812	0.0000	0.3293	151.2000
2/9/2001	21:00:00	0.5000	11.7812	0.0000	0.4168	89.8875
2/9/2001	22:00:00	0.4000	11.7812	0.0000	0.3512	247.1625
2/9/2001	23:00:00	-0.2000	11.7812	0.0000	0.3293	112.3875
2/10/2001	00:00:00	-0.9500	11.7812	0.0000	0.3293	247.0500
2/10/2001	01:00:00	-1.8500	11.7812	0.0000	0.3293	247.0500
2/10/2001	02:00:00	-1.1000	11.7812	0.0000	0.3293	269.5500
2/10/2001	03:00:00	-2.4500	11.7812	0.0000	0.3293	89.8875
2/10/2001	04:00:00	-2.1000	11.7812	0.0000	0.3293	224.6625
2/10/2001	05:00:00	-3.8000	11.7812	0.0000	0.3293	157.2750
2/10/2001	06:00:00	-4.6000	11.7812	0.0000	0.3184	269.5500
2/10/2001	07:00:00	-3.3500	11.7812	0.0000	0.3293	292.0500
2/10/2001	08:00:00	-3.0500	11.7812	0.0000	0.3293	228.8250
2/10/2001	09:00:00	-3.1500	11.7812	0.0022	0.6466	135.0000
2/10/2001	10:00:00	-3.3000	11.7812	8.2055	0.6247	69.5250
2/10/2001	11:00:00	-2.1500	13.8125	23.0494	0.3293	224.6625
2/10/2001	12:00:00	-0.6500	63.7812	75.3938	0.3621	291.9375
2/10/2001	13:00:00	1.3500	11.7812	25.3932	0.3403	135.0000
2/10/2001	14:00:00	1.6500	11.3750	21.8775	0.3293	45.0000
2/10/2001	15:00:00	1.8500	11.3750	15.6274	0.5153	223.8750
2/10/2001	16:00:00	1.8000	11.3750	0.3929	2.9877	247.1625
2/10/2001	17:00:00	1.7000	11.7812	0.0000	2.4845	247.1625
2/10/2001	18:00:00	1.4500	11.7812	0.0000	2.2766	247.1625
2/10/2001	19:00:00	1.4500	11.7812	0.0000	3.3925	247.1625
2/10/2001	20:00:00	0.3500	11.7812	0.0000	0.4825	134.8875
2/10/2001	21:00:00	-0.8000	11.7812	0.0000	1.4999	135.2250

2/10/2001	22:00:00	-2.0500	11.7812	0.0000	0.6028	135.0000
2/10/2001	23:00:00	-3.3000	11.7812	0.0000	1.4014	135.0000
2/11/2001	00:00:00	-4.5500	11.7812	0.0000	1.6640	135.0000
2/11/2001	01:00:00	-5.6000	11.7812	0.0000	0.3950	135.0000
2/11/2001	02:00:00	-6.2500	11.7812	0.0000	2.1125	134.8875
2/11/2001	03:00:00	-6.6000	11.7812	0.0000	2.2329	134.8875
2/11/2001	04:00:00	-7.1000	11.7812	0.0000	1.2264	178.5375
2/11/2001	05:00:00	-7.1500	11.7812	0.0000	1.1389	125.7750
2/11/2001	06:00:00	-6.2500	11.7812	0.0000	0.4825	155.8125
2/11/2001	07:00:00	-4.5500	11.7812	0.0000	0.3293	179.7750
2/11/2001	08:00:00	-2.3000	11.7812	0.0000	2.8455	226.4625
2/11/2001	09:00:00	-1.8000	11.7812	5.8617	1.2155	270.2250
2/11/2001	10:00:00	-1.3500	11.7812	23.0494	4.5303	247.1625
2/11/2001	11:00:00	-0.9000	12.1875	53.1279	0.3293	67.3875
2/11/2001	12:00:00	0.3000	160.8750	391.8041	2.8674	189.0000
2/11/2001	13:00:00	0.3000	81.2500	266.4119	2.8674	202.2750
2/11/2001	14:00:00	-0.2500	15.8437	66.8000	1.9922	224.6625
2/11/2001	15:00:00	0.4500	12.5937	46.8778	1.9594	186.8625
2/11/2001	16:00:00	0.7000	11.7812	3.9085	1.6859	224.6625
2/11/2001	17:00:00	0.9000	11.7812	0.0000	0.9638	112.3875
2/11/2001	18:00:00	1.0000	11.7812	0.0000	0.5919	148.2750
2/11/2001	19:00:00	0.8000	11.7812	0.0000	2.3095	226.0125
2/11/2001	20:00:00	0.7500	11.7812	0.0000	2.3751	224.6625
2/11/2001	21:00:00	0.5500	11.7812	0.0000	1.3358	135.0000
2/11/2001	22:00:00	0.2000	11.7812	0.0000	0.4825	247.2750
2/11/2001	23:00:00	0.0500	11.7812	0.0000	0.4606	179.6625
2/12/2001	00:00:00	-0.1000	11.7812	0.0000	1.1279	171.5625
2/12/2001	01:00:00	-0.2500	11.7812	0.0000	1.8281	135.0000
2/12/2001	02:00:00	-0.3000	11.7812	0.0000	3.1409	135.0000
2/12/2001	03:00:00	-0.2500	11.7812	0.0000	1.2592	112.3875
2/12/2001	04:00:00	-0.4000	11.7812	0.0000	2.1016	134.8875
2/12/2001	05:00:00	-0.3500	11.7812	0.0000	1.7078	157.2750
2/12/2001	06:00:00	-0.4500	11.7812	0.0000	1.9813	135.0000
2/12/2001	07:00:00	-0.5500	11.7812	0.0000	2.2766	135.0000
2/12/2001	08:00:00	-0.6500	11.7812	0.0000	4.4428	135.0000
2/12/2001	09:00:00	-0.3500	11.7812	7.8148	1.1826	118.4625

2/12/2001	10:00:00	0.0000	12.1875	23.8307	2.4954	157.2750
2/12/2001	11:00:00	0.2500	45.0938	55.4717	0.8107	135.0000
2/12/2001	12:00:00	0.7000	62.5625	76.9563	1.9047	157.8375
2/12/2001	13:00:00	0.8000	17.0625	33.2058	2.0688	179.1000
2/12/2001	14:00:00	0.9000	16.6562	35.9402	2.5064	137.8125
2/12/2001	15:00:00	0.8500	11.7812	24.2213	2.2985	134.8875
2/12/2001	16:00:00	0.8500	11.7812	8.5961	4.3115	135.0000
2/12/2001	17:00:00	0.8500	11.7812	0.0000	3.0753	135.0000
2/12/2001	18:00:00	0.9500	11.7812	0.0000	2.2985	135.0000
2/12/2001	19:00:00	0.9500	11.7812	0.0000	0.7669	135.0000
2/12/2001	20:00:00	1.0500	11.7812	0.0000	1.2155	157.2750
2/12/2001	21:00:00	1.1000	11.7812	0.0000	1.4124	135.0000
2/12/2001	22:00:00	1.2000	11.7812	0.0000	0.3293	202.2750
2/12/2001	23:00:00	2.1500	11.3750	0.0000	0.4715	132.4125
2/13/2001	00:00:00	3.3000	11.3750	0.0000	0.9967	47.0250
2/13/2001	01:00:00	3.2000	11.3750	0.0000	0.7888	72.2250
2/13/2001	02:00:00	3.2000	11.3750	0.0000	2.2329	67.3875
2/13/2001	03:00:00	3.0500	11.3750	0.0000	2.1782	88.0875
2/13/2001	04:00:00	2.9500	11.3750	0.0000	2.5173	112.0500
2/13/2001	05:00:00	2.4000	11.3750	0.0000	0.9638	94.1625
2/13/2001	06:00:00	2.6500	11.3750	0.0000	2.4298	67.3875
2/13/2001	07:00:00	2.4500	11.3750	0.0000	0.7669	135.0000
2/13/2001	08:00:00	2.4000	11.3750	0.0022	0.7888	202.2750
2/13/2001	09:00:00	2.7000	11.3750	6.2523	0.3293	224.7750
2/13/2001	10:00:00	3.0000	26.0000	23.0494	2.2438	247.1625
2/13/2001	11:00:00	4.0500	33.7187	28.1276	1.4452	226.8000
2/13/2001	12:00:00	4.1500	50.7812	37.8933	1.3030	224.6625
2/13/2001	13:00:00	4.1500	43.4688	33.9870	3.8520	271.4625
2/13/2001	14:00:00	4.1000	27.6250	25.7838	2.8893	247.1625
2/13/2001	15:00:00	4.0500	11.3750	10.1586	5.4383	292.1625
2/13/2001	16:00:00	4.3000	11.3750	1.1741	7.9436	244.3500
2/13/2001	17:00:00	4.4000	11.3750	0.0000	4.0270	203.1750
2/13/2001	18:00:00	4.7000	11.3750	0.0000	0.3293	212.4000
2/13/2001	19:00:00	5.6500	11.3750	0.0000	3.9176	247.1625
2/13/2001	20:00:00	5.9000	11.3750	0.0000	4.3662	224.7750
2/13/2001	21:00:00	6.2500	11.3750	0.0000	1.0185	64.6875

2/13/2001	22:00:00	6.3000	11.3750	0.0000	3.4910	247.1625
2/13/2001	23:00:00	6.5000	11.3750	0.0000	0.3293	72.5625
2/14/2001	00:00:00	6.4000	11.3750	0.0000	1.9484	269.6625
2/14/2001	01:00:00	6.5000	11.3750	0.0000	1.8609	273.4875
2/14/2001	02:00:00	6.3500	11.3750	0.0000	1.4233	247.1625
2/14/2001	03:00:00	6.3500	11.3750	0.0000	3.4582	248.1750
2/14/2001	04:00:00	6.2000	11.3750	0.0000	1.7734	335.0250
2/14/2001	05:00:00	6.1500	11.3750	0.0000	1.3467	74.7000
2/14/2001	06:00:00	6.1500	11.3750	0.0000	3.3597	72.3375
2/14/2001	07:00:00	6.1000	11.3750	0.0000	0.5591	241.7625
2/14/2001	08:00:00	6.0000	11.3750	0.0000	1.6093	313.0875
2/14/2001	09:00:00	6.0000	11.3750	1.5647	0.3621	334.8000
2/14/2001	10:00:00	6.0500	11.3750	7.4242	2.0250	247.1625
2/14/2001	11:00:00	6.2500	18.2812	21.8775	2.5173	67.5000
2/14/2001	12:00:00	6.4000	12.1875	13.2836	2.5392	79.7625
2/14/2001	13:00:00	6.3500	37.7812	34.3777	4.6616	66.4875
2/14/2001	14:00:00	6.2000	11.3750	10.1586	2.4189	292.2750
2/14/2001	15:00:00	6.1500	11.3750	7.0336	3.8411	292.1625
2/14/2001	16:00:00	6.2500	11.3750	0.0000	0.6356	248.4000
2/14/2001	17:00:00	6.4500	11.3750	0.0000	0.5262	70.4250
2/14/2001	18:00:00	6.6000	11.3750	0.0000	3.6660	69.3000
2/14/2001	19:00:00	6.5500	11.3750	0.0000	0.9529	67.3875
2/14/2001	20:00:00	6.4500	11.3750	0.0000	2.1891	292.3875
2/14/2001	21:00:00	6.4000	11.3750	0.0000	0.9638	71.7750
2/14/2001	22:00:00	6.4000	11.3750	0.0000	1.1279	334.8000
2/14/2001	23:00:00	6.3000	11.3750	0.0000	1.4671	269.7750

Appendix D

Details of the Airflow-Network

Components		Start node (node 1)	h1 (h_{comp}-h_{node1})	End node (node 2)	h2 (h_{comp}-h_{node2})
Name	Details				
Air intake louver (N)	Opening (A=0.62m^2)	Exterior (N)	0.0m	Supply duct	3.5m
Air intake louver (SW)	Opening (A=0.62m^2)	Exterior (SW)	0.0m	Supply duct	3.5m
Air intake louver (SE)	Opening (A=0.62m^2)	Exterior (SE)	0.0m	Supply duct	3.5m
Filter	Power law component (coefficient a=0.41, exponent b=0.7)	Supply duct	1.0m	Heating coil unit section	-1.0m
Heating coil	Power law component (coefficient a=0.35, exponent b=0.7)	Heating coil unit section	0.0m	Underground culvert	0.0m
Air inlet to room 119	Opening (A=0.05m^2×4=0.2m^2)	Underground culvert	1.0m	Room 119	-1.75m
Air inlet to room 120,121	Opening (A=0.05m^2×8=0.4m^2)	Underground culvert	1.0m	Room 120,121	-1.75m
Air inlet to room 122,123	Opening (A=0.05m^2×8=0.4m^2)	Underground culvert	1.0m	Room 122,123	-1.75m
Air inlet to room 124,125	Opening (A=0.05m^2×8=0.4m^2)	Underground culvert	1.0m	Room 124,125	-1.75m
Air inlet to room 126	Opening (A=0.05m^2×4=0.2m^2)	Underground culvert	1.0m	Room 126	-1.75m
Air inlet to room 116	Opening (A=0.05m^2×2=0.1m^2)	Underground culvert	1.0m	Room 116	-1.63m
Air inlet to room 129	Opening (A=0.05m^2×2=0.1m^2)	Underground culvert	1.0m	Room 129	-1.63m
Air inlet to room 130	Opening (A=0.05m^2×2=0.1m^2)	Underground culvert	1.0m	Room 130	-1.63m
Air inlet to room 131	Opening (A=0.05m^2×2=0.1m^2)	Underground culvert	1.0m	Room 131	-1.63m
Air inlet to corridor	Opening (A=0.05m^2×14=0.7m^2)	Underground culvert	1.0m	Corridor	-1.5m
Air outlet from room119	Opening (A=0.18m^2×2=0.36m^2)	Room 119	1.25m	Exhaust channel	-0.75m
Air outlet from 120,121	Opening (A=0.18m^2×4=0.72m^2)	Room 120,121	1.25m	Exhaust channel	-0.75m
Air outlet from 122,123	Opening (A=0.18m^2×4=0.72m^2)	Room 122,123	1.25m	Exhaust channel	-0.75m
Air outlet from 124,125	Opening (A=0.18m^2×4=0.72m^2)	Room 124,125	1.25m	Exhaust channel	-0.75m
Air outlet from 126	Opening (A=0.18m^2×2=0.36m^2)	Room 126	1.25m	Exhaust channel	-0.75m
Air outlet from room 116	Opening (A=0.18m^2×1=0.18m^2)	Room 116	1.37m	Exhaust channel	-0.75m
Air outlet from room 129	Opening (A=0.18m^2×1=0.18m^2)	Room 129	1.37m	Exhaust channel	-0.75m
Air outlet from room 130	Opening (A=0.18m^2×1=0.18m^2)	Room 130	1.37m	Exhaust channel	-0.75m
Air outlet from room 131	Opening (A=0.18m^2×1=0.18m^2)	Room 131	1.37m	Exhaust channel	-0.75m

Components		Start node (node 1)	h1 (h_{comp}-h_{node1})	End node (node 2)	h2 (h_{comp}-h_{node2})
Name	Details				
Air outlet from corridor	Opening ($A=0.18m^2 \times 3=0.54m^2$)	Corridor	1.5m	Exhaust channel	-0.75m
Heat exchanger	Power law component (coefficient a=0.32, exponent b=0.7)	Exhaust channel	0.75m	Exhaust tower	-3.75m
Exhaust tower louver (N)	Opening ($A=0.62m^2$)	Exhaust tower	0.0m	Exterior	0.0m
Exhaust tower louver (SW)	Opening ($A=0.62m^2$)	Exhaust tower	0.0m	Exterior	0.0m
Exhaust tower louver (SW)	Opening ($A=0.62m^2$)	Exhaust tower	0.0m	Exterior	0.0m
Exterior door	Crack (width=0.5mm, length=10.2m)	Exterior (W)	0.0m	Corridor	0.0m
Exterior door	Crack (width=0.5mm, length=10.2m)	Exterior (W)	0.0m	Room 102	0.0m
Exterior door	Crack (width=0.5mm, length=10.2m)	Exterior (E)	0.0m	Room 102	0.0m
Exterior door	Crack (width=0.5mm, length=10.2m)	Exterior (E)	0.0m	Room 103	0.0m
Exterior door	Crack (width=0.5mm, length=10.2m)	Exterior (SW)	0.0m	Corridor	0.0m
Exterior door	Crack (width=0.5mm, length=10.2m)	Exterior (SW)	0.0m	Room 134	0.0m
Exterior door	Crack (width=0.5mm, length=10.2m)	Exterior (NE)	0.0m	Room 134	0.0m
Interior door	Crack (width=1mm, length=6m)	Corridor	0.0m	Room 119	0.0m
Interior door	Crack (width=1mm, length=6m×2=12m)	Corridor	0.0m	Room 120,121	0.0m
Interior door	Crack (width=1mm, length=6m×2=12m)	Corridor	0.0m	Room 122,123	0.0m
Interior door	Crack (width=1mm, length=6m×2=12m)	Corridor	0.0m	Room 124,125	0.0m
Interior door	Crack (width=1mm, length=6m)	Corridor	0.0m	Room 126	0.0m
Interior door	Crack (width=1mm, length=6m)	Room 119	0.0m	Room 120, 121	0.0m
Interior door	Crack (width=1mm, length=6m)	Room 120, 121	0.0m	Room 122,123	0.0m
Interior door	Crack (width=1mm, length=6m)	Room 124, 125	0.0m	Room 126	0.0m
Interior door	Crack (width=1mm, length=6m)	Corridor	0.0m	Room 110	0.0m
Interior door	Crack (width=1mm, length=6m)	Corridor	0.0m	Room 112	0.0m
Interior door	Crack (width=1mm, length=6m)	Corridor	0.0m	Room 113	0.0m
Interior door	Crack (width=1mm, length=6m)	Corridor	0.0m	Room 116	0.0m

Components		Start node (node 1)	h1 (h_{comp}-h_{node1})	End node (node 2)	h2 (h_{comp}-h_{node2})
Name	Details				
Interior door	Crack (width=1mm, length=6m)	Corridor	0.0m	Room 129	0.0m
Interior door	Crack (width=1mm, length=6m)	Corridor	0.0m	Room 130	0.0m
Interior door	Crack (width=1mm, length=6m)	Corridor	0.0m	Room 131	0.0m
Opening	Doorway ($A=2.94m^2$)	Corridor	0.0m	Room 102	0.0m
Opening	Doorway ($A=2.94m^2$)	Corridor	0.0m	Room 103	0.0m
Opening	Doorway ($A=2.94m^2$)	Corridor	0.0m	Room 134	0.0m
Undercut	Opening ($A=0.018m^2$)	Corridor	-0.15m	Room 110	-1.63m
Toilet exhaust fan	Constant flow rate ($10l/s \times 3=30l/s$)	Room 102	1.25m	Exterior (S)	0.0m
Toilet exhaust fan	Constant flow rate ($10l/s \times 3=30l/s$)	Room 103	1.25m	Exterior (S)	0.0m
Toilet exhaust fan	Constant flow rate ($10l/s \times 3=30l/s$)	Room 134	1.25m	Exterior (SE)	0.0m
Laundry room exhaust fan	Constant flow rate ($10l/s$)	Room 110	1.25m	Exterior (E)	0.0m
Main supply fan	Constant flow rate ($10000m^3/h$)	Supply duct	0.0m	Heating coil unit section	-2.0m

Appendix E

Outputs of Zone Heating Load

Zone : 102

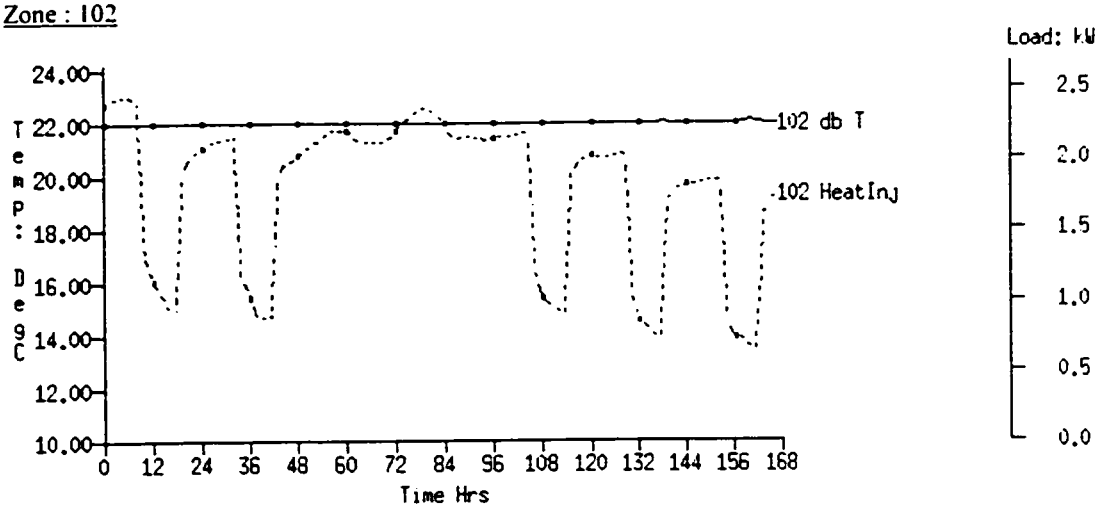

Zone : 103

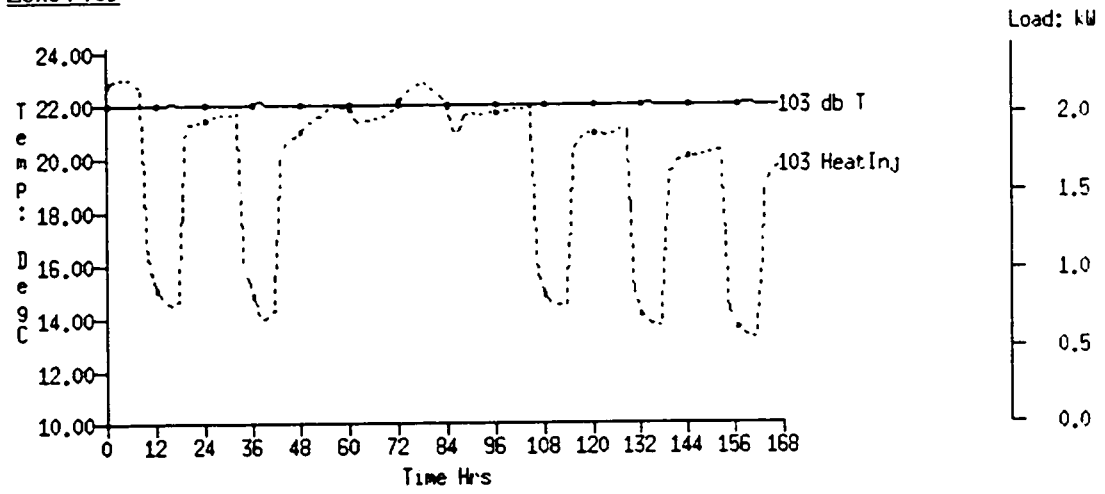

Zone : 110

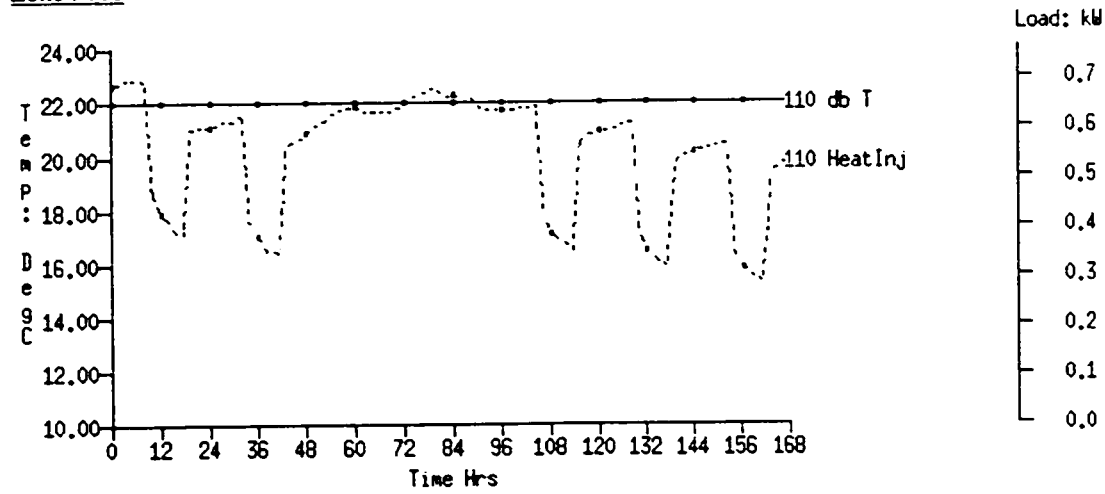

Zone : 112

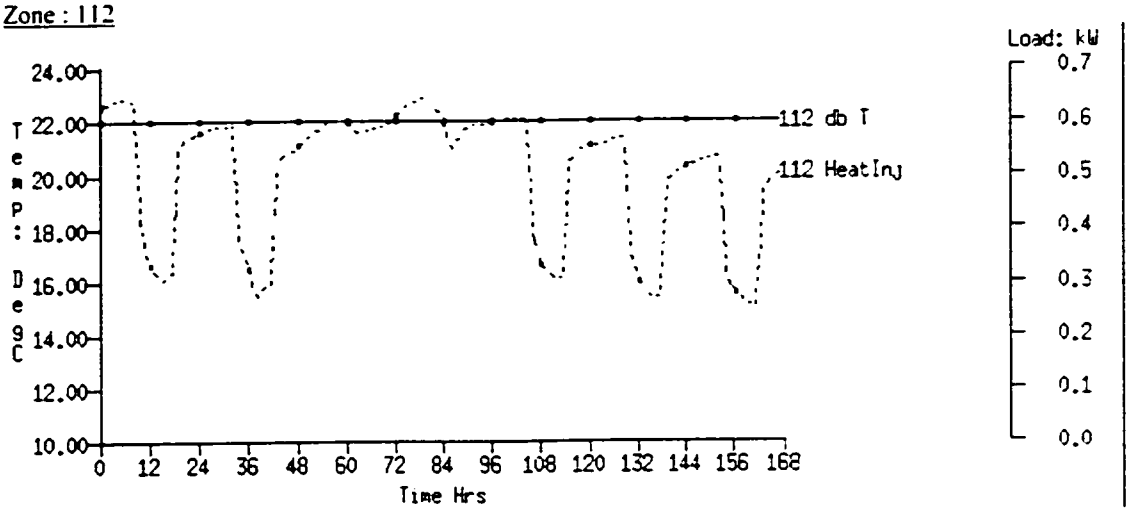

Zone : 113

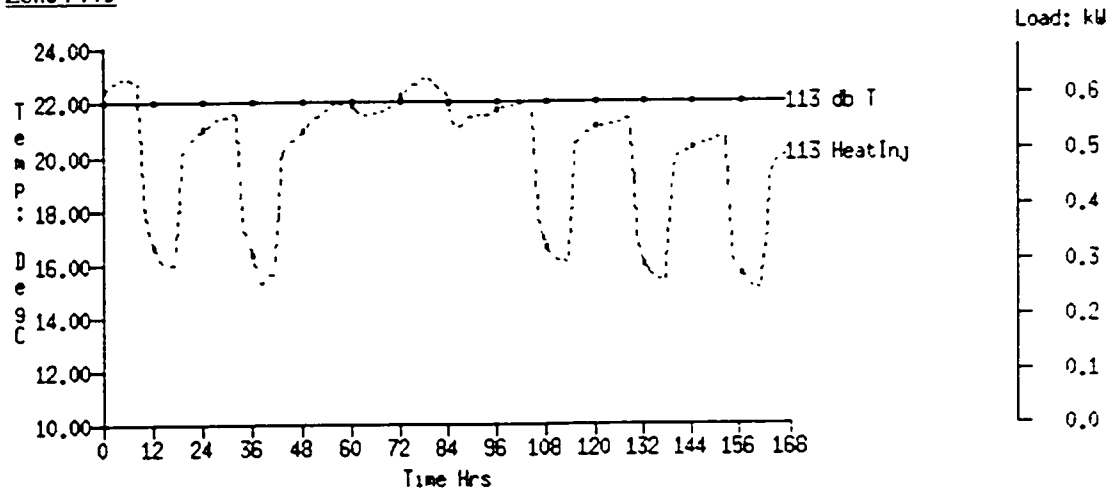

Zone : 116

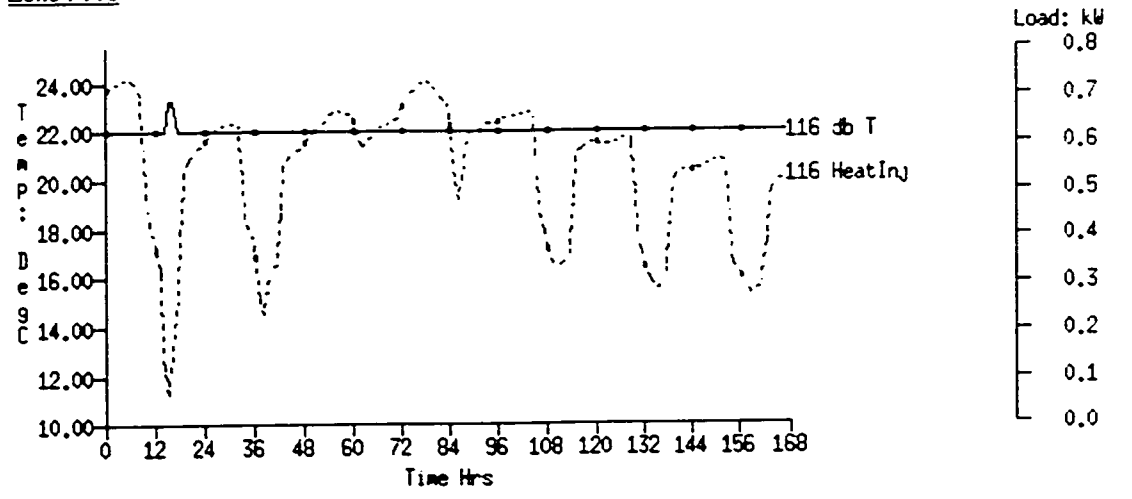

Zone : 119

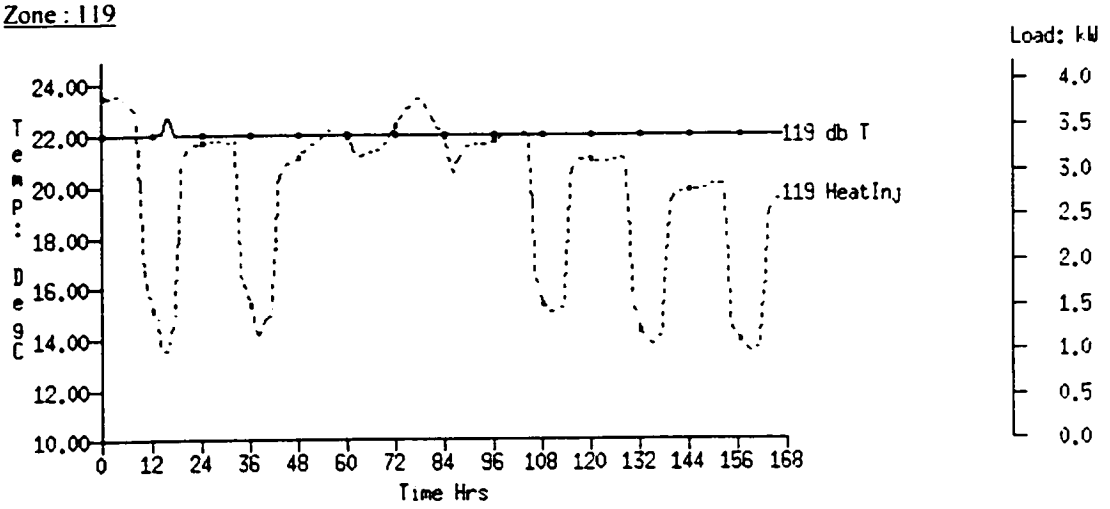

Zone : 120&121

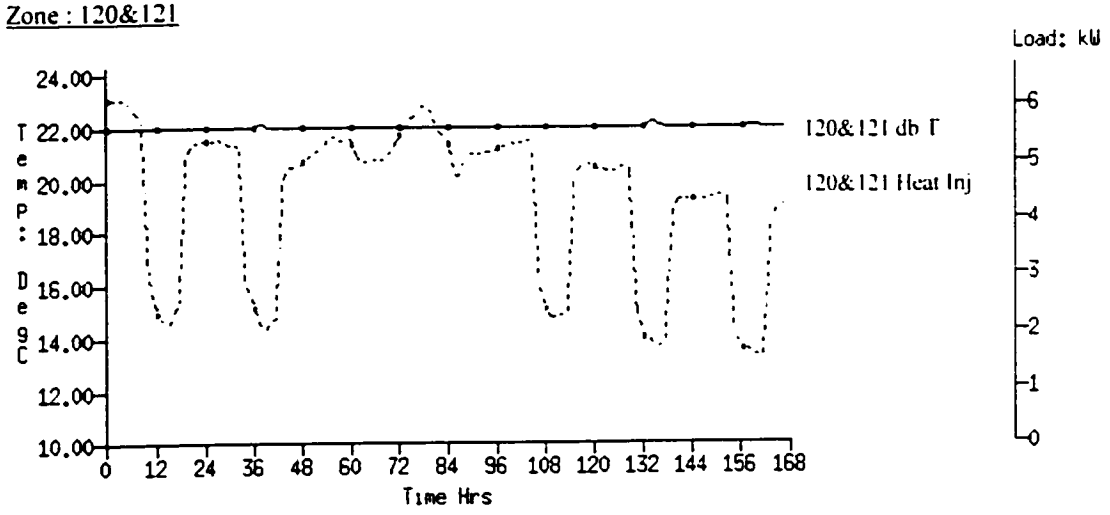

Zone : 122&123

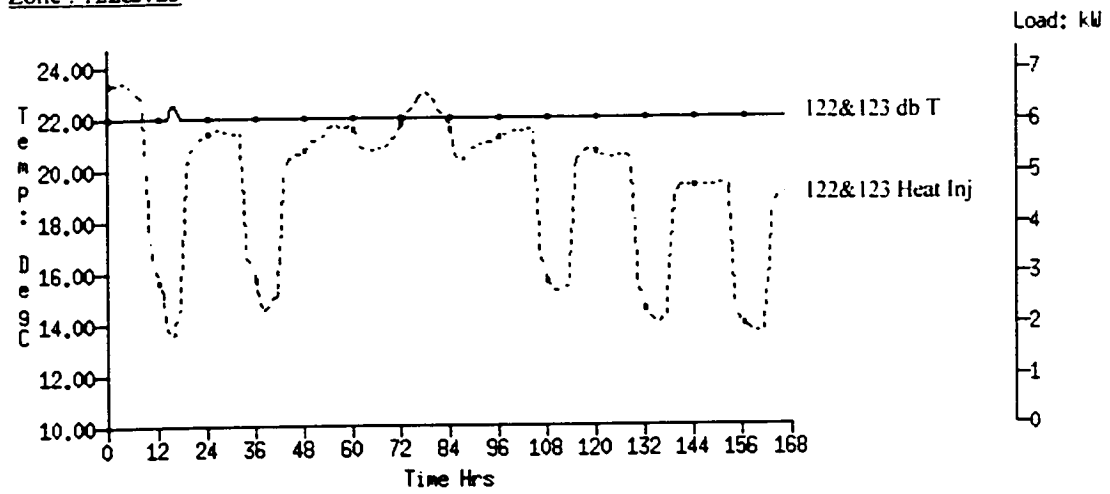

Zone : 124&125

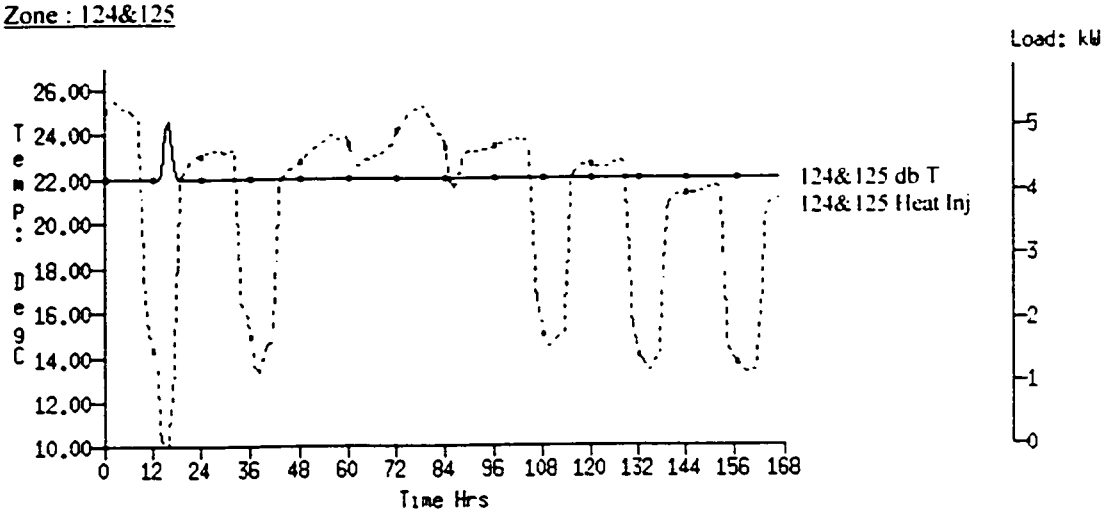

Zone : 126

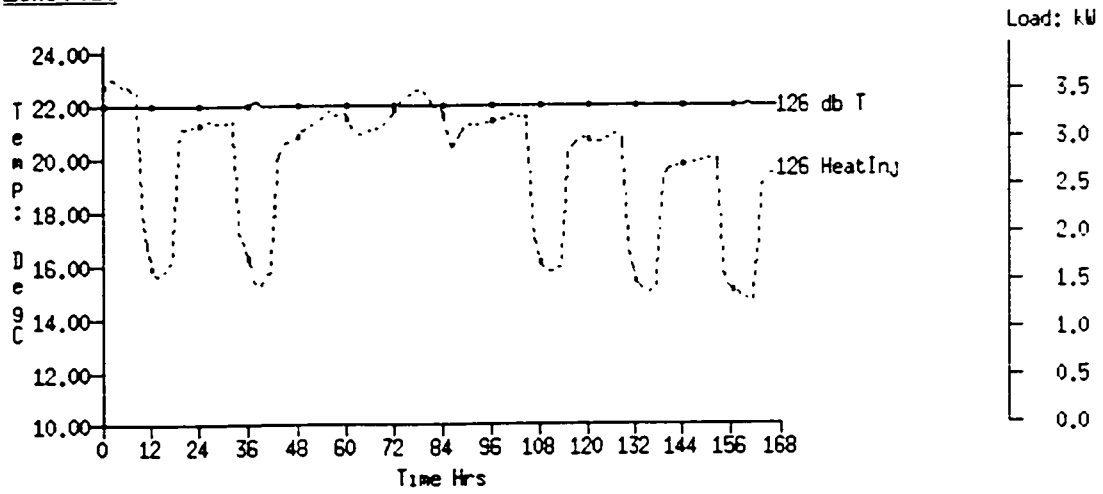

Zone : 129

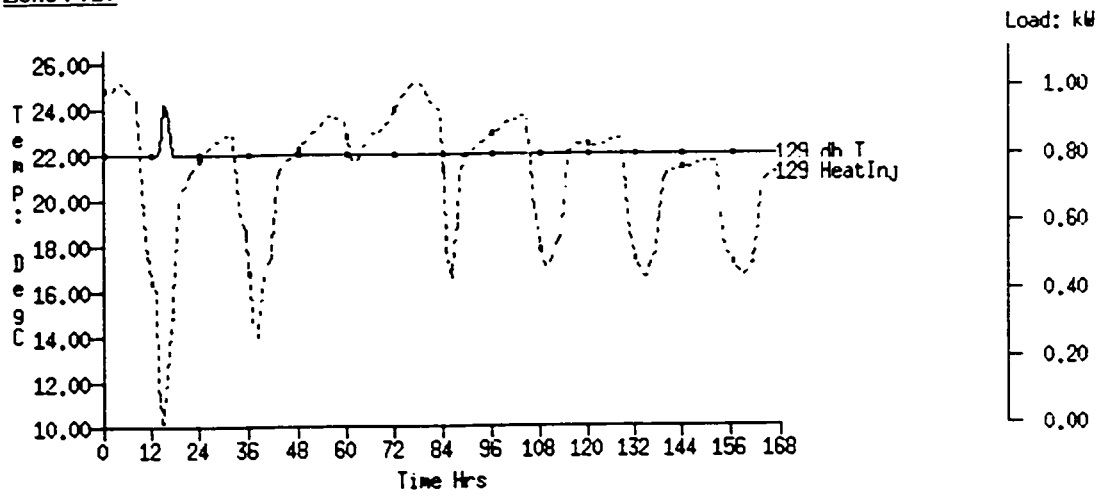

Zone : 130

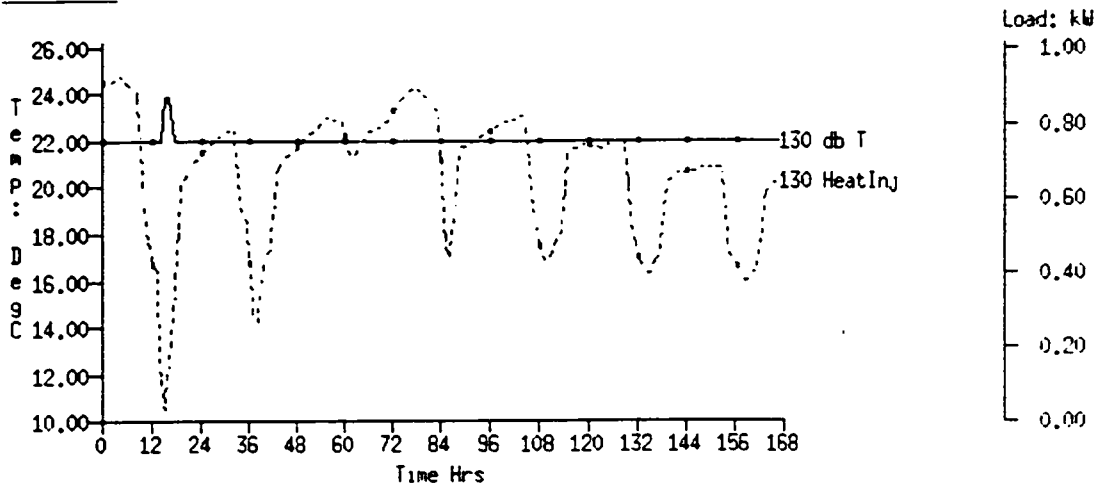

Zone : 131

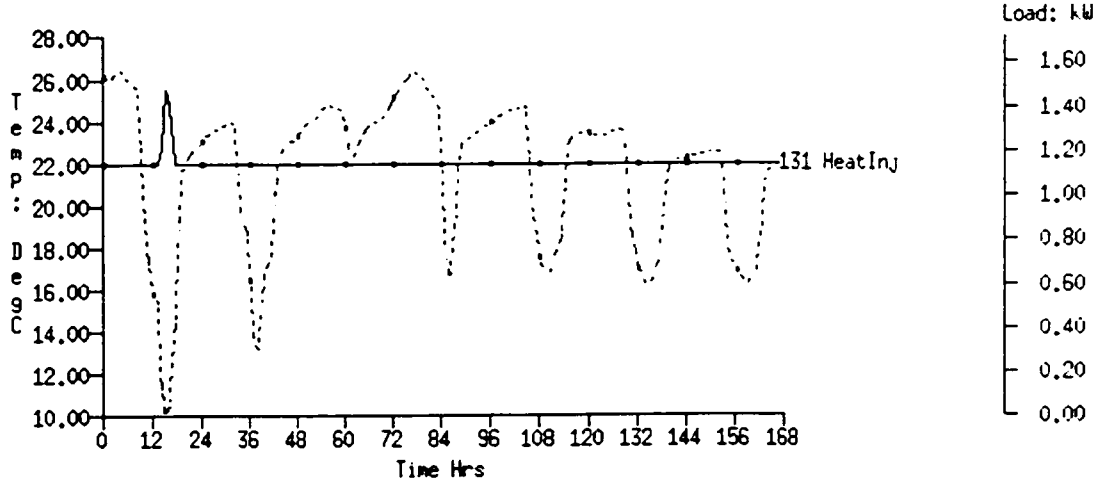

Zone : 134

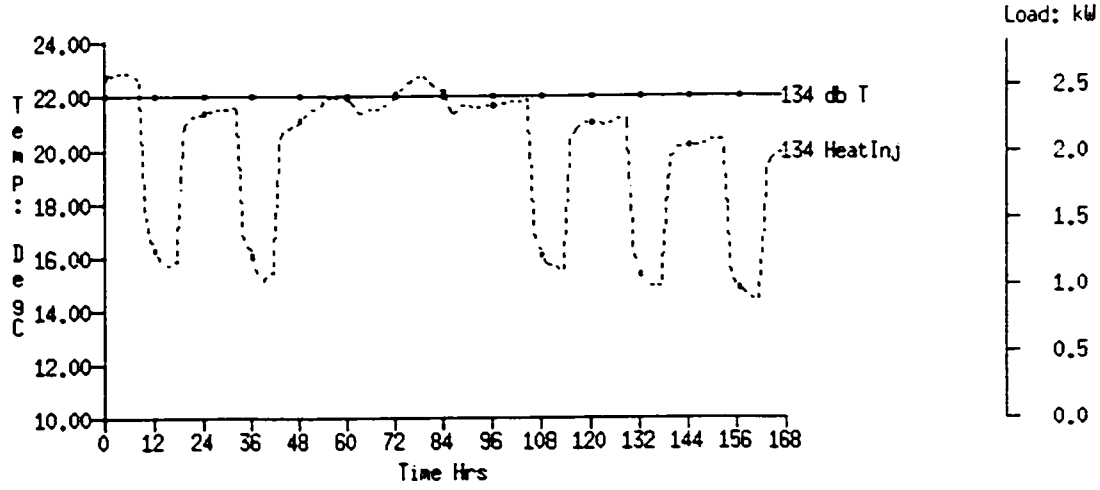

Zone : corridor

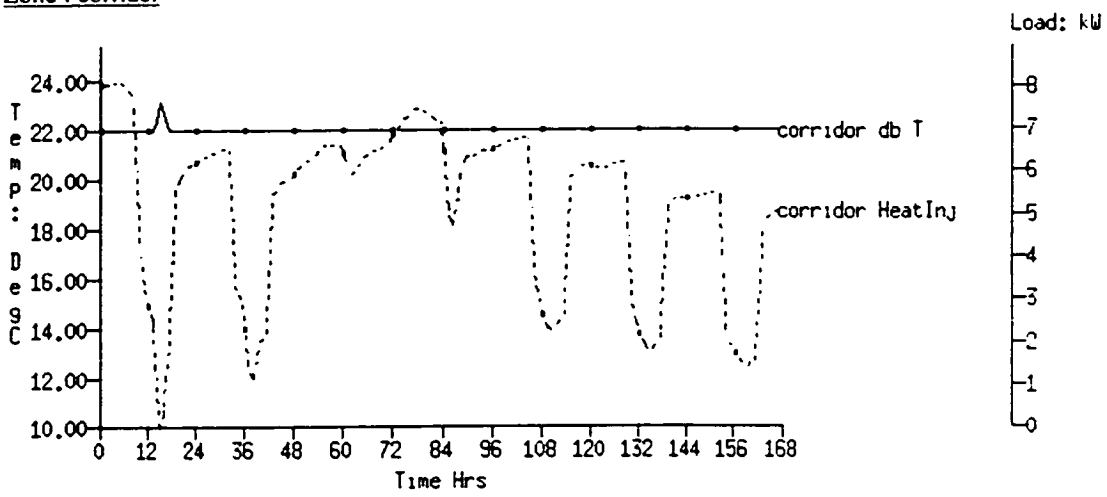

Appendix F

Outputs from the Integrated Simulation

Temperature Outputs

Zone : supply duct

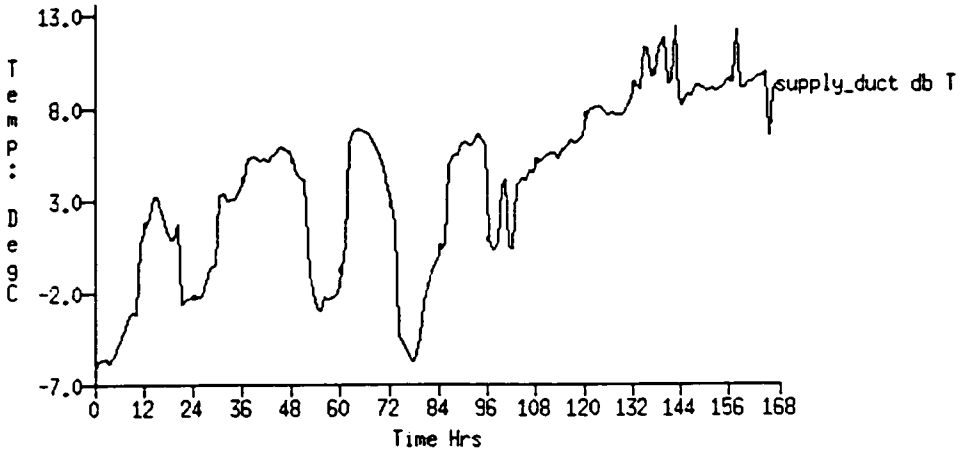

Zone : heating coil unit section

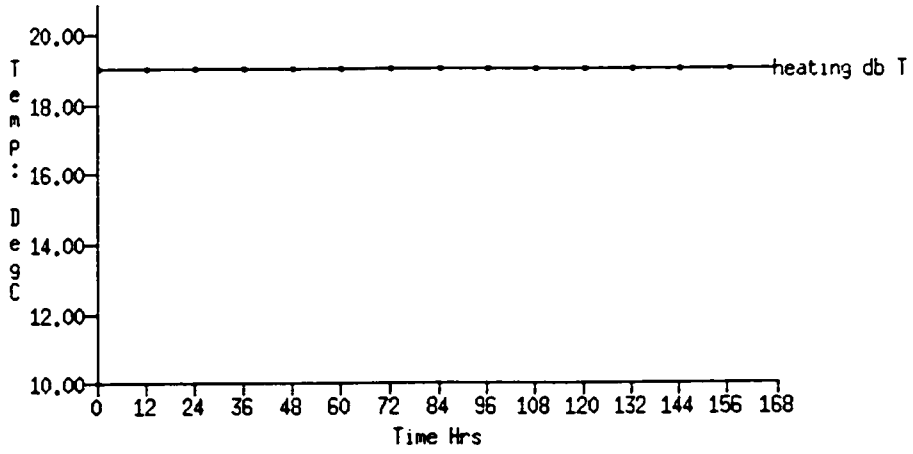

Zone : underground culvert

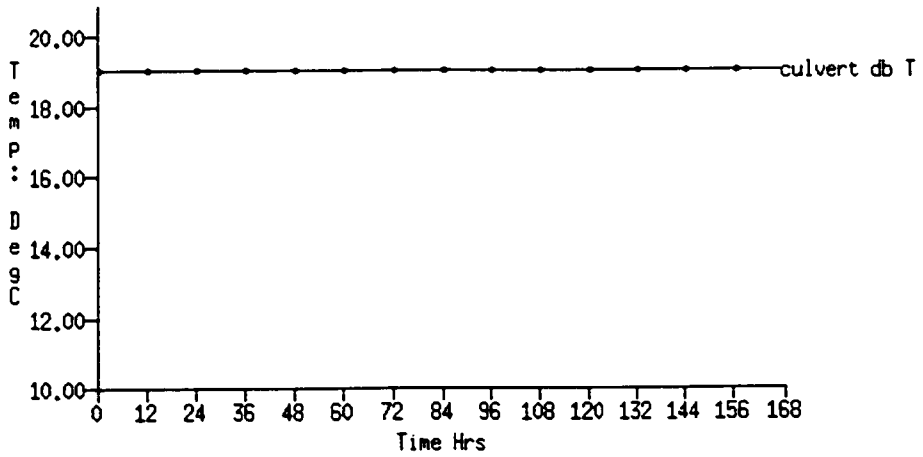

Zone : 102

Zone : 103

Zone : 110

Zone : 112

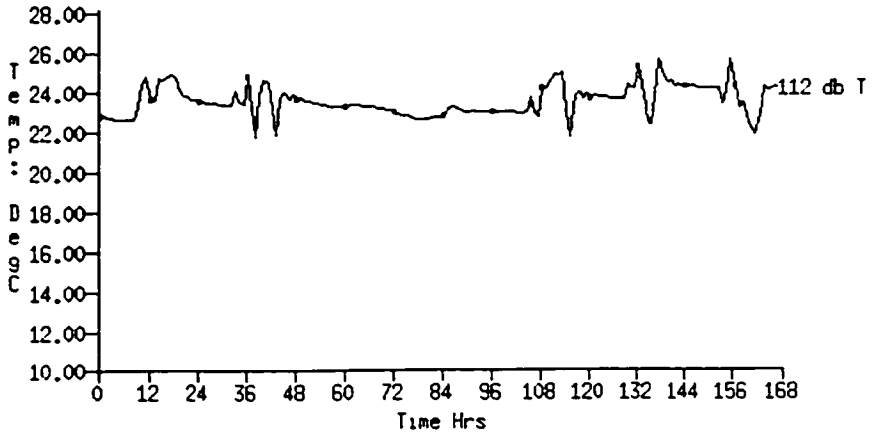

Zone : 113

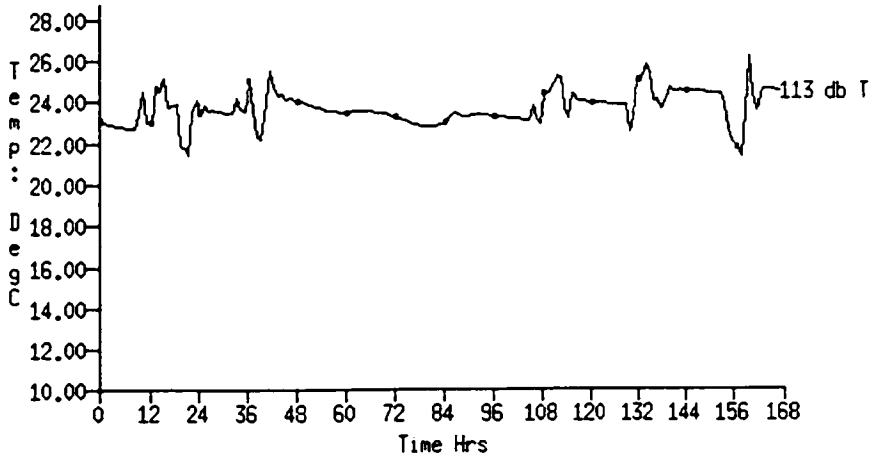

Zone : 116

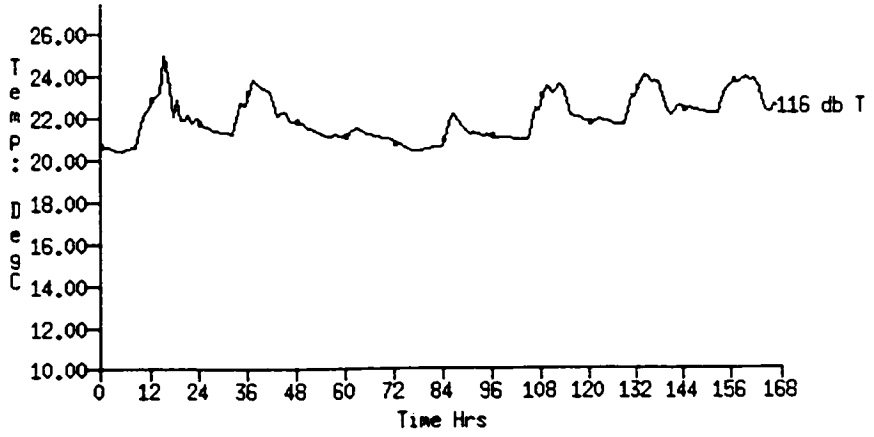

Zone : 119

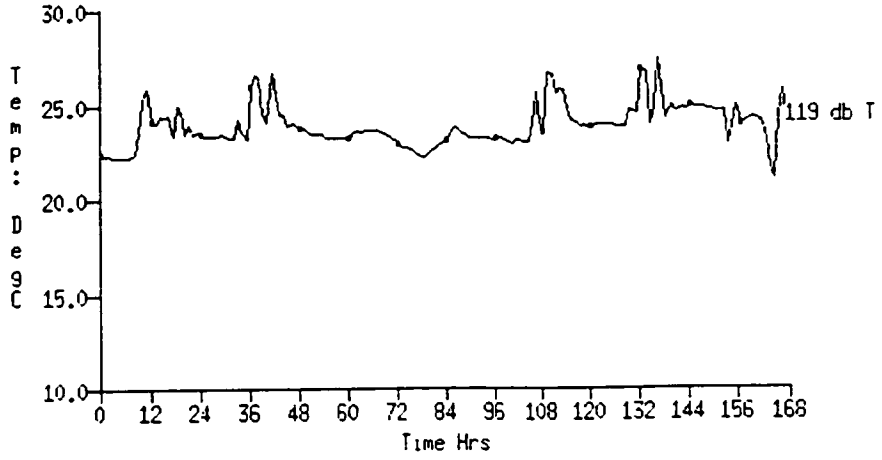

Zone : 120&121

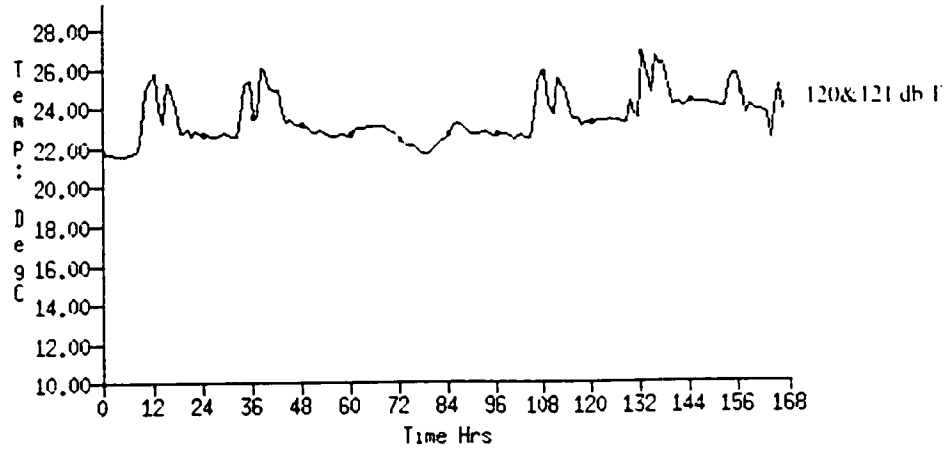

Zone : 122&123

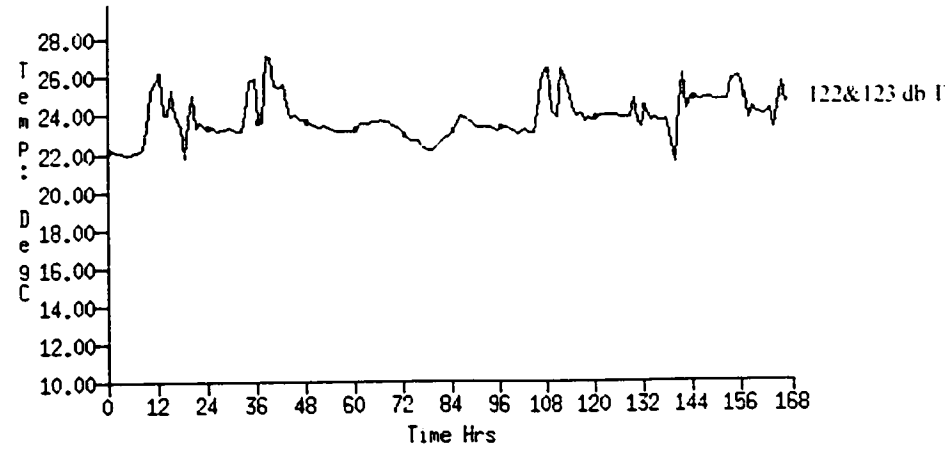

Zone : 124&125

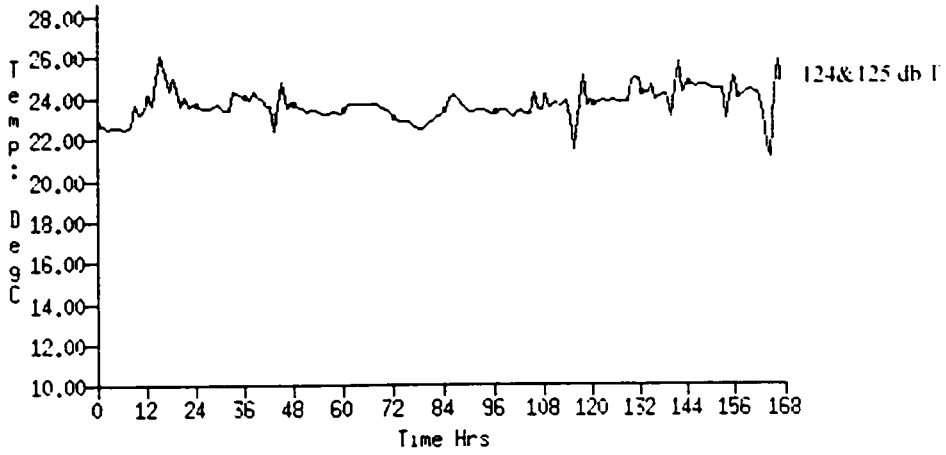

Zone : 126

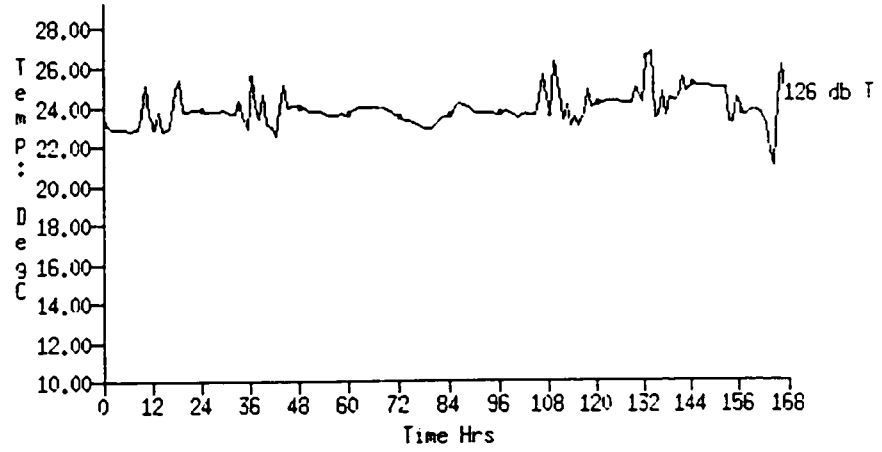

Zone : 129

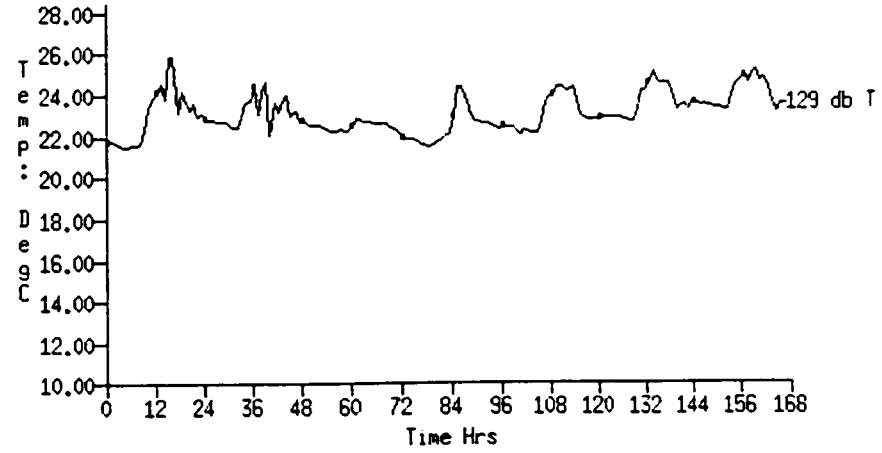

Zone : 130

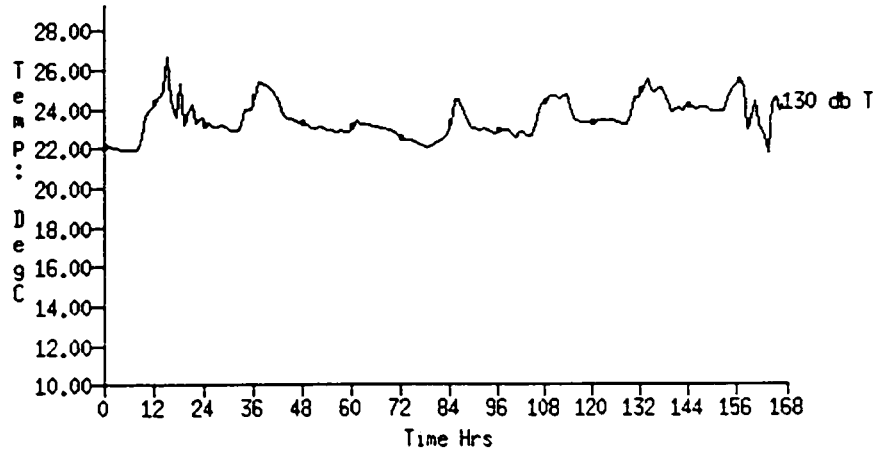

Zone : 131

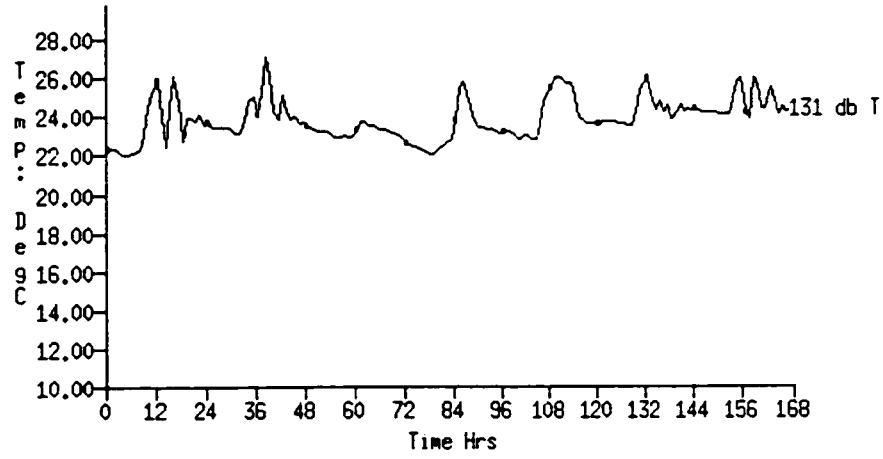

Zone : 134

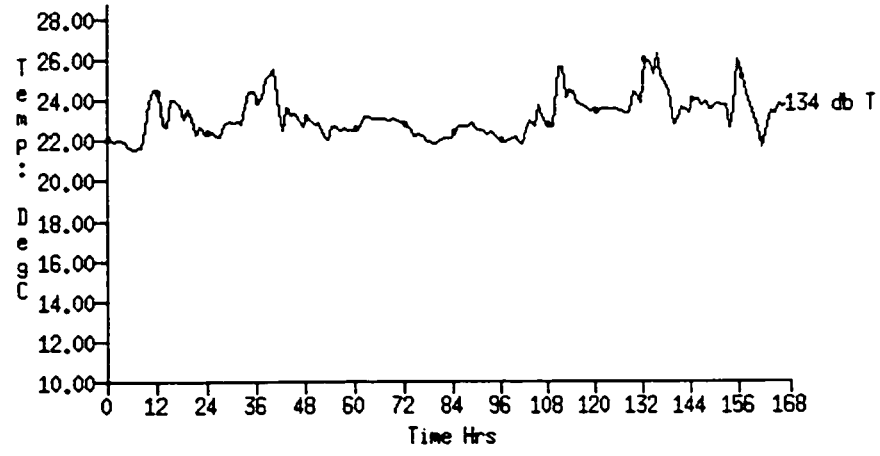

Zone : corridor

Zone : exhaust channel

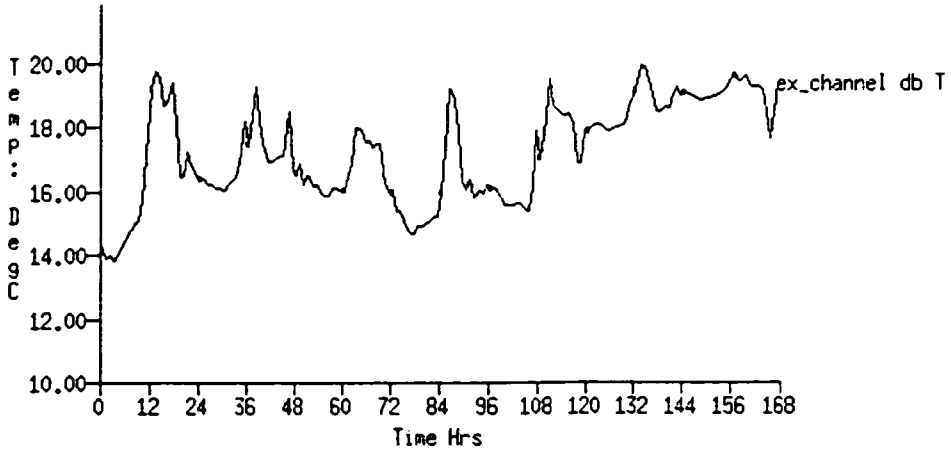

Zone : exhaust tower

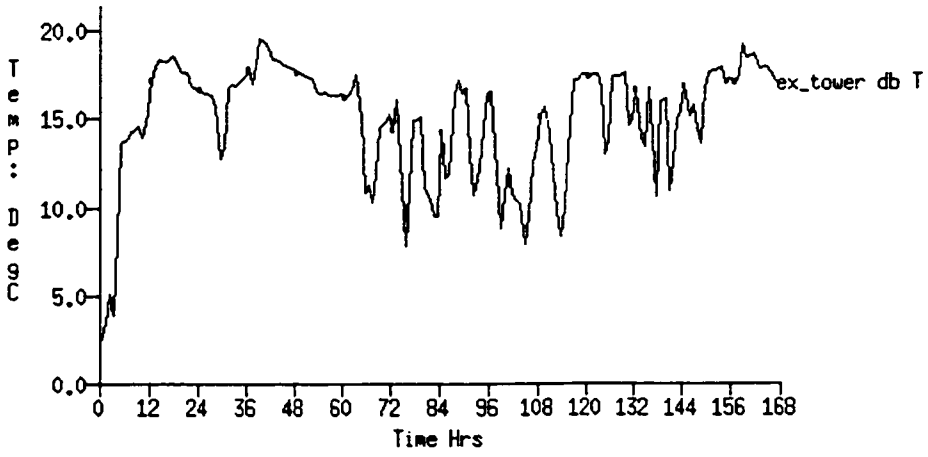

Airflow Outputs

Zone : supply duct

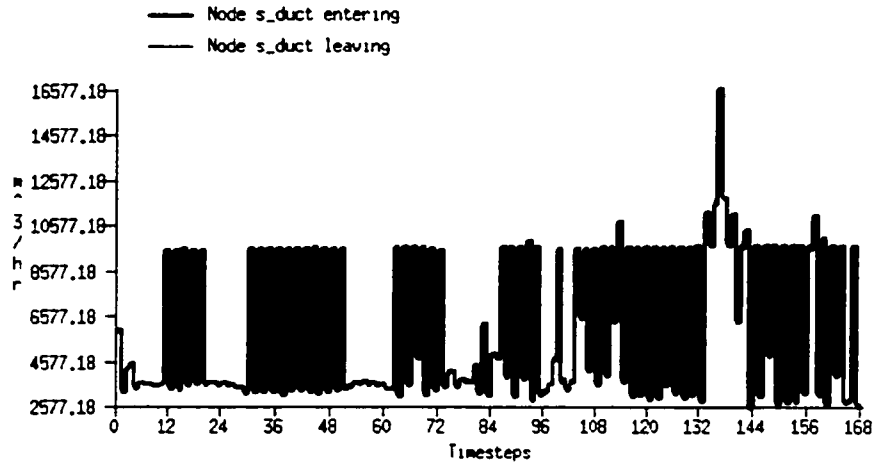

Zone : heating coil unit section

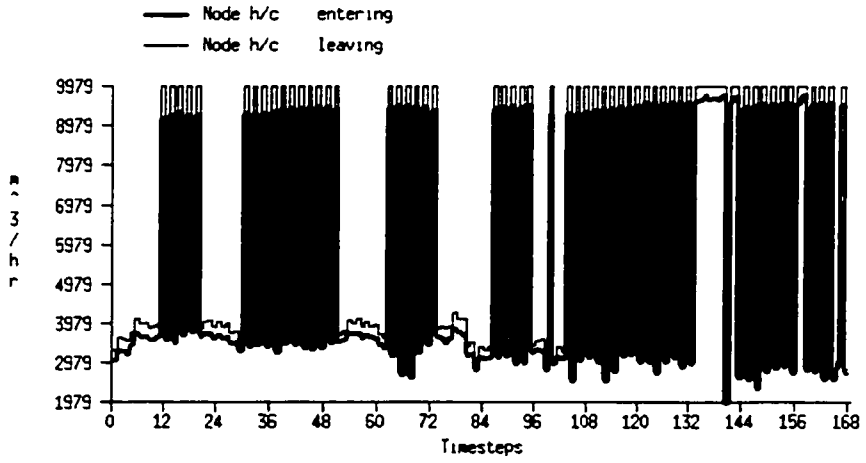

Zone : underground culvert

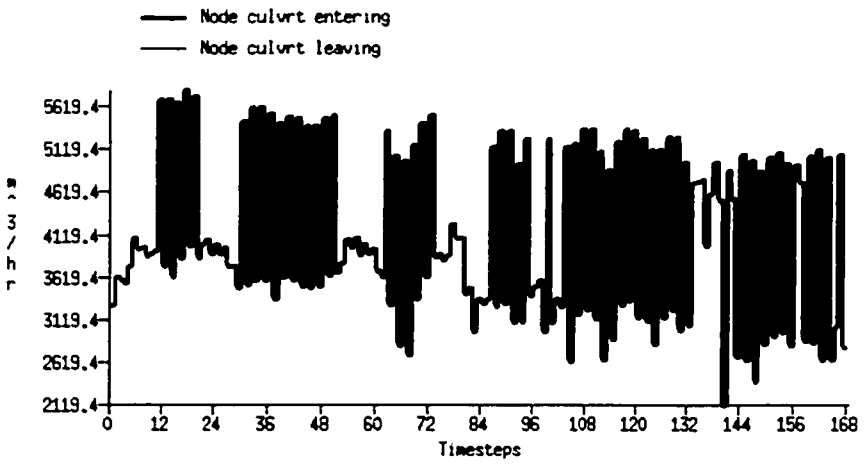

Zone : 102

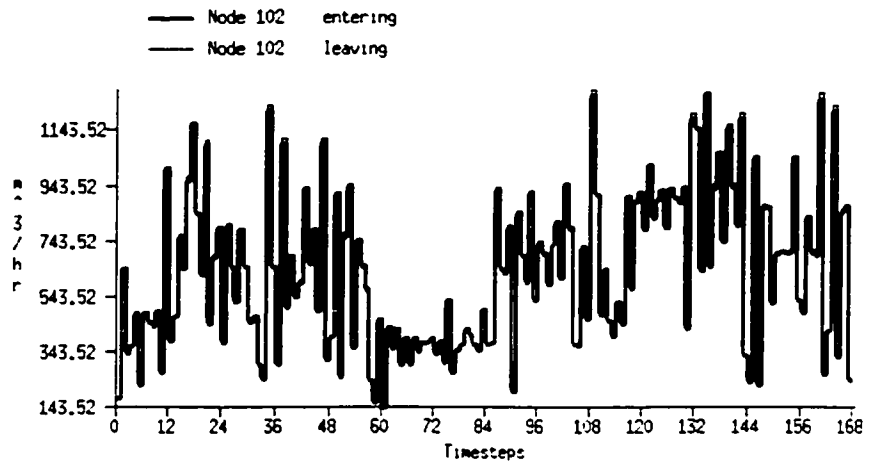

Zone : 103

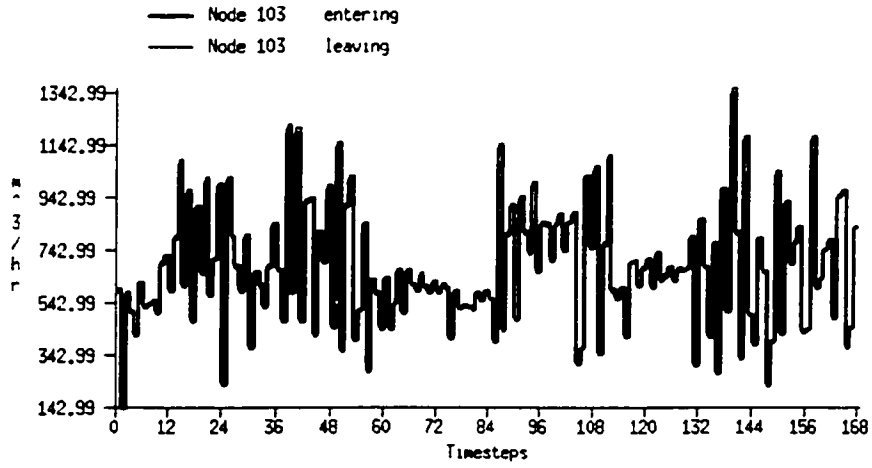

Zone : 110

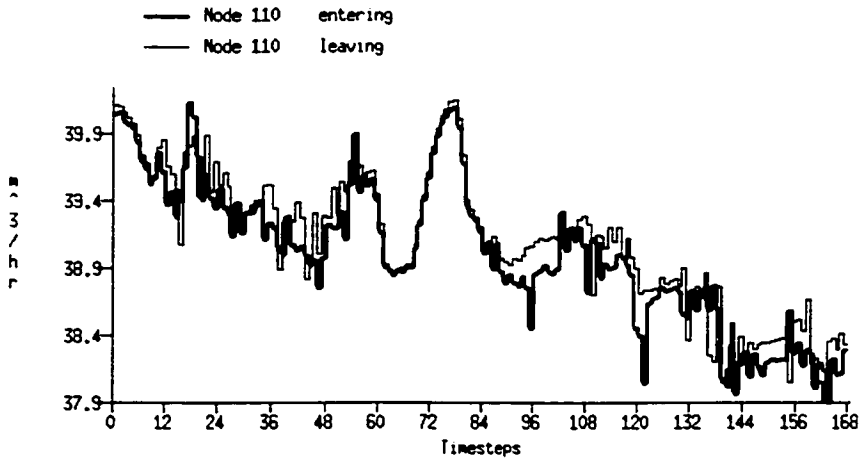

Zone : 112

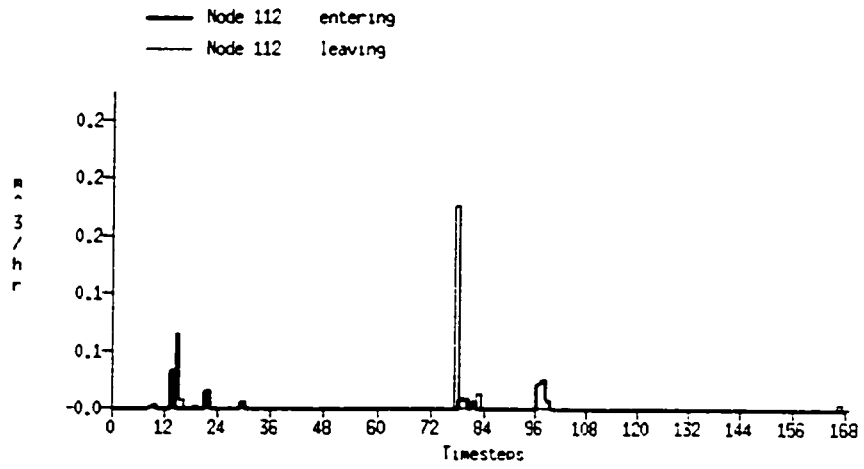

Zone : 113

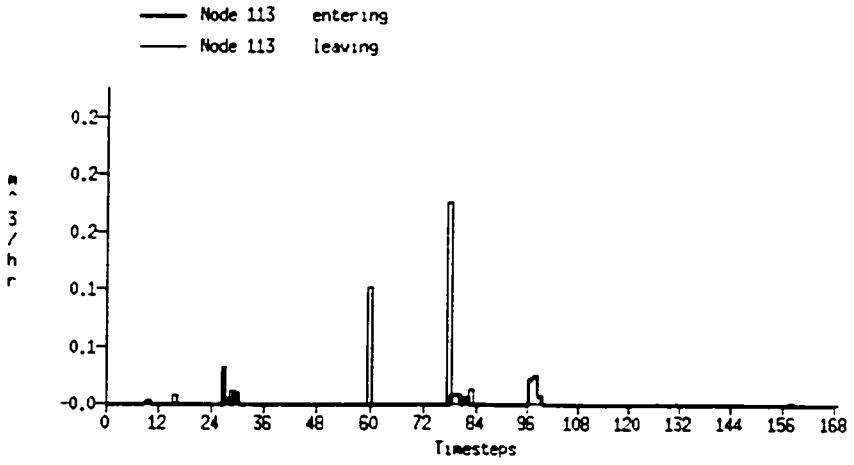

Zone : 116

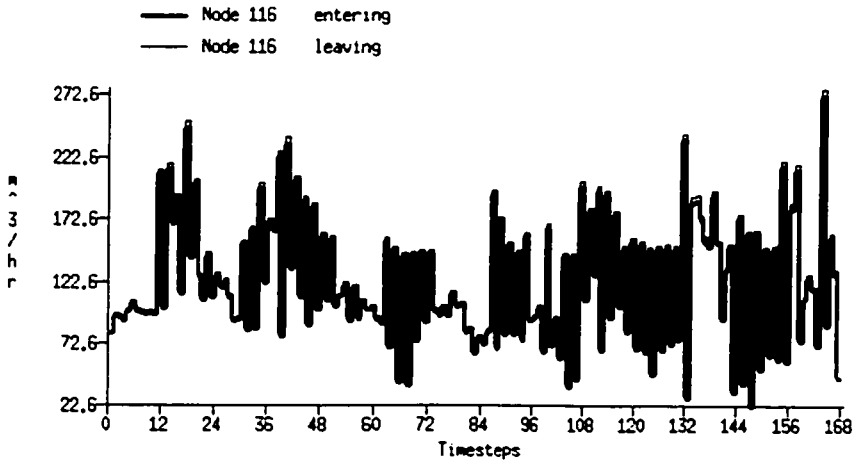

Zone : 119

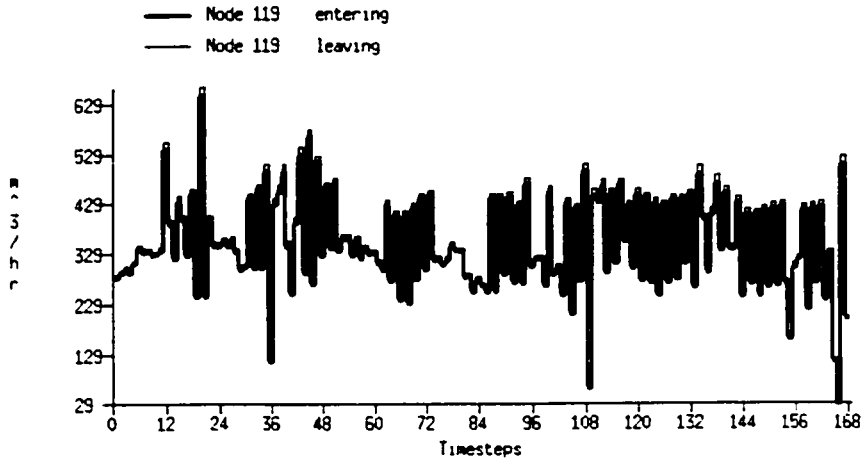

Zone : 120&121

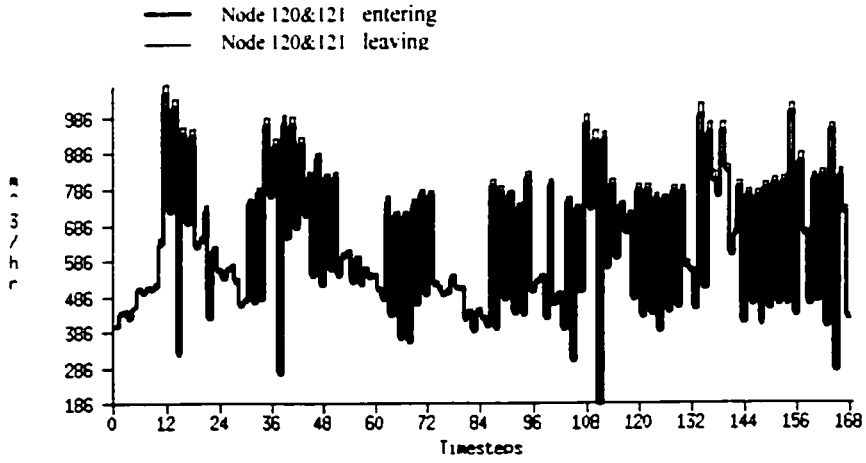

Zone : 122&123

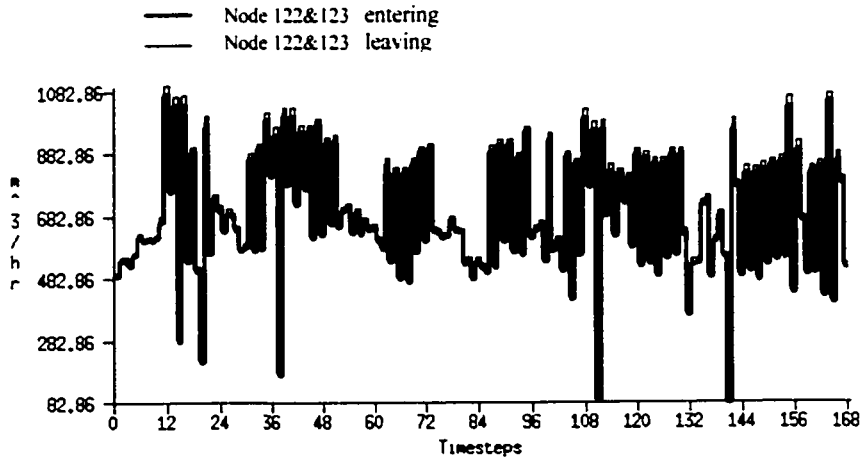

Zone : 124&125

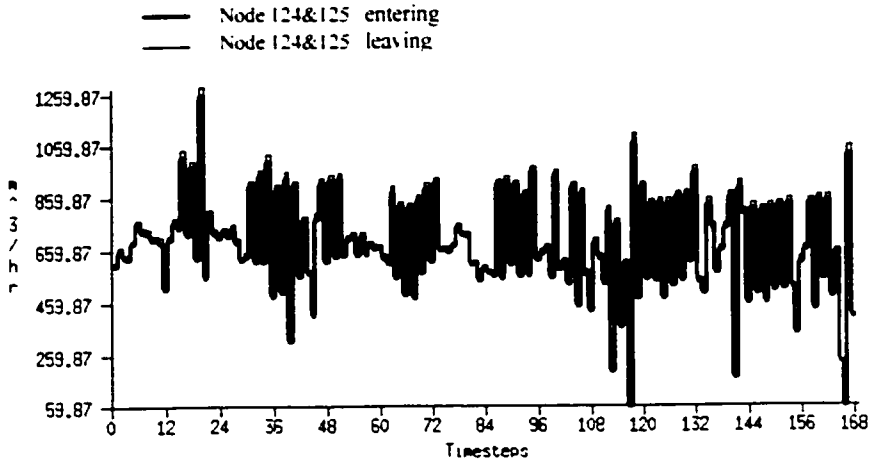

Zone : 126

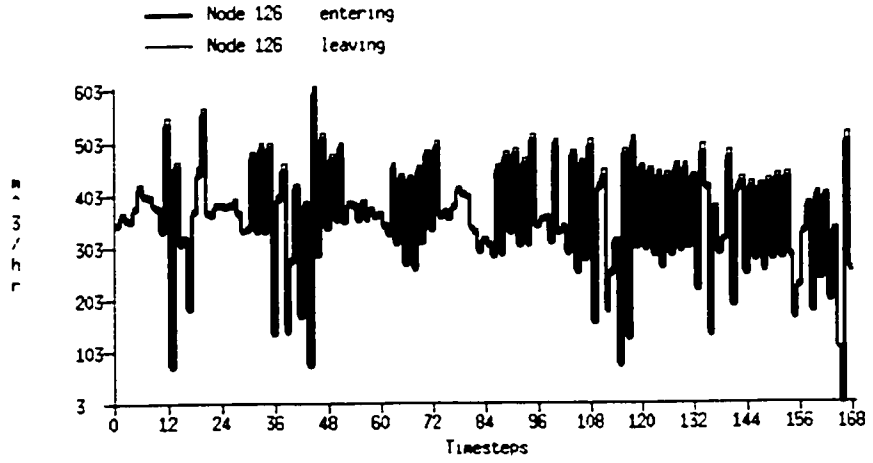

Zone : 129

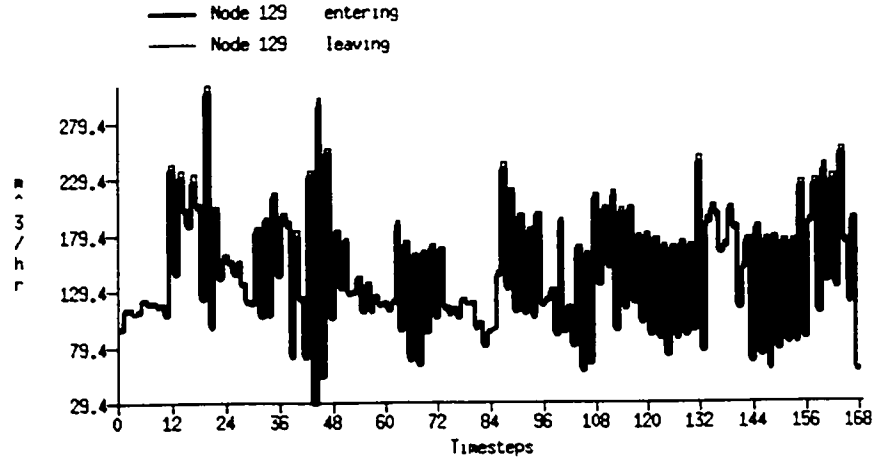

Zone : 130

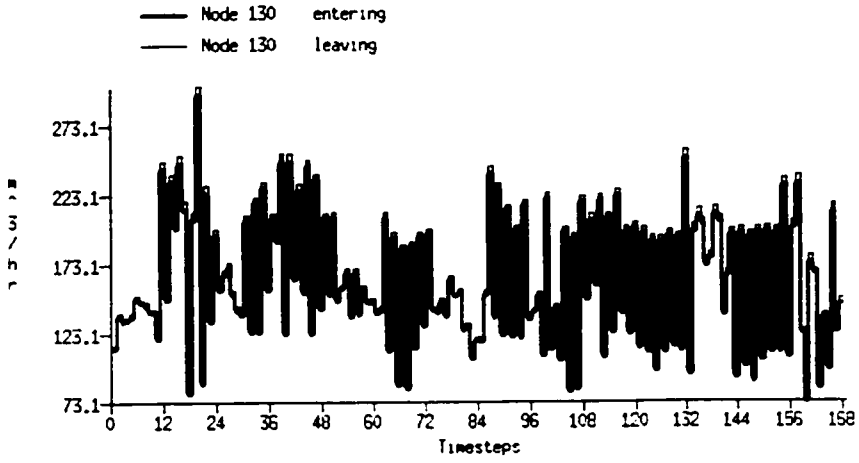

Zone : 131

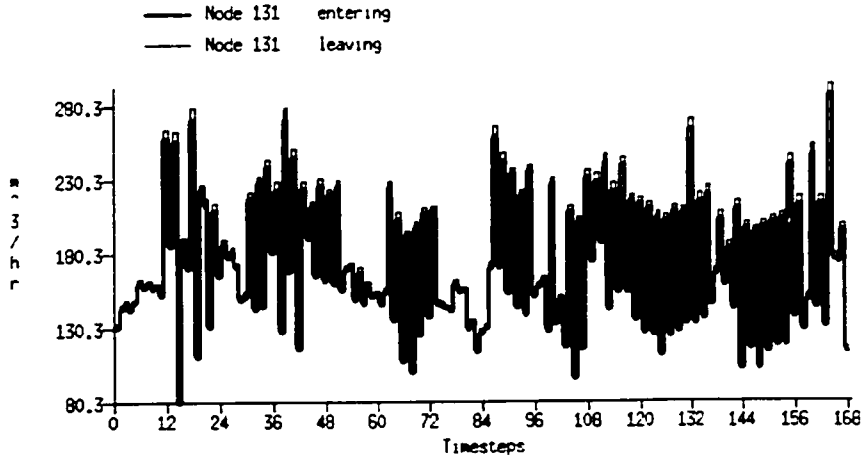

Zone : 134

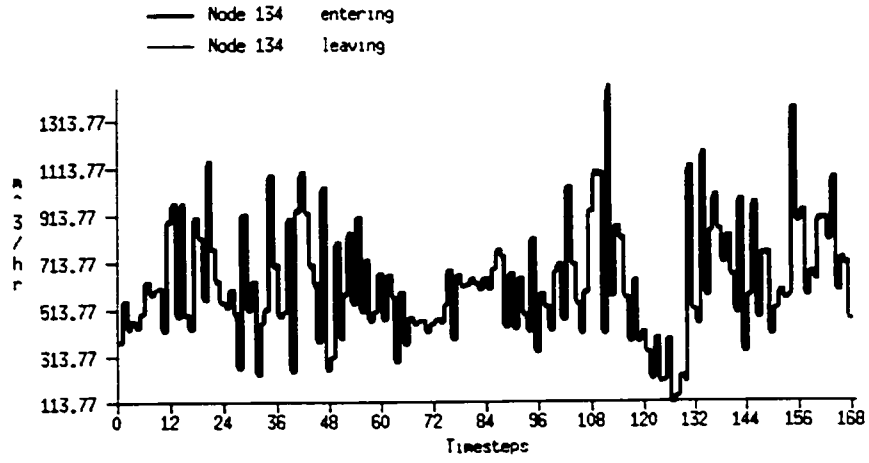

Zone : corridor

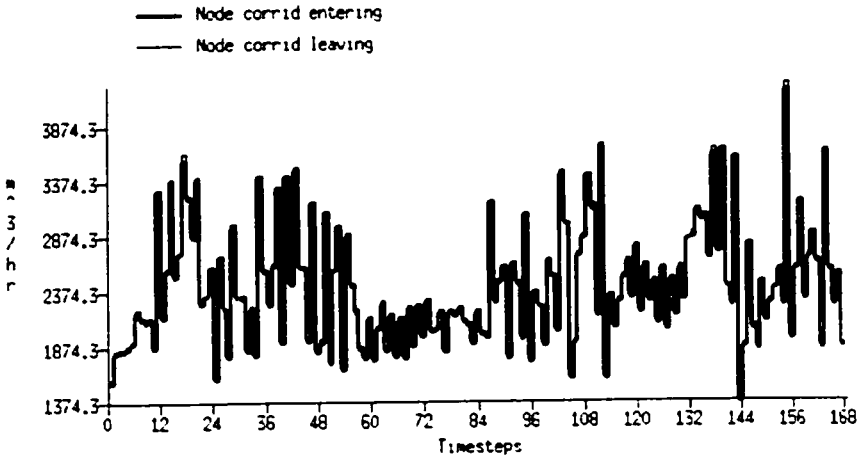

Zone : exhaust channel

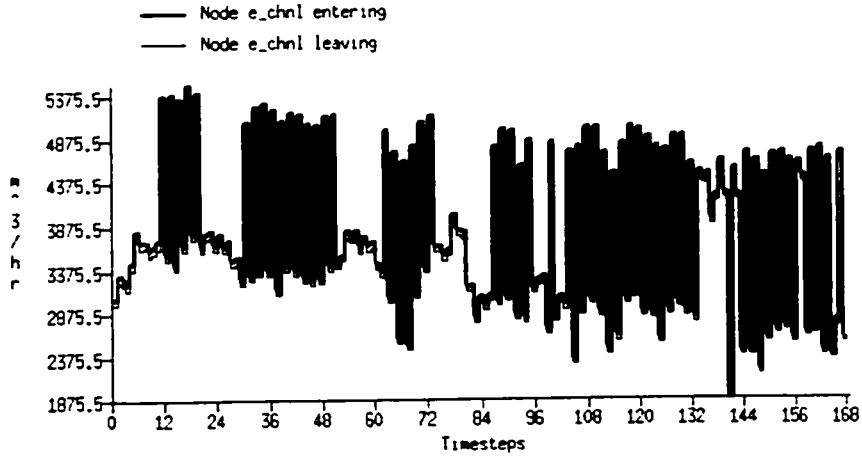

Zone : exhaust tower